



NTNU – Trondheim
Norwegian University of
Science and Technology

Numerical and Analytical Analysis of Geogrid Reinforced Soil Wall Subjected to Dynamic Loading

Martin Holst

Civil and Environmental Engineering

Submission date: June 2012

Supervisor: Steinar Nordal, BAT

Co-supervisor: Amir Kaynia, NGI

Norwegian University of Science and Technology
Department of Civil and Transport Engineering



Report Title: Numerical and Analytical Analysis of Geogrid Reinforced Soil Wall Subjected to Dynamic Loading	Date: June 11 th 2012		
	Number of pages (incl. appendices): 102		
	Master Thesis	x	Project Work
Name: Martin Holst			
Professor in charge/supervisor: Prof. Steinar Nordal, NTNU			
Other external professional contacts/supervisors: Prof. Amir M. Kaynia, NGI/NTNU			

Abstract: The potential human and economic loss due to structural collapse of geo-synthetic reinforced soil walls during earthquakes is huge. This substantiates the need for reliable design of such structures. The focus of this study was numerical and analytical design of geo-synthetic reinforced soil walls under dynamic loading. Two topics were addressed; the effect of reinforcement parameters and verification of pseudo-static methods.

The study is based on a 1 m high reduced-scale shaking table model loaded using stepped-amplitude harmonic base acceleration amplitude. A numerical PLAXIS model was developed and verified using physical model data. Material properties of the components (e.g. backfill and reinforcements) were based on information from a similar model developed using FLAC. The numerical model was used in a parameter study of the effects of reinforcement length and strength on the failure surface, facing displacements and reinforcement loads. The accuracy of pseudo-static methods was studied by comparing physical model results with predictions using the Mononobe-Okabe, the horizontal slices and two-part wedge method. Furthermore, guidelines for the Mononobe-Okabe method in different seismic design codes (i.e. Eurocode, FHWA/AASHTO and PIANC) were compared. Based on this comparison a new pseudo-static coefficient was developed.

The reinforcement length and strength were found to have a significant effect on model response. For example, an increase in reinforcement axial stiffness will give a shallower failure surface and reduced the lateral facing displacements. Neither the Mononobe-Okabe, nor the horizontal slice, or the two-part wedge method was able to predict both the failure surface and the earth forces for a wide range of acceleration amplitudes. It was found that different pseudo-static methods are suitable for different predictions (e.g. of the failure surface) at different acceleration amplitudes. For example, single wedge pseudo-static methods gave good predictions for the active earth force and failure surface shape for acceleration amplitudes up to 0.30g, but not for higher amplitudes. FHWA/AASHTO were found to give better predictions for the failure surface and earth forces (when using Mononobe-Okabe) than the Eurocode and PIANC guidelines. Even so, the failure surface predicted using FHWA/AASHTO was too shallow compared to the physical measurements for acceleration amplitudes up to 0.30g.

Keywords:

1. Pseudo-static methods
2. Reinforced soil walls
3. Numerical modelling
4. PLAXIS

(sign.)

Master Thesis
(TBA 4900 Geotechnical Engineering, master thesis)
Spring 2012
for
Stud. Techn. Martin Holst,

Numerical and analytical analysis of geogrid reinforced soil wall subjected to dynamic loading

Analytisk og numerisk analyse av dynamiske belastninger på en støttemur som er forsterket med «geonett»

Background

Geosynthetics are planar products manufactured from polymeric materials (the synthetic) used with soil, rock, or other geotechnical- related material (the geo) as part of a civil engineering project or system. A geogrid is a geosynthetic which are primarily used for reinforcement; they are formed by a regular network of tensile elements with apertures of sufficient size to interlock with surrounding fill material. They are in some cases used to construct stable slopes at much steeper angles than would otherwise be possible.

The analysis of the stability of soil masses and forces in the geosynthetics has traditionally been based on the classical principles of failure mechanisms and limit equilibrium. More recently, the use of numerical solutions such as finite elements has become more common following the development of special elements.

Task description

The ultimate objective for this thesis is to create a numerical model and verify it by using physical model test results for dynamic forces. Such models can be used for optimum design of geosynthetics layout in practical applications. The study will also highlight key reinforcement parameters and their role on the performance of geosynthetics under earthquake loading. In addition, the use of analytical methods for calculations of dynamic forces (earthquakes) on retaining walls and their accuracy should be studied.

The following activities should be included:

- Literature review on earthquake (or general dynamic) response of retaining walls. In this part the objective is to find a relevant case on which the numerical models (see later bullet-points) can be calibrated, e.g.:
 - Experimental studies
 - Empirical solutions
 - Numerical analysis
- Numerical modelling of the case found in the literature review on earthquake response of retaining walls (or embankments), verification of model by use of case data.
- Study of the effect of key reinforcement parameters using the developed numerical model.
- Literature review of analytical methods used to analyse retaining walls or embankments, focus on pseudo-static methods.
- Study of analytical methods accuracy by use of case data and current design guidelines.



Fakultet for ingeniørvitenskap og teknologi
Institutt for bygg, anlegg og transport

Professor in charge: Prof. Steinar Nordal, NTNU

Other supervisors: Prof. Amir M. Kaynia, NGI and NTNU

Trondheim, January 16, 2012. (revised: June 8.2012)

A handwritten signature in blue ink that reads "Amir M. Kaynia".

Prof. Amir M. Kaynia

Abstract

The potential human and economic loss due to structural collapse of geo-synthetic reinforced soil walls during earthquakes is huge. This substantiates the need for reliable design of such structures. The focus of this study was numerical and analytical design of geo-synthetic reinforced soil walls under dynamic loading. Two topics were addressed; the effect of reinforcement parameters and verification of pseudo-static methods.

The study is based on a 1 m high reduced-scale shaking table model loaded using stepped-amplitude harmonic base acceleration amplitude. A numerical PLAXIS model was developed and verified using physical model data. Material properties of the components (e.g. backfill and reinforcements) were based on information from a similar model developed using FLAC. The numerical model was used in a parameter study of the effects of reinforcement length and strength on the failure surface, facing displacements and reinforcement loads. The accuracy of pseudo-static methods was studied by comparing physical model results with predictions using the Mononobe-Okabe, the horizontal slices and two-part wedge method. Furthermore, guidelines for the Mononobe-Okabe method in different seismic design codes (i.e. Eurocode, FHWA/AASHTO and PIANC) were compared. Based on this comparison a new pseudo-static coefficient was developed.

The reinforcement length and strength were found to have a significant effect on model response. For example, an increase in reinforcement axial stiffness will give a shallower failure surface and reduced the lateral facing displacements. Neither the Mononobe-Okabe, nor the horizontal slice, or the two-part wedge method was able to predict both the failure surface and the earth forces for a wide range of acceleration amplitudes. It was found that different pseudo-static methods are suitable for different predictions (e.g. of the failure surface) at different acceleration amplitudes. For example, single wedge pseudo-static methods gave good predictions for the active earth force and failure surface shape for acceleration amplitudes up to 0.30g, but not for higher amplitudes. FHWA/AASHTO were found to give better predictions for the failure surface and earth force (when using Mononobe-Okabe) than the Eurocode and PIANC guidelines. Even so, the failure surface predicted using FHWA/AASHTO was too shallow compared to the physical measurements for acceleration amplitudes up to 0.30g.

Sammendrag (Norwegian Abstract)

Kollaps av geo-syntetisk forsterkede støttemurer som følge av seismiske laster kan potensielt føre til store menneskelige og økonomiske tap. Dette illustrerer et behov for pålitelige designkriterier for slike konstruksjoner. I denne oppgaven har fokuset vært numerisk og analytisk analyse av geo-syntetisk forsterkede støttemurer utsatt for dynamisk belastning. To temaer har vært berørt; effekten av forsterkingsparametere og verifikasjon av pseudo-statistiske modeller.

Grunnlaget for oppgaven er en 1m høy ristebordsmodell som ble belastet med en stegvis økende harmonisk akselerasjonsamplitude. En numerisk PLAXIS-modell ble utviklet og verifisert ved hjelp av data fra det fysiske modellforsøket. Materialeegenskapene til de ulike komponentene (for eksempel jorden og jordforsterkingene) ble basert på informasjon fra en lignende modell, utviklet i FLAC. Den numeriske modellen ble benyttet i en parameterstudie hvor jordforsterkningens lengde og styrke ble studert med hensyn på deres påvirkning på utvikling av bruddflaten, forskyvningen av støttemuren og kreftene i forsterkningene.

De pseudo-statistiske modellenes pålitelighet ble vurdert ved å sammenligne prediksjonene til Mononobe-Okabemetoden, «Horizontalskivemetoden» og «Todelskilemetoden» med resultatene fra det fysiske modellforsøket. I tillegg ble retningslinjene for Mononobe-Okabemetoden i ulike veiledere (dvs. Eurocode, FHWA/AASTHO og PIANC) sammenlignet. Basert på denne sammenligningen ble det også forslått en ny pseudo-statistisk koeffisient.

De numeriske undersøkelsene viste at jordforsterkningslengden og –styrken har betydelig effekt på responsen i støttemuren. For eksempel vil en økning av den aksiale stivheten i forsterkningene føre til en grunnere bruddflate og redusere de horisontale forskyvningene på støttemuren. Ingen av de studerte pseudo-statistiske metodene var i stand til å beregne både bruddflaten og jordkreftene for et bredt spekter av akselerasjonsamplituder. Den analytiske studien viste at ulike pseudo-statistiske metoder egner seg for ulike prediksjoner (f.eks. av bruddflaten) ved ulike akselerasjonsamplituder. For eksempel, single-kilemetoder viste seg vel egnet til å bestemme de aktive jordkreftene og formen på bruddflaten for akselerasjonsamplituder opp til 0.30g. Ellers ble retningslinjene i FHWA/AASTHO funnet å gi et bedre estimat en Eurokode 8 og PIANC for bruddflaten og jordkreftene ved bruk av Mononobe-Okabemetoden.

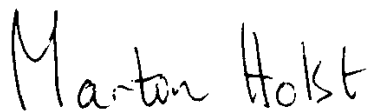
Preface

This report is the result of a Geotechnical Master thesis at the Norwegian University of Science and Technology (NTNU) in spring 2012 and deals with analytical and numerical studies of dynamic loading on retaining walls. The thesis was suggested by the Norwegian Geotechnical Institute (NGI).

I would like to thank my supervisor's: Professor Amir M. Kaynia for his commitment and positive attitude and Professor Steinar Nordal for always taking his time to explain and point me in the right direction. I would also like to thank Dr. Richard J. Bathurst at the Royal Military College of Canada (RMC) for sharing his knowledge and for providing data, rapports and articles that made my studies possible.

I've completed this rapport (and thus completed a 5 year Master of Science program at NTNU) knowing that this is more than most people expected of me growing up. For my family who always believed in me: Thank you. And for my engineering ancestors, Ole Martin Vik and Harold Strafford Holst; I hope I've made you proud.

Trondheim, June 10th 2012



Martin Holst

Table of Contents

Abstract	V
Sammendrag (Norwegian Abstract)	VII
Preface.....	IX
Table of Contents	XI
List of Figures.....	XV
List of Tables	XVII
List of Notation and Symbols.....	XIX
1 Introduction.....	1
1.1 Choice of Subject	1
1.2 Problem Definition	1
1.3 Objective.....	2
1.4 Research Methodology	2
1.5 Thesis Organisation	2
1.6 Previous Work	3
2 Background Material	5
2.1 Reinforced Soil Walls.....	5
2.2 Fast Fourier Transformation and Spectral Density.....	5
2.3 Hardening Soil Model in Dynamic Analysis	6
2.4 Rayleigh Damping.....	7
2.5 Displacement Drift.....	7
3 Shaking Table Experiments at RMC: Background.....	9
3.1 General	9
3.2 Geometry.....	9
3.3 Soil Properties	10
3.4 Reinforcement and Facing.....	10
3.5 Natural Frequency and Base Excitation.....	11
3.6 Failure Surface.....	11
4 Shaking Table Experiments at RMC: Numerical Modelling	13
4.1 PLAXIS 2D Dynamics	13
4.2 Model Properties.....	13
4.2.1 Geometry.....	13
4.2.2 Excitation	14
4.2.3 Mesh and Time Step.....	15

4.2.4	Loads and Boundary Conditions.....	15
4.2.5	Material Models and Material Properties.....	16
4.3	Model Verification.....	17
4.3.1	Fundamental Frequency.....	17
4.3.2	Lateral Displacements at the Top of the Facing Panel	18
4.3.3	Zone of Movement.....	19
4.3.4	Total Earth Forces.....	22
4.4	Comments and Discussion.....	23
4.5	Summary of Numerical Model Development and Verification.....	24
5	Numerical Study: Effect of Reinforcement Parameters.....	25
5.1	Effect on Failure Surface	25
5.2	Effect on Facing Displacements.....	28
5.3	Effect on Reinforcement Connection Loads.....	29
5.4	Comments and Discussions.....	31
5.5	Summary of Numerical Study on Effect of Reinforcement Parameters	32
6	Literary Review: Analytical Methods for Seismic Design	33
6.1	Introduction to Pseudo-Static Analysis	34
6.2	Mononobe-Okabe Method (M-O).....	34
6.2.1	Assumptions	34
6.2.2	Earth Pressure Coefficient and Critical Surface.....	35
6.3	Two-Part Wedge Method (TPW).....	36
6.4	Horizontal Slice Method (HSM).....	37
6.4.1	Assumptions	37
6.4.2	Formulation	38
7	Shaking Table Experiments at RMC: Pseudo-Static Analysis.....	41
7.1	Pseudo-Static Coefficient	41
7.2	Material Parameters.....	42
7.3	Failure Surface.....	42
7.4	Earth Forces on the Retaining Wall.....	46
7.5	Comments and Discussions.....	47
7.6	Summary of the Pseudo-Static Analysis of the Shaking Table Experiments at RMC	48
8	Pseudo-static Analysis: Different Guidelines.....	49
8.1	Guidelines for the Horizontal Pseudo-Static Coefficient.....	49
8.1.1	Eurocode 8.....	49

8.1.2	FHWA(2001)/AASHTO(2002).....	49
8.1.3	PIANC (2001)	49
8.2	Predictions using EC8, PIANC (2001) and FHWA(2001)/AASHTO(2002)	50
8.2.1	Assumptions and Limitations	50
8.2.2	Failure Surface	50
8.2.3	Earth Forces.....	52
8.2.4	Observations.....	53
8.3	Predictions using ABC-coefficient.....	53
8.3.1	Failure Surface	53
8.3.2	Earth Forces.....	55
8.4	Comments and Discussions	55
8.5	Summary of the Pseudo-Static Analysis using Different Guidelines	56
9	Summary and Conclusions	57
9.1	Limitations	57
9.2	Conclusions.....	58
9.3	Possible Future Work	59
10	References.....	61
Appendix 1 – Reinforcement connection loads		67
	Effect of reinforcement stiffness.....	67
	Effect of reinforcement length.....	68
Appendix 2 – Pseudo-static methods – MATLAB code		69
	Mononobe-Okabe method.....	69
	Two-part wedge method.....	71
	Horizontal slices method - Linear and polylinear.....	75
Appendix 3 – Horizontal Pseudo-static Coefficients from Current Seismic Design Codes.....		79
Appendix 4 – Effect of changing A, B and C.....		81

List of Figures

Figure 2.1 Reinforced soil retaining wall illustration.....	5
Figure 2.2 Acceleration time series, velocity shift and displacement drift	8
Figure 3.1 Reduced-scale shaking table model (El-Emam, 2003).....	9
Figure 3.2 General cross section (El-Emam & Bathurst, 2005)	10
Figure 3.3 Base acceleration input time series (El-Emam & Bathurst, 2004)	12
Figure 3.4 Base acceleration input for the first second	12
Figure 4.1 Illustration of the PLAXIS model.....	14
Figure 4.2 Base velocity input for the first 7 seconds	15
Figure 4.3 Fourier amplitude spectrum for the lateral displacements at the top of the model wall during the free vibration	18
Figure 4.4 Numerical and measured time histories for horizontal displacements at the top of facing panel.....	18
Figure 4.5 Numerical and observed soil failure zone surfaces.....	21
Figure 4.6 Total earth force (P_{AE}), measured and numerically predicted (El-Emam, 2003).....	22
Figure 5.1 Change in failure surface: Effect of reinforcement stiffness.....	26
Figure 5.2 Change in failure surface: Effect of reinforcement length	27
Figure 5.3 Top facing lateral displacements: Effect of reinforcement stiffness.....	28
Figure 5.4 Top facing lateral displacements: Effect of reinforcement length.....	29
Figure 5.5 Total reinforcement connection loads	30
Figure 6.1 Mononobe-Okabe Method (Kramer, 1996)	35
Figure 6.2 The two-part wedge method (Shukla, et al., 2002)	37
Figure 6.3 Horizontal slices method a) general b) one slice (Shahgholi, et al., 2001).....	38
Figure 6.4 Polylinear and linear failure surfaces (Ahmad & Choudhury, 2008).....	40
Figure 7.1 Outward soil amplification factor at backfill surface (El-Emam & Bathurst, 2004)	41
Figure 7.2 Observed and calculated failure surface geometry (El-Emam, 2003).....	45
Figure 7.3 Total active earth force on the back of the facing.	46
Figure 8.1 Predicted failure surfaces using M-O and Eurocode 8,	51
Figure 8.2 Predicted active earth forces using Eurocode, PIANC and FHWA/AASHTO (El-Emam, 2003)	52
Figure 8.3 Failure surface predicted using k_h^{ABC-MO}	54
Figure 8.4 Active earth forces calculated using k_h^{ABC-MO}	55

List of Tables

Table 3.1 Soil properties.....	10
Table 3.2 Reinforcement properties	11
Table 4.1 PLAXIS Model Material Properties	17
Table 6.1 Dynamic pressures and displacements on retaining walls – Various calculation methods ..	33
Table 6.2 Recommended horizontal seismic coefficients (Melo & Sharma, 2004)	34
Table 7.1 Horizontal pseudo-static coefficient.....	42
Table 7.2 Material parameters in the pseudo-static studies	42
Table 7.3 Safety factors used for the two-part wedge calculations.....	42
Table 8.1 Factor for calculation of the horizontal seismic coefficient according to the Eurocode.....	49

List of Notation and Symbols

Symbol	Explanation
$a(t)$	Time dependent acceleration
a_0	Acceleration amplitude (Displacement drift)
a_b	Amplitude of the input base acceleration in the shaking-table tests
a_{h_v}, a_v	Pseudo-static horizontal and vertical accelerations (Mononobe-Okabe method)
a_k	Amplitude of harmonic function (Spectral density)
a_g	Design ground acceleration on type A ground (Eurocode 8)
AF	Soil amplification factor
b_i	Width of slice base (Horizontal slices method)
b_k	Amplitude of harmonic function (Spectral density)
c_k	Amplitude of harmonic function (Spectral density)
c	Cohesion
C	Damping matrix (Rayleigh damping)
EA	Reinforcement axial stiffness
FS	Factor of safety
g	Gravity constant
G	Shear modulus
h_i	Thickness of slice I (Horizontal slices method)
H	Height of retaining wall
H_i	Horizontal interslice force (Horizontal slices method)
HMS	Horizontal method of slices
k_h, k_v	Dimensionless horizontal and vertical pseudo-static (seismic) coefficients
k_h^{ABC-MO}	Horizontal seismic coefficient (ABC method)
k_h^{EC}	Horizontal seismic coefficient (Eurocode 8)
k_h^{FHWA}	Horizontal seismic coefficient (FHWA(2001)/AASHTO(2002))
k_h^{spes}	Pseudo-static coefficient (based on data from these specific model test)
k_h^{PIANC}	Horizontal seismic coefficient (PIANC (2001))
K	Stiffness matrix (Rayleigh damping)
K_{AE}, K_{PE}	The dynamic active and passive earth pressure coefficient
L	Reinforcement length
L_c	Maximum distance between the fail surface and the face of the slope (Horizontal slices method)
l_i	Length of the top horizontal border of slice i (Horizontal slices method)
m_i	the mass of the i th slice (Horizontal slices method)
M	Mass matrix (Rayleigh damping)
M-O	Mononobe- Okabe method
n	Number of slices (Horizontal slices method)
N_i	Normal force upon base of slice (Horizontal slices method))
P_A, P_P	Static component of the active and passive thrust
$\Delta P_A, \Delta P_P$	Dynamic component of the active and passive thrust
P_{AE}, P_{PE}	Total active and passive thrust
P_1	Horizontal force acting on the 2 nd wedge from the 1 st (Two-part wedge method)
q_{hi}, q_{vi}	Inertia forces in the horizontal and vertical direction for the i th slice (Horizontal slices method)
R_{inter}	Interface strength reduction (PLAXIS)
S_i	Shear force upon base of slice (Horizontal slices method)

Symbol	Explanation
S_x	One sided spectral density
t	Time
t_j	Tensile force of the reinforcements, layer j (Horizontal slices method)
T	Period of seismic shaking (Horizontal slices method)
TPW	Two-part wedge method
$u(t)$	Time dependent displacement
$v(t)$	Time dependent velocity
V_i	Vertical interslice force (Horizontal slices method)
V_1	Shear force acting on the 2 nd wedge from the 1 st (Two-part wedge method)
V_p	Primary wave velocity
W_i	Weight of slice (Horizontal slices method)
W_1, W_2	Weight of 1 st and 2 nd wedge (Two-part wedge method)
z	depth below the surface (Horizontal slices method)
α	Ratio of the design ground acceleration on type A ground, a_g , to the acceleration on gravity g (Eurocode 8)
α_{base}	linear failure surface angle (Horizontal slices method)
α_r	Rayleigh damping coefficient
α_i	Inclination angle of the base of the slice (Horizontal slices method)
α_{AE}	Critical failure surface for active and passive pressure conditions (Mononobe-Okabe method)
β	The inclination angle of the slope
β_r	Rayleigh damping coefficient
φ	Internal friction angle of soil
φ_f	$= \tan^{-1}(\tan \varphi/FS)$ (Two-part wedge method)
$\varphi_{residual}$	Residual value of internal friction angle of soil (physical shaking table model)
φ_{peak}	Peak value of internal friction angle (physical shaking table model)
θ_1, θ_2	Angle of the failure surface, 1 st and 2 nd wedge (Two-part wedge method)
γ	Unit weight of soil
γ_d	The dry density of the soil
γ'	Effective soil unit weight
λ	Inter-wedge shear mobilization ratio (Two-part wedge method)
τ_r	Required shear resistance (Horizontal slices method)
τ_f	Available shear resistance (Horizontal slices method)
ξ	Damping ratio
ψ	Dilation angle

1 Introduction

Earth retaining structures are common to many projects. Their main function is to resist lateral earth forces, both under static and earthquake loading. Geo-synthetically reinforced soil wall is a retaining structure that has become popular in the last decades, partly due to their cost effectiveness compared to conventional gravity retaining walls, and partly because they have performed well during recent earthquakes (McCarthy p.613, 1998; El-Emam p. 1-2, 2003).

The potential human and economic loss due to structural collapses during earthquakes is significant and the need for reliable and effective design guidelines is therefore crucial (Kramer, 1996). A number of devastating earthquakes occur each year all around the world. Even in Norway, where seismic activity is relatively low, there are requirements for seismic design. Until recently, seismic design of structures in Norway has been mainly considered for offshore structures, but the implementation of Eurocodes in 2010 has generated a need for Norwegian engineers to improve their knowledge about earthquake resistant design also for onshore structures (NORSAR Engineering, 2011).

This study describes a numerical model created in the finite element program PLAXIS 2D Dynamics with the intention of optimum design of geo-synthetics layout. In addition, the technical computing language MATLAB was used to develop programs for studying the accuracy of pseudo-static methods, and for developing a more suitable coefficient for use in the Mononobe-Okabe method.

1.1 Choice of Subject

The subject of numerical and analytical analysis of geo-synthetically reinforced soil wall model, subjected to dynamic loading, was suggested by Professor Amir M. Kaynia at the Norwegian Geotechnical Institute (NGI). Problem definition and research method was worked out in consultation with Professor Kaynia.

This study was tailored to the author's academic interests and to the notion that Norwegian engineers need to improve their knowledge related to seismic design. An important focus has been to understand the limitations by using PLAXIS 2D with respect to dynamic analysis. It has also been a focus on studying the pseudo-static methods and understanding their limitations.

1.2 Problem Definition

Geo-synthetics are planar products manufactured from polymeric materials (the synthetic) used with soil, rock, or other geotechnical- related material (the geo) as part of a civil engineering project or system. They are in some cases used to construct stable slopes at much steeper angles than would otherwise be possible.

Traditionally, the seismic design of reinforced soil walls is based on classical failure mechanics and limit equilibrium (analytical) approaches. There are a variety of analytical approaches, but the pseudo-static methods are most common. Recently, the use of numerical solutions, such as finite elements, has become more frequent following the development of special elements.

Two topics were identified as relevant for this study:

- The effect of key reinforcement parameters, since “relatively few studies have investigated the effect of key reinforcement parameters on the response of reinforced soil walls” (El-Emam & Bathurst, 2007).
- According to El-Emam & Bathurst (2004); “few pseudo-static methods have been verified using physical tests” and their accuracy is therefore not well documented. Different codes also give different suggestions for using these methods; the differences between them are thus also relevant.

1.3 Objective

Based on the topics identified above the following objectives were identified:

- The ultimate objective of this study is to create a numerical model and verify it by using physical test results.
- Study key reinforcement parameters and their role on the retaining wall performance under dynamic loading.
- Use physical model to investigate the accuracy of different pseudo-static methods.
- Study differences in seismic design codes with respect to the suggested pseudo-static coefficients, the Mononobe-Okabe method and their accuracy compared to physical results.
- On this basis, find a more suitable guideline for selecting the pseudo-static coefficient for the Mononobe-Okabe method.

1.4 Research Methodology

The current study contains two quite distinct parts; one numerical study and one analytical based on pseudo-static solutions. Thus to achieve the various objectives, the work was divided in to the following tasks:

- Literature review on general dynamic response of retaining walls. In this part the objective is to find a relevant case against which the numerical models (see later points) can be calibrated. These include:
 - Experimental studies
 - Empirical solutions
 - Numerical analysis
- Numerical modelling of the case history/model test identified in the literature review on general dynamic response of retaining walls, and verification of model by use of case data.
- Study of the effect of key reinforcement parameters using the developed numerical model.
- Literature review of analytical methods used for analysing retaining walls with focus on pseudo-static methods.
- Study of existing pseudo-static methods accuracy by use of literature data.
- Study of differences in current guidelines for pseudo-static methods and suggest improvements

1.5 Thesis Organisation

The following three chapters (2-5) are mainly concerned with topics related to the numerical study. Chapter 2 presents background material on retaining walls in general, and theory used in connection with the numerical simulations. The result of a literary review on general dynamic response is presented in Chapter 3. Here, a small-scale shaking table model experiment conducted in Canada is

presented. This forms the basis for development of a numerical model, which is described in Chapter 4. Relevant information about the numerical model's geometry, loading and material parameters are given before it is compared to the physical shaking table model. Chapter 5 presents a numerical study of the influence of the strength and length of reinforcement on the failure surface, wall displacements and reinforcement loads.

The next three chapters (6 -8) are concerned with topics related to pseudo-static methods of calculating the seismic pressures on retaining walls. The result of a review of analytical methods used to analyse retaining walls is presented in Chapter 6. First, a general summary of different analytical methods is presented before three pseudo-static methods (the Mononobe-Okabe, horizontal slices and two-part wedge method) are investigated further. Chapter 7 presents a study to determine the suitability of these methods for calculating the failure surface geometry and total earth force on the back of the facing panel of the shaking table model presented in Chapter 3. In Chapter 8, firstly, a short presentation of different design guidelines for calculating the failure surface using the Mononobe-Okabe method is given. This is followed by a comparison of these codes, before a suggestion for improving the selection of the pseudo-static coefficient is presented. All results are discussed in the individual chapters, but a summary of the most important findings is given in Chapter 9 together with a presentation of the limitations in this study and proposals for further work.

1.6 Previous Work

A major background for the research presented in this study is the PhD thesis by El-Emam (2003) and articles related to it (El-Emam & Bathurst, 2004; El-Emam & Bathurst, 2005; El-Emam & Bathurst, 2007; Zarnani, et al., 2011). It should be noted that the influence of reinforcement parameters in design of earth retaining walls has been investigated using numerical modelling (Bathurst & Hatami, 1998) and by small-scale shaking table models (El-Emam & Bathurst, 2007). Furthermore, numerical and analytical analyses for reinforced soil walls have been carried out by Zarnani et al. (2011). Details and lessons from this work are compared to the findings in this thesis where relevant.

2 Background Material

This chapter gives a short description of retaining walls in general and focuses on giving the reader a basic understanding of terms used later. Subsequently, theory relevant for the development of the numerical model (Chapter 4) is presented.

2.1 Reinforced Soil Walls

There are different types of retaining walls (e.g. gravity, cantilever and tieback walls) and they are used to secure embankments against sliding, or as key elements of harbours. Tall retaining walls are often constructed as what is called *reinforced soil retaining walls* (Figure 2.1). This type of retaining wall consists of a facing with a reinforced soil zone behind it (Kramer, 1996). Traditionally, the reinforcements consisted of thin steel elements, today the use of geo-grids are becoming more common. A geo-grid is a geo-synthetic and is a regular network of tensile elements with apertures of sufficient size to interlock with surrounding fill material.

During an earthquake, the retaining wall is subjected to inertial forces due to the backfill inertia. Reinforced soil walls must be designed to withstand the static lateral earth pressure, in addition to additional forces that are introduced in case of an earthquake (Kramer, 1996).

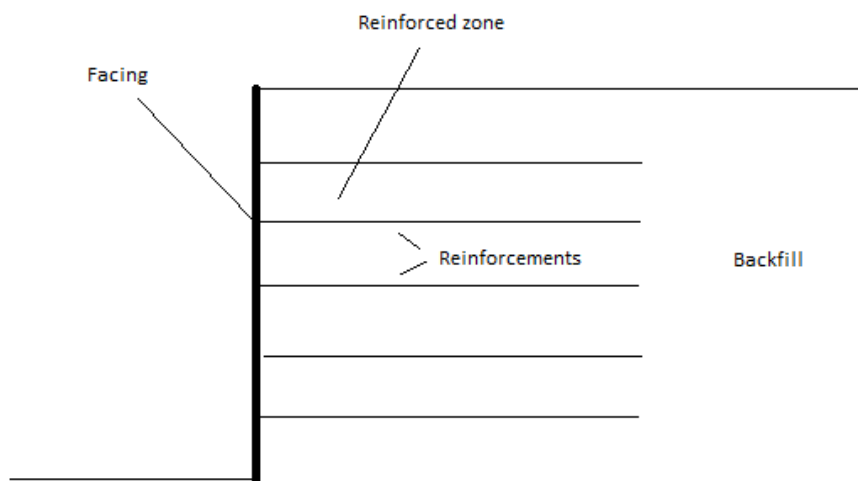


Figure 2.1 Reinforced soil retaining wall illustration

2.2 Fast Fourier Transformation and Spectral Density

As defined in Strømmen (2010); “the auto spectral density contains the frequency domain properties of the process, i.e. it is the frequency domain counterpart to the concept of variance”. The spectral density of a displacement measurement (e.g. for a tower subjected to wind loading) contains information about the distribution of displacements with frequency. There are different ways of determining spectral density, one way is to use a Fourier transforms. The discrete Fourier transform is often used to convert a time series from time domain to frequency domain. A plot of frequencies against the spectral densities of amplitudes, found by using a Fourier transform is called a Fourier amplitude spectrum.

For transforming of a continuous time series, $x(t)$, from the time domain to the frequency domain, the Fourier transform is:

$$X(\omega) = \int_{-\infty}^{\infty} x(t)e^{-ti\omega} dt \quad (2.1)$$

Where t is time and ω is the angular frequency.

By using discrete Fourier transformation one may approximate $x(t)$ as a sum of harmonic components, $X_k(\omega_k, t)$, where $k=0,1,\dots,N-1$. According to Strømmen (2010) the one sided spectral density, $S_x(\omega_k)$ is given by:

$$S_x(\omega_k) = \frac{c_k^2}{\Delta\omega} \quad (2.2)$$

Where

$$c_k = \sqrt{a_k^2 + b_k^2} \quad (2.3)$$

$$\begin{bmatrix} a_k \\ b_k \end{bmatrix} = \frac{2}{T} \int_0^T x(t) \begin{bmatrix} \cos(\omega_k t) \\ \sin(\omega_k t) \end{bmatrix} dt \quad (2.4)$$

There have been developed numerous programs for calculating the spectral densities, e.g. Holst (2011) presents a simple program developed using MATLAB (The Mathworks, Inc., 2011).

2.3 Hardening Soil Model in Dynamic Analysis

When modelling the behaviour of a soil body, it is essential to consider the inertia of the soil, the time dependence of the loading and damping. In principle all the soil models in PLAXIS are able to account for these effects, but it should be noted that these models are not developed specifically for dynamic analysis. Thus, all these models have significant limitations when used in dynamic modelling (Plaxis bv, 2010).

The HS model was initially developed for use on sand but can also be used for other soil types. It is an advanced soil model based on the theory of hardening plasticity. Compared to, for example Mohr-Coulomb, the HS model describes soil stiffness more accurately by using three input stiffness' from loading/unloading triaxial and oedometer loading (E_{50} , E_{ur} and E_{oed} respectively). Another advantage of the HS model is that the yield surface can expand due to plastic straining. (Nordal, 2011; Auleda, 2011).

Although the HS model is an advanced model, there are limitations for what it is able to model. For example; it does not account for softening due to soil dilatancy and de-bounding effects and it does not model hysteretic and cyclic loading. Another shortcoming of the HS model is increased calculation time, although it is not as high as for example for the Hardening Soil model with small-strain stiffness. Furthermore, the soil models in PLAXIS do not include viscosity in the material

damping term, instead Rayleigh damping is used to account for this (Plaxis bv, 2010; Plaxis, 2011). Further details regarding the Hardening Soil model can be found in Schans et. al. (1999).

2.4 Rayleigh Damping

As explained by Liu & Gorman (1995), the Rayleigh damping assumes that the damping matrix (**C**) is proportional to the mass (**M**) and stiffness (**K**) matrices, thus

$$\mathbf{C} = \alpha_r \mathbf{M} + \beta_r \mathbf{K} \quad (2.5)$$

From this a relationship between the damping ratio (ξ), the angular frequency (ω) and the two Rayleigh damping coefficients (α_r and β_r) can be established:

$$\alpha_r + \beta_r \omega^2 = 2\omega\xi \quad (2.6)$$

By selecting two frequencies (1 and 2) and corresponding damping ratios equation (2.6) can be solved by

$$\alpha = 2\omega_1\omega_2 \frac{\omega_1\xi_2 - \omega_2\xi_1}{\omega_1^2 - \omega_2^2} \quad (2.7)$$

$$\beta = 2 \frac{\omega_1\xi_1 - \omega_2\xi_2}{\omega_1^2 - \omega_2^2} \quad (2.8)$$

2.5 Displacement Drift

For a numerical simulation of a shaking table experiment, one often wishes to use a zero initial velocity and displacement condition. In a finite element model this introduces a shift in the velocity term and this causes a drift in the displacement term due to the integration procedure. Madabhushi (1990) presents the effect of the initial velocity and displacement conditions on the numerical integrations in detail. The following gives a short introduction to the problem.

Starting with a simple sinusoidal acceleration we obtain the velocity and displacement by integration

$$a(t) = a_0 \sin(\omega t) \quad (2.9)$$

$$v(t) = -\frac{a_0}{\omega} \cos(\omega t) + C_1 \quad (2.10)$$

$$u(t) = -\frac{a_0}{\omega^2} \sin(\omega t) + C_1 t + C_2 \quad (2.11)$$

Where $a(t)$, $v(t)$ and $u(t)$ is the time-dependent acceleration, velocity and displacement respectively. C_1 and C_2 are integration constants, a_0 the acceleration amplitude, t is time and ω the angular frequency.

When using the initial condition $v(t=0)=0$ and $u(t=0)=0$ the velocity and displacement becomes

$$v(t) = -\frac{a_0}{\omega} \cos(\omega t) + \frac{a_0}{\omega} \quad (2.12)$$

$$u(t) = -\frac{a_0}{\omega^2} \sin(\omega t) + \frac{a_0}{\omega} t \quad (2.13)$$

In Figure 2.2 the acceleration, velocity and displacement-time series for the above equations are illustrated using an angular frequency of 2π (corresponding to a frequency of 1 Hz) and acceleration amplitude of 1m/s^2 . From the figure, drift in displacement is observed. This has an impact on how the excitation is applied to numerical model and is discussed further in the presentation of the numerical model.

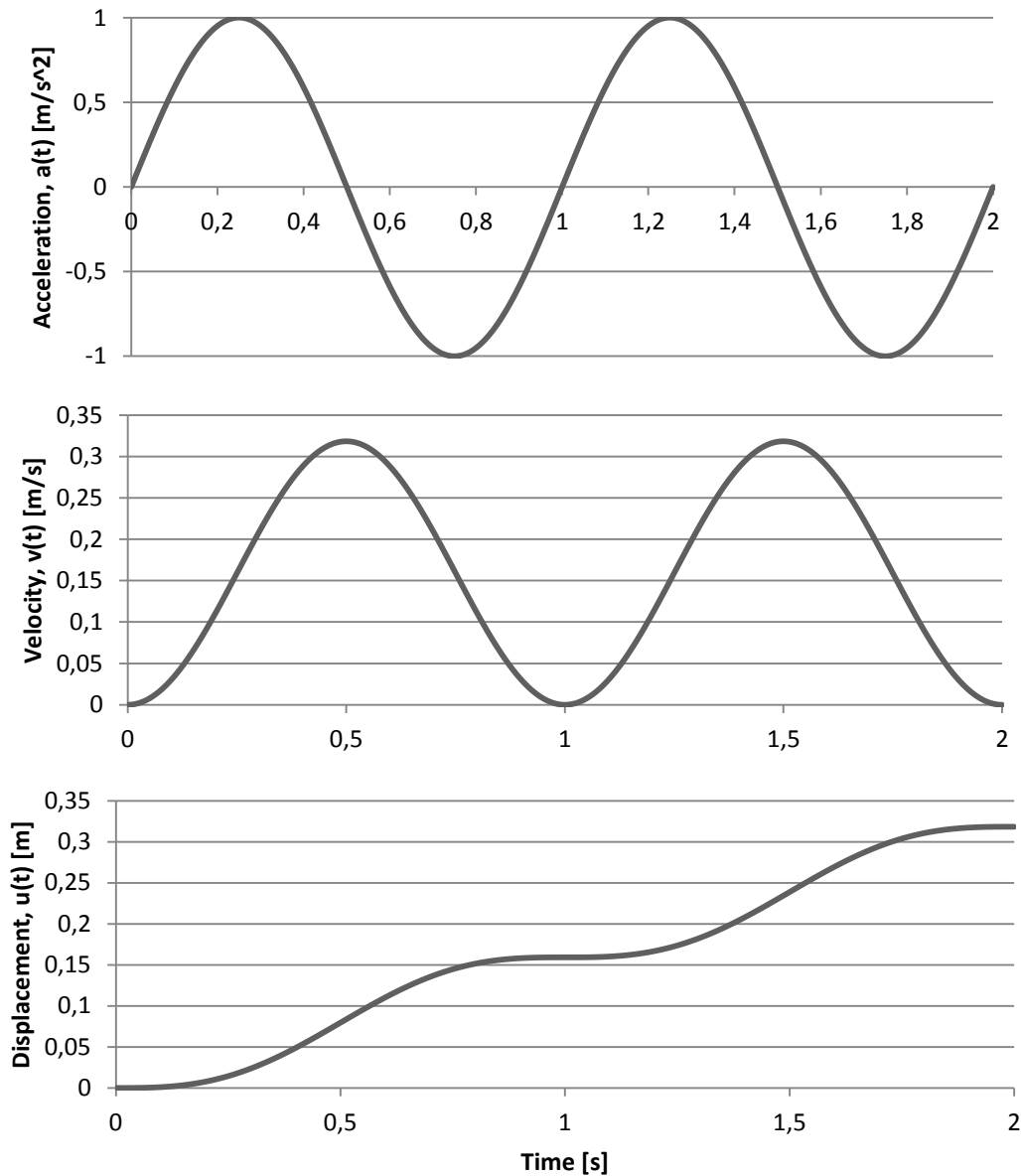


Figure 2.2 Acceleration time series, velocity shift and displacement drift

3 Shaking Table Experiments at RMC: Background

A number of dynamic shaking table experiments performed around 2004 at the Royal Military College of Canada (RMC). This chapter gives an introduction to relevant aspects of these experiments that are relevant for the investigations in this thesis. It should be noted that all the information presented in this chapter is based on the PhD thesis by El-Emam (2003) and its related articles, see section 1.6.

3.1 General

The main goal of the investigations at RMC is to use the results from the scale model shaking table tests to refine analytical models and develop guidelines for numerical modelling of reinforced soil walls. To achieve this El-Emam and Banthurst investigated the effects of different toe boundary conditions, facing panel configurations and reinforcement layouts.

Fourteen 1/6-scale models with different properties were investigated. The models were all excited by the same horizontal sinusoidal vibration at the base and the amplitude was increased in steps until failure. A rigid strong box (1.4m wide by 2.7 m long) with a rigid back wall was used to confine the models. Although El-Emam (2003) contains information on many different shaking table models only one of these is used as basis for this study. The reason is the limited data about relevant measurements (e.g. regarding the failure surface) on the other models.

3.2 Geometry

The model is referred to as “Wall 1” in El-Emam (2003), an illustration of it is shown in Figure 3.1. It was constructed using a hinged-type toe boundary condition (which means that it can rotate but not move in the vertical or horizontal direction) and a vertical facing with a thickness of 76 mm. The vertical spacing of the reinforcement layers is 185 mm.

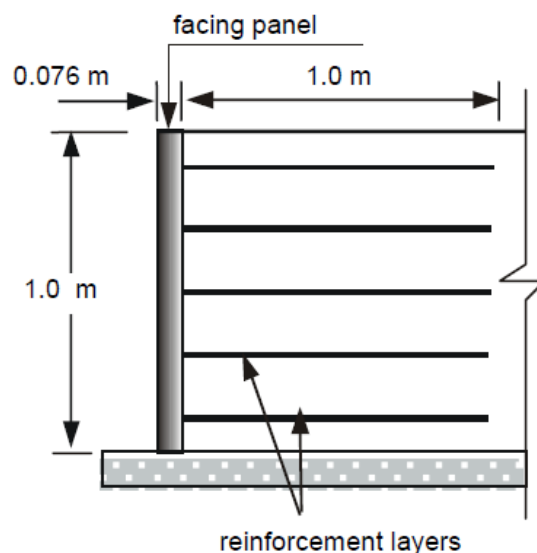


Figure 3.1 Reduced-scale shaking table model (El-Emam, 2003)

In

Figure 3.2 we see a typical cross section of a model from the shaking table tests at RMC and it shows where the different measurements of strains and displacements are conducted (note that this setup

is not identical to the one used in the relevant model). In this study, results from the extensometers are used in both the numerical and analytical parts. The extensometers consisted of a 1 mm-diameter lightly pre-tensioned steel wire encircled by a stiff plastic tube. The measurements were made by a linear potentiometer.

Plywood was placed between the rigid back wall and base to allow for the placement of measuring instruments. The layer between the plywood and the sand was glued to achieve the necessary friction. Steps were also taken to reduce the friction of the model against the side wall and to make sure that the predicted internal failure surface did not intersect the back wall.

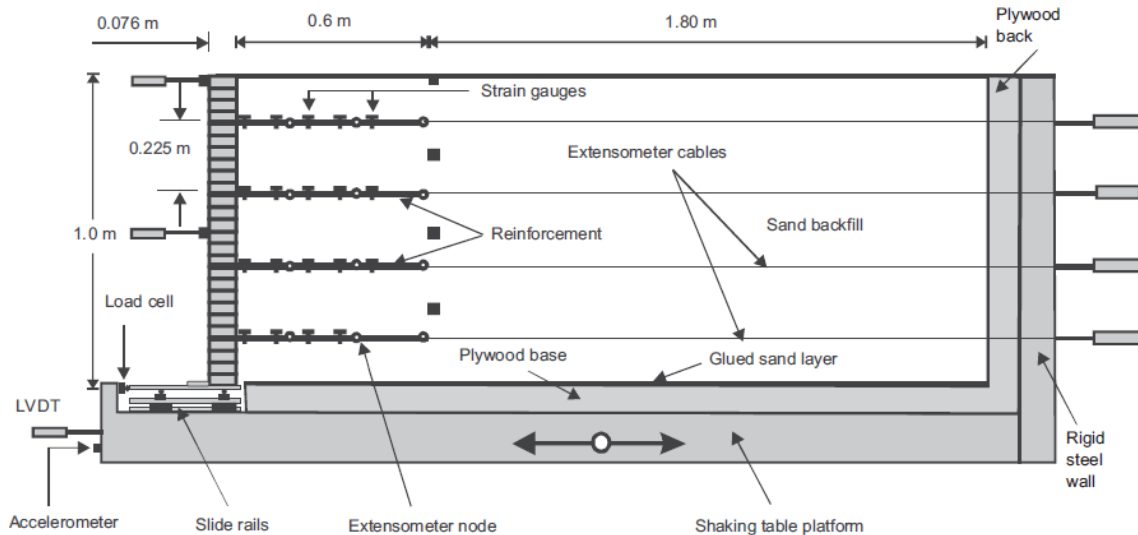


Figure 3.2 General cross section (El-Emam & Bathurst, 2005)

3.3 Soil Properties

Table 3.1 presents the most important properties for the soil used in the shaking table tests. A direct shear test was used by El-Emam (2003) to find the friction angle, dilation angle and cohesion.

Table 3.1 Soil properties

Soil property	Value
Peak friction angle, $\phi_{\text{peak,ds}}$	51°
Residual friction angle, $\phi_{\text{residual,ds}}$	46°
Dilation angle, ψ	15°
Cohesion, c	0
Unit weight, γ	15,7kN/m ³

3.4 Reinforcement and Facing

The reinforcement in the models consisted of a polyester rigid with openings of 21mm by 25mm. The properties of this geo-grid are given in Table 3.2. Figure 3.1 illustrates the number for reinforcements and how they are placed.

A 76 mm thick, full height facing was used in these tests and it was designed to be perfectly stiff. The facing panel was constructed using hollow steel sections which were bolted together using steel rods

with a diameter of 25 mm. Connections between the reinforcements and the facing panel were designed to be perfectly rigid.

Table 3.2 Reinforcement properties

Reinforcement properties from wide-width strip tensile tests	Value
Axial stiffness, J	90 kN/m
Yield strength, T_y	13 kN/m
Compressive strength, T_c	0 kN/m
Thickness, t	0,002m

3.5 Natural Frequency and Base Excitation

Walls of height lower than 10 meters are dominated by their fundamental frequency (Hatami & Bathurst, 2000). El-Emam & Bathurst (2004) showed that the natural frequencies of the models were much higher than the frequency of the input motion. Therefore it is reasonable to assume that a resonance state did not occur to disrupt the physical test results.

Frequencies of 2 to 3 Hz are suitable to represent most of the frequencies of typical design earthquakes in North America (Bathurst & Hatami, 1998). According to lai (1989) a frequency of 5-7Hz should be used for representing such design earthquakes in a 1/6 scale model. El-Emam (2003) used a frequency of 5 Hz in their shaking table tests. In Figure 3.3 and Figure 3.4 the base input acceleration against time in the shaking table tests are shown.

3.6 Failure Surface

In the following, the failure surface of this shaking table model is widely referred to (both in the numerical and analytical part). Both the terms *predicted failure surface* and *observed failure surface* are used. To avoid confusion, please note that: The *predicted failure surface* refers to the failure geometry interpreted from extensometer readings at different input base accelerations (factor of safety > 1). The *observed failure surface* is the failure surface geometry at actual failure (factor of safety = 1). In this study the failure surface when FS=1 is referred to as the *ultimate failure surface*.

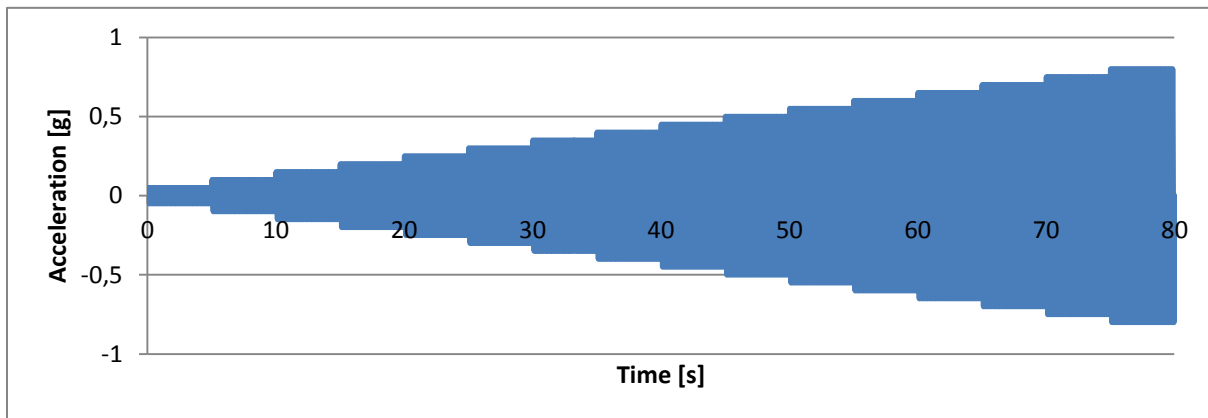


Figure 3.3 Base acceleration input time series (El-Emam & Bathurst, 2004)

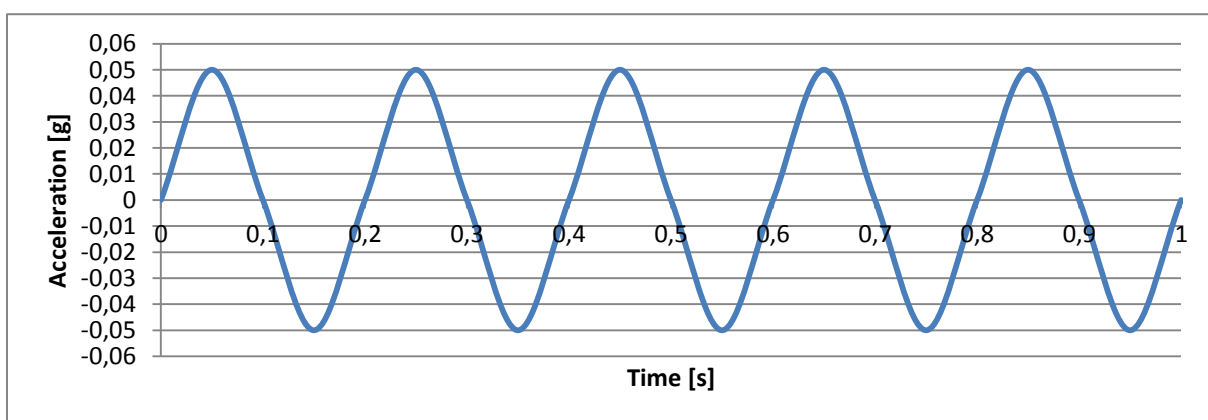


Figure 3.4 Base acceleration input for the first second

4 Shaking Table Experiments at RMC: Numerical Modelling

This chapter described the development of a numerical model using the finite element program PLAXIS 2D Dynamics (Plaxis bv, 2011) for the reduced-scale shaking table model described above. The aim of the following is to develop a model to be used in a parametric study by verifying it using results from the physical model.

El-Emam (2003) created a similar model using FLAC (Itasca Consultion Group, 2001) which is presented in Zarnani et al. (2011). Zarnani et al. (2011) is used as a basis and as inspiration for creating the numerical model in this study.

4.1 PLAXIS 2D Dynamics

PLAXIS 2D is a finite element program used for two-dimensional analysis in the geotechnical field. PLAXIS Dynamics is an addition to this program and makes it possible to perform dynamic analyses (Plaxis bv, 2011). PLAXIS was chosen for the numerical investigations in this study because of:

- It's ability to simulate the soil behaviour in both static and dynamic conditions.
- Its ability to create illustrations and videos of the soil behaviour during dynamic excitation (i.e. before the calculations are complete), making it simple to locate irregularities in the model without having to finish time-consuming analyses.
- Its advanced soil models.

4.2 Model Properties

4.2.1 Geometry

The facing panel, soil and back wall were all modelled using 15-node triangular elements. Reinforcements were modelled using flexible elastic elements (geo-grid elements (Plaxis bv, 2011)) and these were rigidly attached to the facing. The back wall was modelled as rigid and without mass.

The soil placement was modelled using five construction phases. Displacements were set to zero between each phase. After the soil construction, the entire base of the models was subjected to a velocity-time record obtained from the base acceleration-time record used in the physical test. I.e. the acceleration is not applied directly since this would create a drift in the displacement term as explained in the background material (section 2.5).

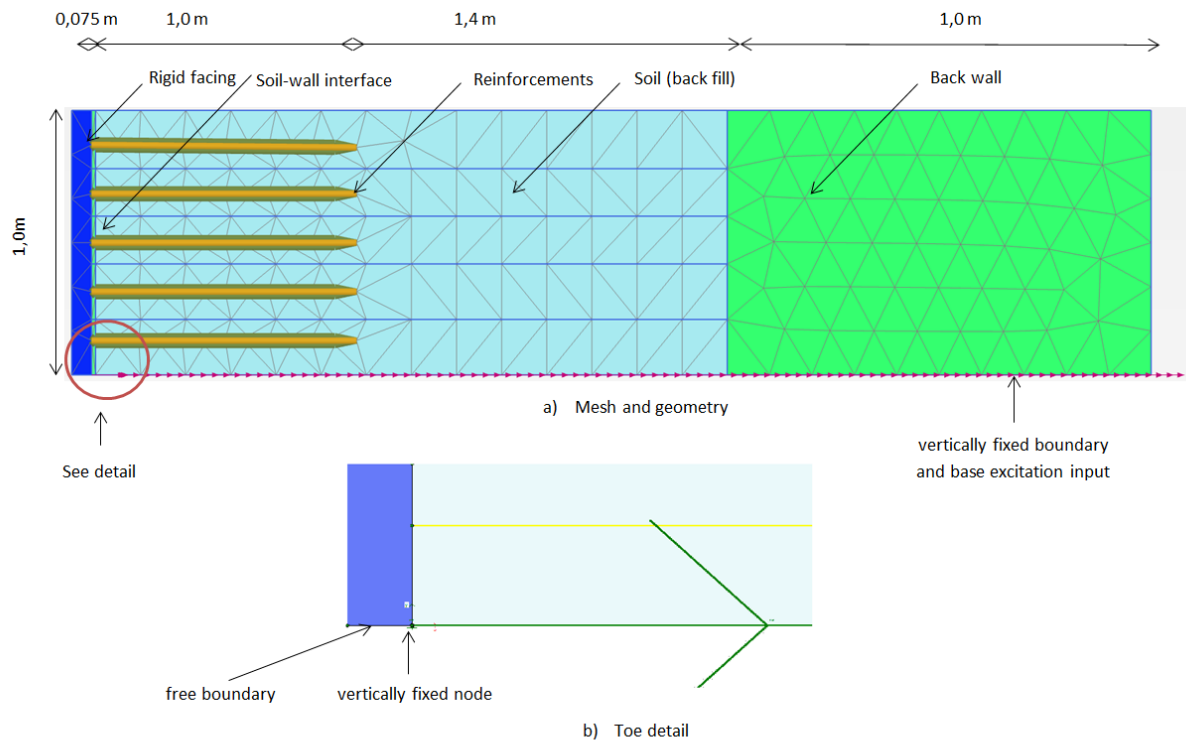


Figure 4.1 Illustration of the PLAXIS model
a) Mesh and Geometry b) toe detail

4.2.2 Excitation

Base input excitation, similar to what's illustrated in Figure 3.3 (5 Hz with increasing amplitude), was used in the numerical simulations, but modifications were made to avoid displacement drift; a "soft start" input series was applied. This insured the use of the correct initial condition (zero initial acceleration, velocity and displacement). The soft start equation (eq. 5.1) was selected based on a series of preliminary numerical analyses to reduce the acceleration-time output error to an acceptable level.

$$v(t) = -(1 - e^{-3t}) \frac{a_0}{\omega} \cos(\omega t) \quad (5.1)$$

Where a_0 is the amplitude in the original acceleration time series, see Figure 3.3. A velocity series was chosen since this gave suitable values also for acceleration and displacement input.

A "soft transition" curve was applied in the transitions where the velocity amplitude increased due to an increase in the acceleration amplitude. The applied velocity-time curve is partly shown in Figure 4.2.

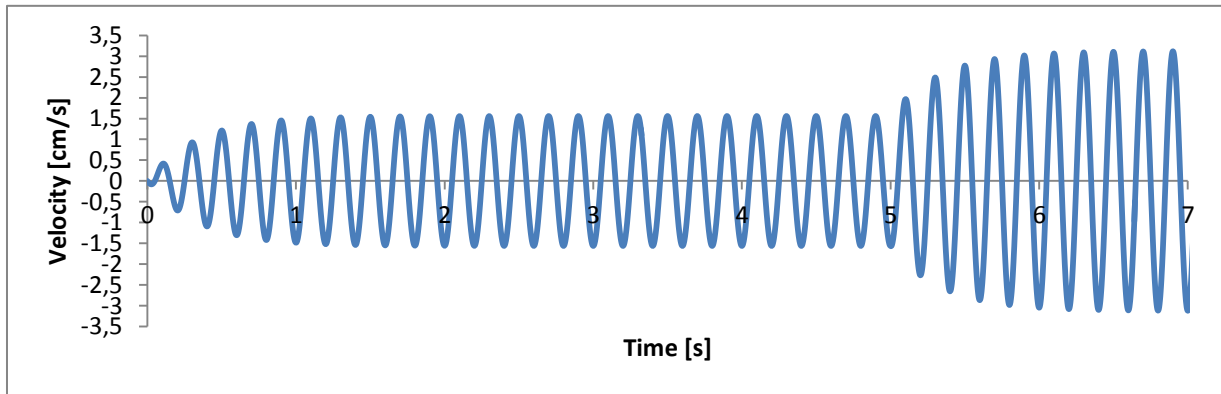


Figure 4.2 Base velocity input for the first 7 seconds

4.2.3 Mesh and Time Step

The dominating frequency in the current study was 5 Hz. According to Kanade & Gakki (1997) the minimum element height (Δh) should be less than one fourth of the minimum wave length ($\lambda_{min}/4$) where

$$\lambda_{min} = \frac{V_{s\ min}}{f_{max}} \quad (5.2)$$

where $V_{s\ min}$ is the minimum shear wave velocity and f_{max} is the maximum frequency. When finding the suitable element height, f_{max} was assumed to be 5Hz.

The time step (Δt) is a function of element height, material shear velocity and material pressure velocity (V_p). According to Kanade & Gakki (1997) this should be

$$\Delta t < \frac{0,8\Delta h}{\sqrt{V_p^2 + V_s^2}} \quad (5.3)$$

The number of steps and mesh size were selected so as to obtain satisfactory accuracy in the numerical integrations. I.e., the number of “dynamic sub steps” was set to 8, the number of “additional steps” to 10000 (for the 80 second time series) and a “fine mesh” was selected (414 soil elements and 3951 nodes).

4.2.4 Loads and Boundary Conditions

A standard absorbent boundary (Plaxis bv, 2011) was applied to the back wall (far right boundary) to absorb the increments of stress on the boundaries due to the dynamic loading. Simulations without this boundary condition showed only minor changes in the results. This is believed to be due to the stiff material parameters of the back wall that effectively reflect the shear and pressure waves.

The hinged toe boundary was modelled using a free boundary on the side and bottom of the facing elements, see Figure 4.1b. At the base a vertical fixity and dynamic load system consisting of prescribed displacements was applied on the entire length of the model, except from on the facing elements.

4.2.5 Material Models and Material Properties

A numerical model can give a good understanding of the soil stress and strain behaviour and other interesting characteristics, but in order to achieve this, the material parameters must be able to correctly represent the soil behaviour. Due to limited information on the material used, it has not been possible to conduct independent laboratory experiments for finding these parameters. Instead, data compiled for use in the FLAC model (Zarnani et al., 2011) has been adopted for use in PLAXIS and used as a basis for the material parameters in this study.

Transferring material parameters from FLAC to PLAXIS was not “a straight forward procedure”, so more suitable values have been found by trial starting with the parameters presented in Zarnani et al. (2011) and following different advices in the PLAXIS Tutorials and adjusting the parameters to these. Table 4.1 summarises the material parameters and material models used for the different components in the numerical models created in PLAXIS.

4.2.5.1 Facing and Back Wall Properties

The facing and back wall was modelled using a linear-elastic material model (L E model) and stiffness parameters were selected to insure rigid behaviour, which the values found in Zarnani et al. (2011) did. Zarnani et al. (2011) found that too high values of the shear and bulk modulus could create numerical instability, this did not prove a problem in the current model. The weight of the facing was found in El-Emam & Bathurst (2004) and the weight of the back wall was neglected.

4.2.5.2 Backfill

The sand was modelled as a cohesion less material and drained conditions was assumed due to the use of dry sand in the physical experiments. In PLAXIS (2011) “it is advised to use the Mohr-Coulomb model (M-C model) for a first analysis of the problem and use the Hardening Soil model (HS model) in additional analysis”. The M-C model was used for the initial analysis (i.e. to determine number of steps, time-step etc.), while HS was used in the final analysis in this study. All the results presented in the current study are using HS.

Although the HS model can generate irreversible plastic strains (and thus material damping), the irreversible strains are too small to fully simulate the correct material damping because the unloading and reloading is perfectly elastic (Plaxis bv, 2011). To be able to simulate the material damping properties of soil, Rayleigh damping was applied. A damping ratio of 5% has been assumed and applied to the backfill (and facing) material.

4.2.5.3 Reinforcements

The axial stiffness for the reinforcements from wide-width strip tensile tests (Table 3.2) showed a higher strength than what was used in the numerical model. When using the stiffness (i.e. EA = 90 kN/m) found in the tensile tests, the numerical values for the top facing lateral displacements was low compared to the model results. By trial it was found that stiffness of 50kN/m was suitable.

4.2.5.4 Interfaces

Zarnani et al. (2011) found that a soil friction angle of 44° was suitable for the soil-facing interface. As in the FLAC model this interface was modelled using a 0.015 m strip of soil directly behind the facing with the same material properties as the backfill, except from the soil friction angle.

To simulate soil-reinforcement interaction, an interface with a reduced strength (R_{inter}) was applied between the reinforcements and backfill. According to Waterman (2006), $R_{inter} = 0.5 - 0.9$ is suitable for interfaces between soil and a geotextiles. $R_{inter} = 0.8$ was assumed in the current model.

Table 4.1 PLAXIS Model Material Properties

The back wall was modelled Parameter	Symbol	Facing	Soil-facing interface	Backfill	Reinforcements	Unit
Material type	Type	Soil	Soil	Soil	Geogrid	-
Material model	Model	L. Elastic	HS	HS	Elastic	-
Dry weight	$\gamma_{sat}/\gamma_{unsat}$	17.20/17.20	15.70/15.70	15.70/15.70	-	kN/m ³
Young's modulus	E'	$2.475 \cdot 10^6$	-	-	-	kN/m ²
Young's modulus	E_{50}^{ref}	-	$15.33 \cdot 10^3$	$15.33 \cdot 10^3$	-	kN/m ²
Oedometer modulus	E_{oed}	-	8000	8000	-	kN/m ²
Power	m	-	0.5	0.5	-	kN/m ²
Unloading modulus	E_{ur}^{ref}	-	$46 \cdot 10^3$	$46 \cdot 10^3$	-	kN/m ²
Poisson's ratio	ν' (nu)	0.1250	-	-	-	-
Reference stress	P_{ref}	-	100	100	-	kN/m ²
Cohesion	c'_{ref}	-	0	0	-	kN/m ²
Friction angle	φ	-	44	51	-	°
Dilatancy angle	ψ	-	15	15	-	°
Stiffness	EA_1/EA_2	-	-	-	50	kN/m
Interface strength reduction	R_{inter}	1.0 (rigid)	1.0 (rigid)	1.0 (rigid)	-	-
Damping	α_r/β_r	0,06277/ 0,00159	0,06277/ 0,00159	0,06277/ 0,00159	-	-

4.3 Model Verification

In this section, the numerical results are compared to the results found in the physical shaking model test. The fundamental frequency, lateral displacements at the top of the facing panel, earth forces and failure surfaces are studied, as these are considered important indications on the model's accuracy. The aim is to show the limitations of the numerical model and see what aspects of the model that might need further study.

4.3.1 Fundamental Frequency

According to Zarnani et al. (2011) it is important that the fundamental input frequency is different from the fundamental frequency of the model wall to avoid early failure due to resonance. To find the fundamental frequency of the model wall, the model was subjected to a base input excitation for six seconds and then left to vibrate freely. The excitation was similar to the first six seconds used to simulate the shaking table excitation which is presented in section 4.2. Lateral displacements were measured for the free vibration at the top of the facing and the fast Fourier transform (FFT) was used to transfer the response to the frequency domain using a program from Holst (2011). The Fourier amplitude spectrum for the numerical model is presented in Figure 4.3, El-Emam (2003) found that the fundamental frequency of the physical model wall was 22 Hz. The fundamental frequency for the PLAXIS model wall is estimated to 19 Hz.

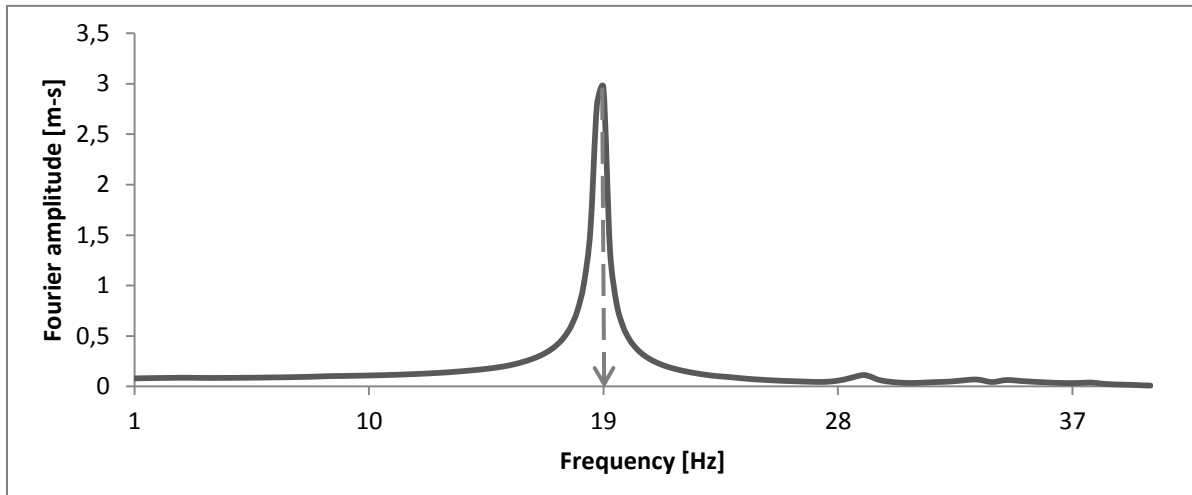


Figure 4.3 Fourier amplitude spectrum for the lateral displacements at the top of the model wall during the free vibration

4.3.2 Lateral Displacements at the Top of the Facing Panel

The measured lateral displacement on the top of the facing panel measured in the shaking table test (El-Emam, 2003) and the numerically predicted lateral displacements are shown in Figure 4.4. The numerical predictions are in satisfactory agreement with the measured displacements for the lower accelerations, up to about 35 seconds (input base acceleration amplitude of 0.35g). From this point on, the physical model experience a sharp increase in the lateral displacement and in the range 35-50 seconds the numerically predicted displacements are too small. Zarnani et al. (2011 p.306) notes that: "Sharp increases in displacement versus peak base acceleration can be found in literature for similar reduced-scale (i.e. physical shaking table) models". The sharp increase occurs because of the change in the soil response from elastic to plastic behaviour. The amplitude where it occurs is referred to as *critical acceleration*. A sharp increase in the numerically predicted lateral displacements is not observed until around 40 s (input base acceleration amplitude of 0.40g) and the facing displacements develops faster than in the physical model.

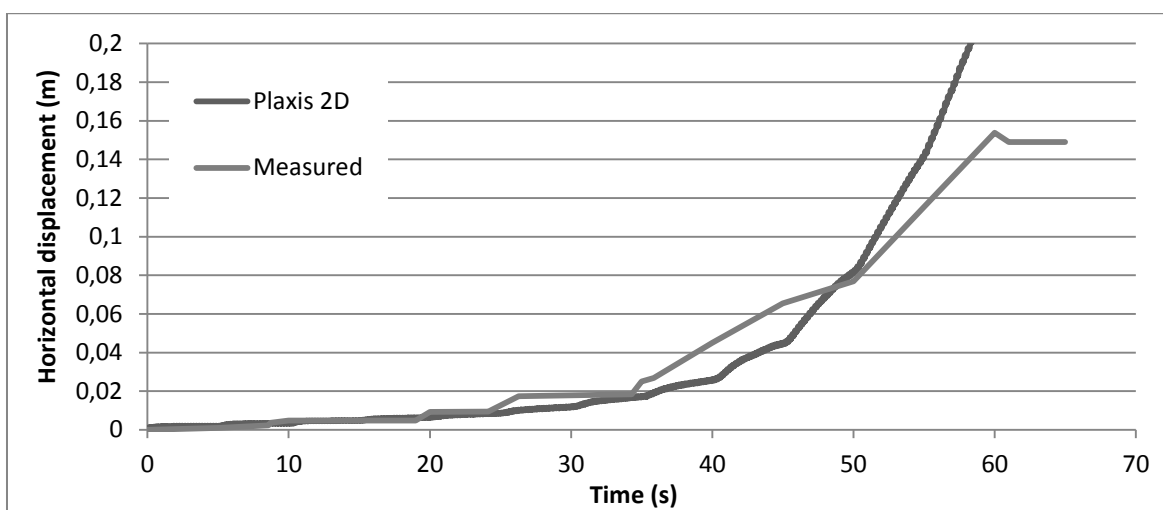


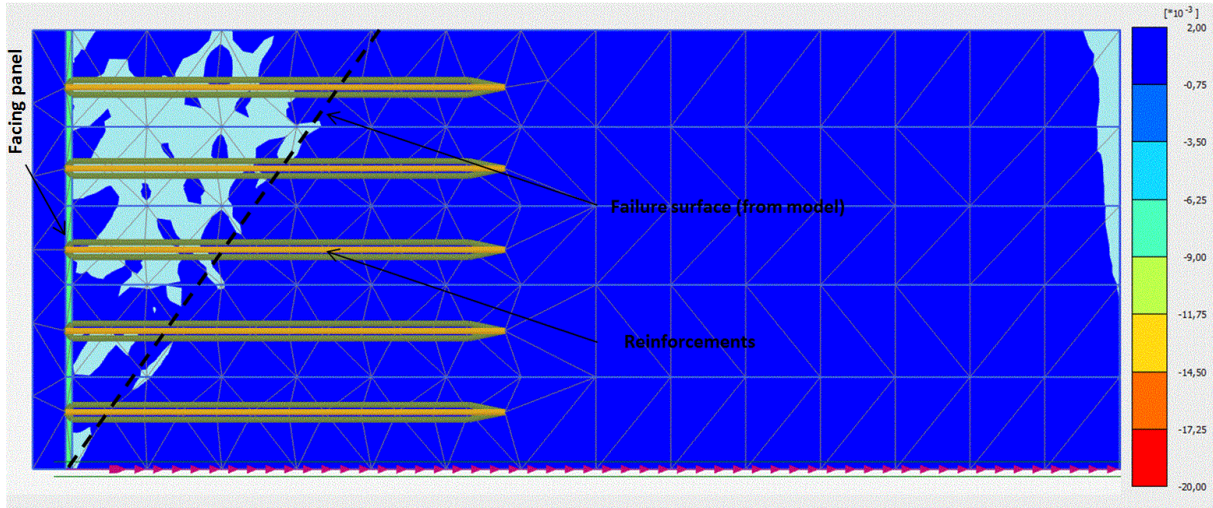
Figure 4.4 Numerical and measured time histories for horizontal displacements at the top of facing panel

4.3.3 Zone of Movement

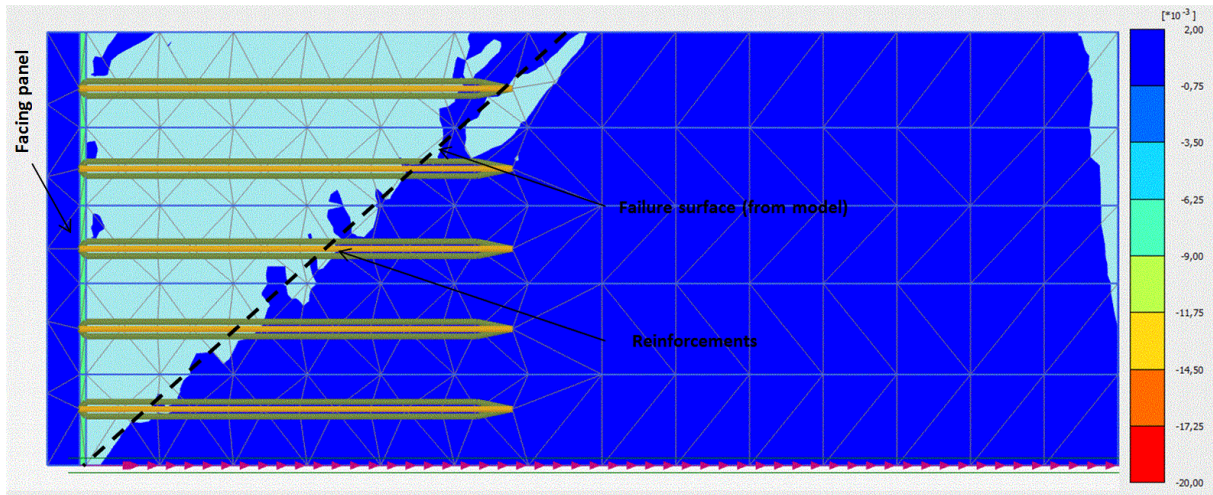
Shear zones for the numerical model for different base accelerations are presented in Figure 4.5 a)-f) using the total deviatoric shear stress plots from PLAXIS. El-Emam (2003 p.205) confirmed that “extensometer readings can be used to estimate the failure surface in shaking table tests” and the inferred failure surfaces for different input accelerations from the extensometer readings in the physical model are also included in the figure.

The predicted failure zone evolves from a single wedge to a two wedge mechanism with increased base accelerations. A similar mechanism can be observed from the physical results (see stapled lines in the figure marked “failure surface (from model)”), but this is not as evident as in the numerical results. A similar observation was made by Zarnani et al. (2011) for the FLAC model. The predicted failure surfaces are in reasonable agreement for base input acceleration amplitudes up to 0.30 g. Above 0.30 g, the agreement between the measured and predicted zones of movement is diminished.

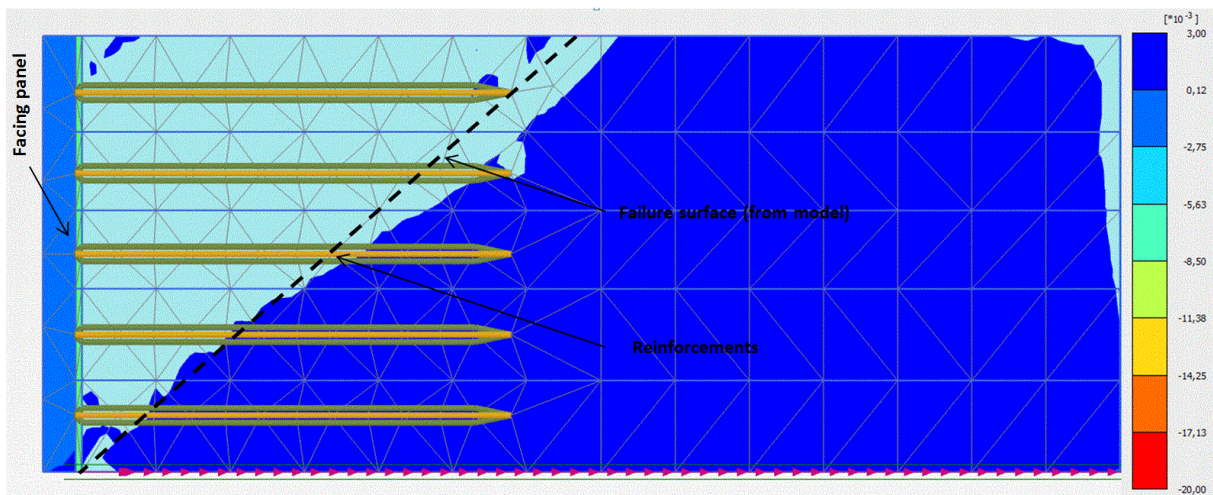
It should also be noted that at lower base input acceleration amplitudes the zone of soil movement intersects all the reinforcement layers. As the acceleration amplitudes increase, only the bottom layers are sufficiently long to intersect the failure surface.



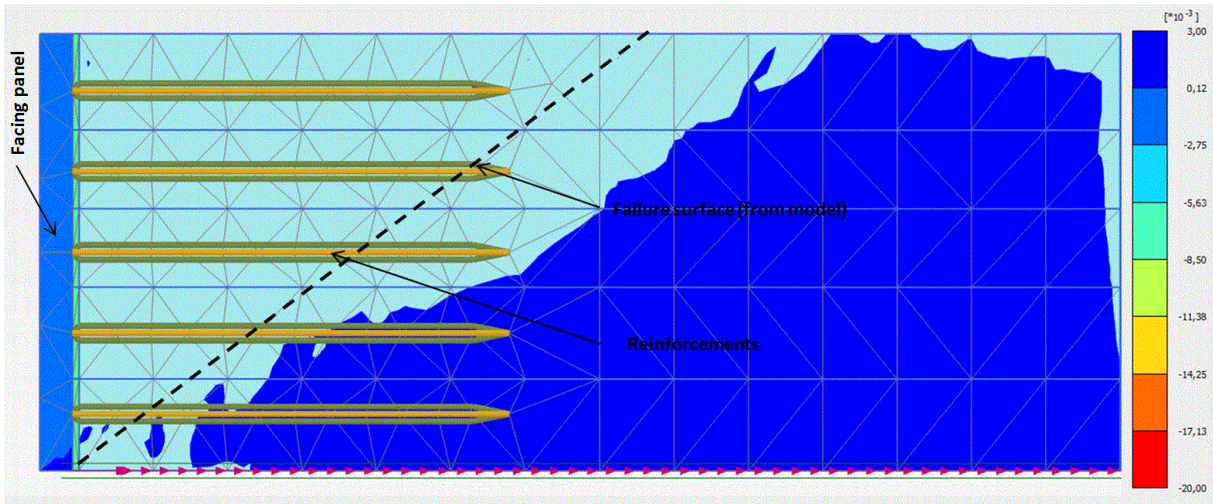
a) Base Acceleration input amplitude = 0.05g



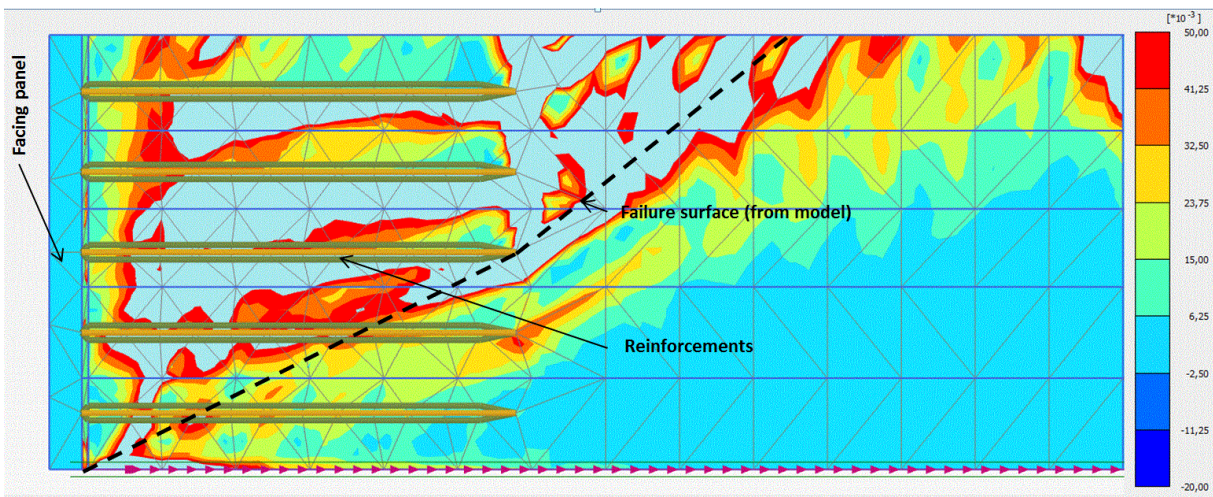
b) Base Acceleration input amplitude = 0.15g



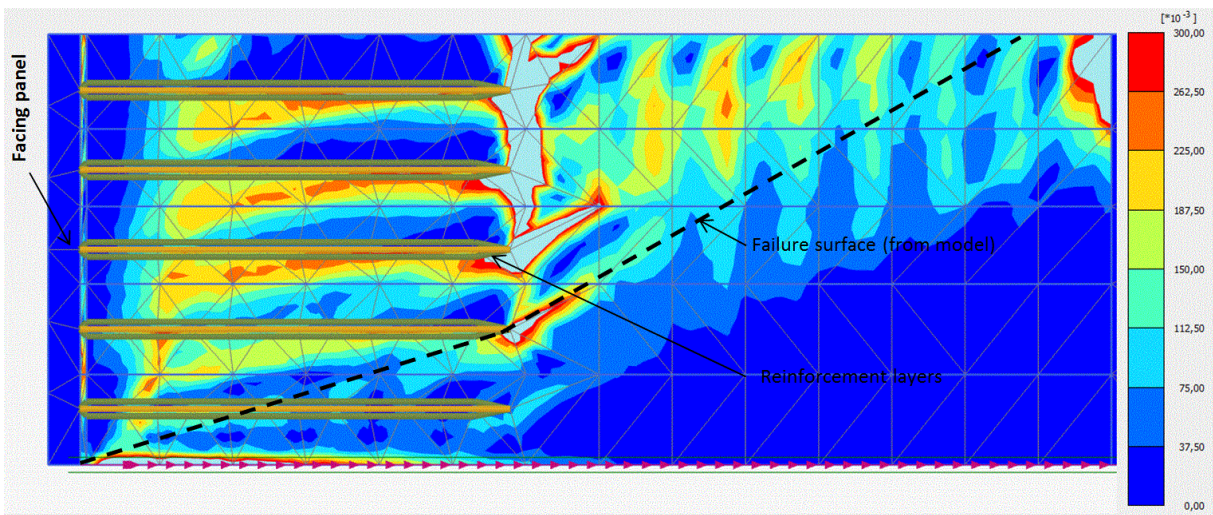
c) Base Acceleration input amplitude = 0.30g



d) Base Acceleration input amplitude = 0.40g



e) Base Acceleration input amplitude = 0.50g



f) Base Acceleration input amplitude = 0.60g

Figure 4.5 Numerical and observed soil failure zone surfaces

4.3.4 Total Earth Forces

The earth force resultant is important in calculations that concern the stability of a retaining wall. El-Emam (2003) noted that “the total earth force at the back of the facing panel is the summation of the total connections loads and the horizontal load developed at the toe”. Figure 4.6 presents the measured total earth force, P_{AE} , acting at the back of the facing panel found by El-Emam (2003) for different input accelerations. From the PALXIS model the numerically predicted reinforcement loads are known and from these the predicted total earth forces are calculated and included in the figure.

El-Emam (2003) only presents data for the reinforcement loads for input base accelerations up to 0.5 g; therefore the following results only cover input base accelerations between 0 g and 0.5 g. Furthermore, El-Emam (2003) does not report measurement for base input acceleration amplitudes of 0.05 and 0.15 g. The “measured” values in Figure 4.6 for these amplitudes are found by interpolation of the values at 0 g, 0.10 g and 0.20 g.

It is observed that the measured and predicted total earth forces are in reasonable agreement for input base accelerations up to 0.15 g, but after this the numerical model overestimates the total earth force.

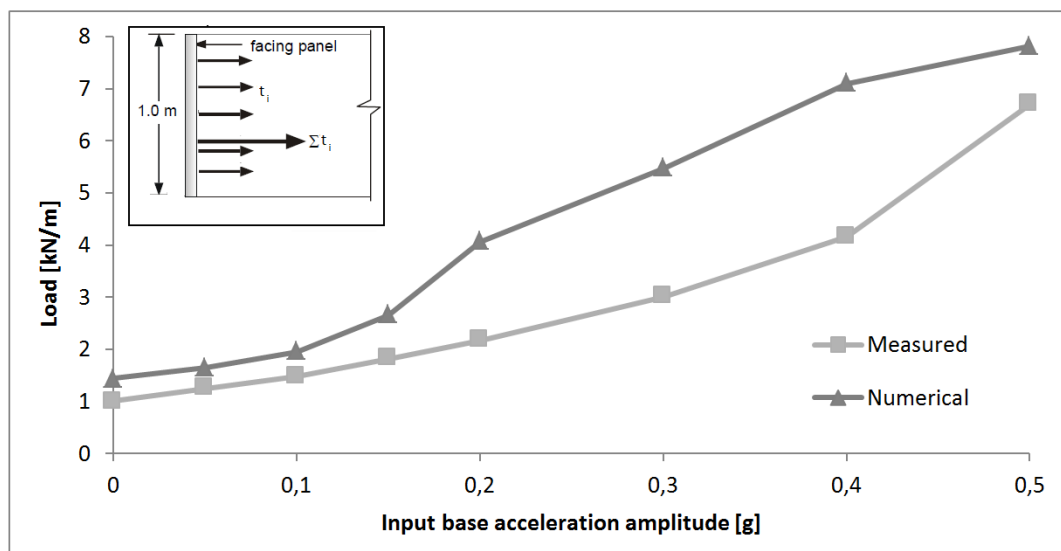


Figure 4.6 Total earth force (P_{AE}), measured and numerically predicted (El-Emam, 2003)

4.4 Comments and Discussion

Zarnani et al. (2011) found that there are no significant difference in numerical results if the entire soil structure is constructed instantaneously, compared to in steps to simulate soil placement. The reason for using steps to simulate soil placement is that this was considered more intuitive to the reader and the extended calculation time proved minimal.

To put a shaking table in the desired motion (as shown in Figure 3.3) requires some type of initial excitation. Details on the exact shape of the initial acceleration, velocity or displacement time series, i.e. details on how the physical model is put in motion, are not known. Thus, it is reasonable to expect that the base input time series in the physical model is not identical to the one used in the numerical simulation where a “soft start” and “soft transition” curve was used. The number of cycles that differ in the two models (physical and numerical respectively) are relatively few for each “amplitude plateau”. The consequence of the use of a “soft start” and “soft transition” in the numerical simulation is therefore considered minor.

A relatively high soil friction angle was used for the backfill material (51°). In PLAXIS, the use of high friction angles are not recommended due to increased calculation requirements (Plaxis, 2011). Furthermore, it is important to note that numerical instability can occur when high values are used. In the current model no instability was observed, but the calculation time was long, in excess of 7 hours. By increasing the number of “dynamic sub steps” and reducing the number of “additional steps” the same numerical accuracy could be obtained, but with a shorter calculation time. The drawback of this is that PLAXIS does not store information on other steps than the additional ones. Thus, high calculation time was accepted to make it possible to extrude data at a great number of time intervals.

One of the main reasons for choosing PLAXIS was its advanced (complex) soil models, but Zarnani et al. (2011) pointed out that one does not simply improve the simulation accuracy by using a complex material model as opposed to a simple one. Thus, the need for complex models is in question. Use of a simpler model (Mohr-Coulomb) would result in a shorter calculation time. Even so, the ability to adjust the stiffness’ proved useful to obtain a better fit for measured results for the lower base input accelerations, e.g. of the lateral displacements on the facing top.

The limitation in all the available PLAXIS material models is that they do not account for softening due to soil dilatancy and they do not model effects due to cyclic loading. The hardening soil model with small-strain stiffness (HSsmall model) “can, to some extent, be used to model cyclic loading” but this model “is not suitable for cyclic loading problems in which softening plays a role and softening due to soil dilatancy are not taken in to account” (Plaxis, 2011). The reason that the HS model was preferred on the expense of the HSsmall model was that the calculation time was much longer for the latter and this proved a great disadvantage when searching for suitable soil parameters.

It has not been possible to obtain a response spectrum for the lateral displacements at the top of the retaining wall for the physical model, thus it has not been possible to do a detailed study of the differences in the two response spectrums. But, the predicted fundamental frequency is well above the fundamental frequency of the base input excitation (5 Hz) and the numerical model will therefore not be affected noteworthy by resonance effects.

It should be noted that the available illustrations from El-Emam (2003) used in the following does not give the observed failure zones for the exact same values as the base input acceleration amplitudes studied in this study (0.05 g, 0.15 g, 0.30 g, 0.40 g, 0.50 g and 0.60 g). E.g. the base input acceleration amplitude for the situation in Figure 4.5 a) is set as 0.05 g, but El-Emam only gives an illustration for 0.06 g for the physical model. It is assumed that the differences between the failure surface for 0.05 g and 0.06 g, thus these illustrations are used in the current study. A similar assumption is made for higher amplitudes.

4.5 Summary of Numerical Model Development and Verification

This chapter described the results from a numerical model created to simulate the shaking table model described in chapter 3. PLAXIS 2D was used together with a Hardening soil model for the backfill. Elastic-plastic material parameters were collected from El-Emam (2003) and used as a basis for a trial procedure to find suitable material parameters suitable for the current study. The numerical model was subjected to a soft start base input series based on the information of the input base acceleration as used in the physical tests.

The overall results suggest that the numerical model is best suited for input base acceleration amplitudes up to 0.30 g. At higher acceleration amplitudes the numerical model over-predict the volume of the disturbed soil zone, this affects the results of the forces that act on the back of the facing and the lateral displacement.

These are some important findings from the current chapter:

- Even though complex soil models are used, it is challenging to create a dynamic model in PLAXIS 2D Dynamic that simulate reinforced retaining wall behaviour for a wide range of acceleration amplitudes.
- The failure surface evolves from a single to a two-wedge mechanism and the inclination of the surface decreases with increasing base input amplitudes.
- The developed numerical model is best suited for parameter studies up to base input acceleration amplitudes up to 0.30 g

5 Numerical Study: Effect of Reinforcement Parameters

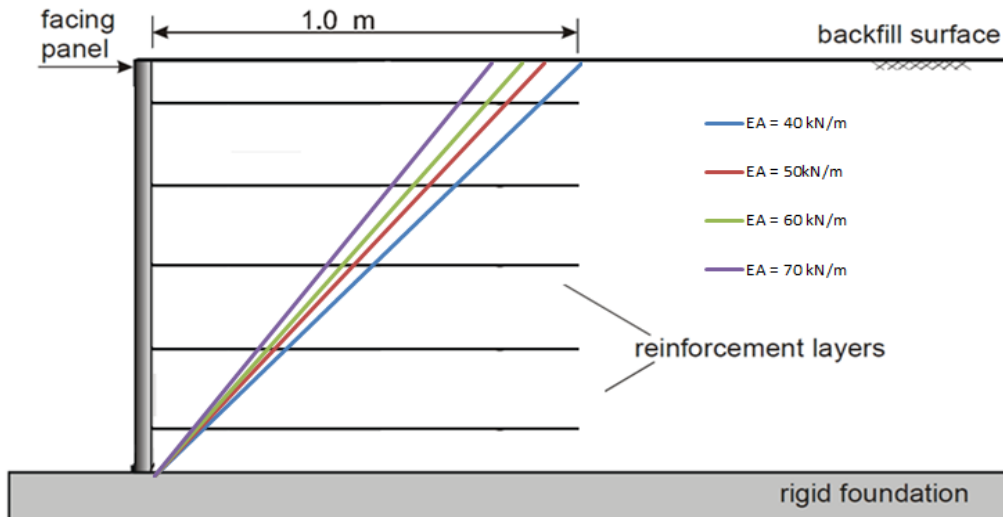
So far in this study a numerical model has been developed and verified using the results from the shaking table tests at RMC. In this chapter, this model is used to study the influence of reinforcement strength and length on the failure surface, wall displacements and reinforcement loads. El-Emam & Bathurst (2007) also studied the effects of reinforcement design parameters (i.e. stiffness, length and vertical spacing), but they used physical shaking table models (El-Emam, 2003). In their study, the influence of reinforcement design parameters on facing displacements, total earth forces at the back of the facing panel and reinforcement connection loads was discussed.

Chapter 4 concluded that the numerical model is best suited for a parametric study for base acceleration amplitudes up to 0.30g. Three base input acceleration amplitudes, 0.05g, 0.15g and 0.30g respectively, are used to illustrate the findings of the reinforcement design parameters study. Please note that the sketch of the reinforced soil wall (used to illustrate the failure surfaces) is obtained from El-Emam (2003).

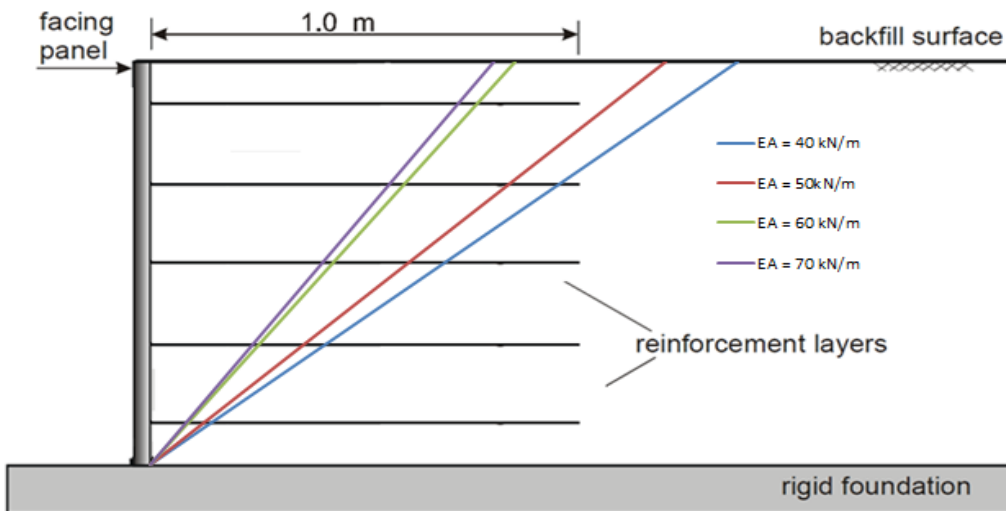
5.1 Effect on Failure Surface

The failure surfaces for models with different reinforcement axial stiffness (EA) are shown in Figure 5.1 for different base input acceleration amplitudes. The effect of axial stiffness on the failure surface development varies with the input base amplitude. How much the failure surface is affected by the increase in axial stiffness varies with the different base amplitudes, i.e. the effect of axial stiffness are not increased with increasing base amplitudes or vice versa, but generally the failure surface becomes shallower with increasing axial reinforcement stiffness. From Figure 5.1 c), the failure surface is not a straight line for the lowest stiffness (EA=40 kN/m).

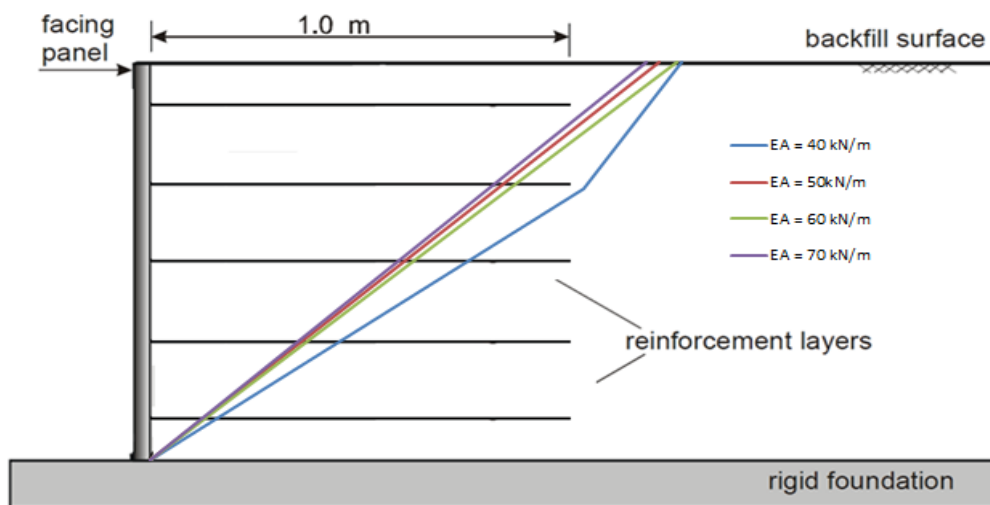
In Figure 5.2, results for different base input acceleration amplitudes and four different reinforcement lengths (L) are presented. From Figure 5.2 a) and c) it is observed that the failure surface generally becomes shallower with increasing reinforcement length. The results shown in Figure 5.2b) do not show the same tendency; the failure surface predicted using the shortest and longest reinforcement length's (L=0.80 m and L=1.40 m respectively) are almost identical. It should also be noted that the failure surface is no longer straight for the shortest reinforcement length in Figure 5.2 c).



a) Base input acceleration amplitude: 0.05 g

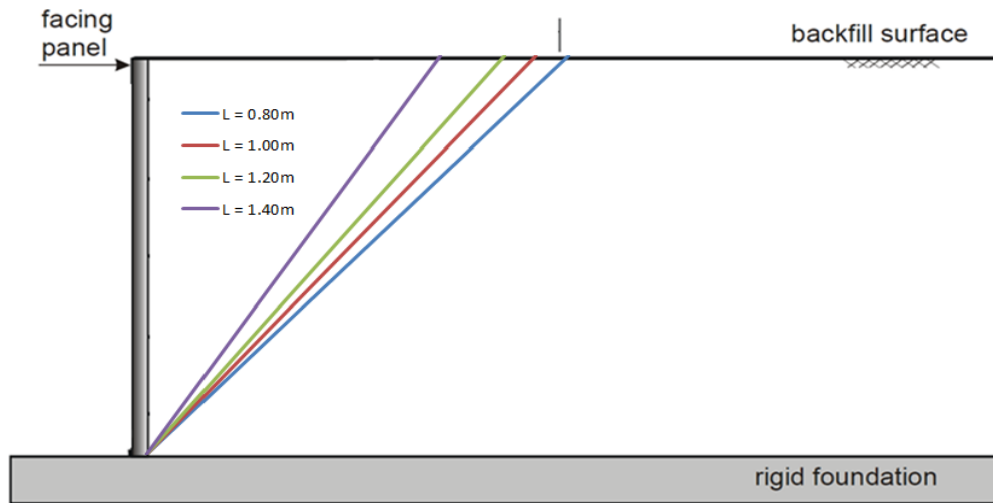


b) Base input acceleration amplitude : 0.15 g

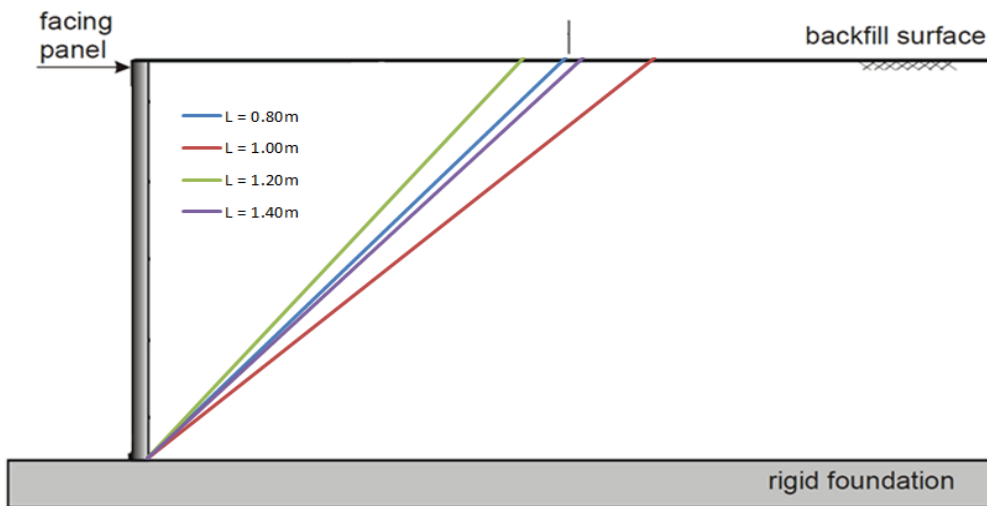


c) Base input acceleration amplitude: 0.30 g

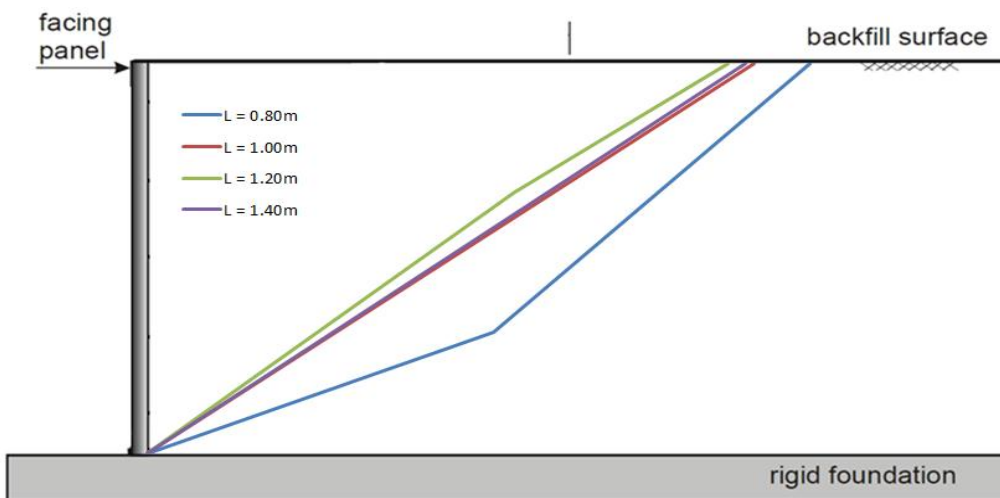
Figure 5.1 Change in failure surface: Effect of reinforcement stiffness



a) Base input acceleration amplitude: 0.05 g



b) Base input acceleration amplitude: 0.15 g



c) Base input acceleration amplitude: 0.30 g

Figure 5.2 Change in failure surface: Effect of reinforcement length

5.2 Effect on Facing Displacements

The lateral displacement at the top of the facing as a function of time is shown in Figure 5.3 for models with different reinforcement axial stiffness (EA). Increasing the reinforcement stiffness reduces the lateral facing displacements significantly, e.g. it is observed that an increase in stiffness from 40 to 90 kN/m results in a reduction of top facing lateral displacements by 50 % for an input base amplitude of 0.30g (at 30 s). Figure 5.3 also shows that the decrease in the displacements is non-linear with respect to the reinforcement stiffness; increasing the stiffness from 40 to 50kN/m results in a larger decrease in displacements than increasing the stiffness from 50 to 60kN/m for an input base amplitude of 0.30g (at 30 s).

Figure 5.4 shows the lateral displacement at the top of the facing as a function of time for models with different reinforcement lengths. Decreasing the reinforcement length has little effect on the lateral facing displacements for peak base input values under 0.20 g (20 s), but for values over 0.20 g a significant effect of increasing the length is observed; e.g. increasing the reinforcement length from 0.8 to 1.4 m results in a 30 % decrease in lateral facing displacements for a peak base input value of 0.30 g (30 s).

These results are supported by El-Emam & Bathurst (2007) who found that higher reinforcement axial stiffness resulted in smaller lateral facing displacements for peak base input values up to 0.24g. They also found that an increase in reinforcement length results in a decrease in the wall's lateral displacement.

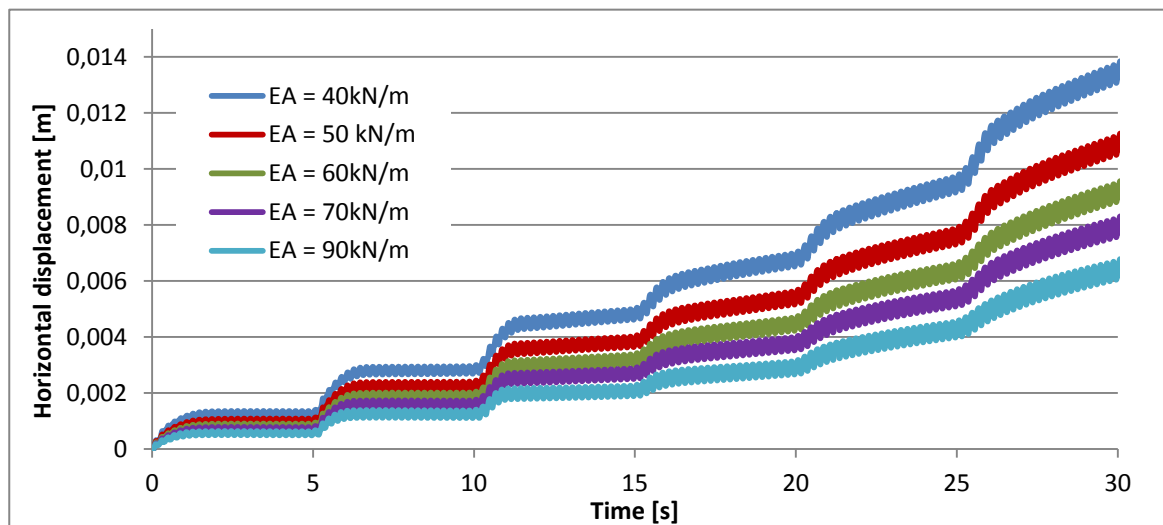


Figure 5.3 Top facing lateral displacements: Effect of reinforcement stiffness

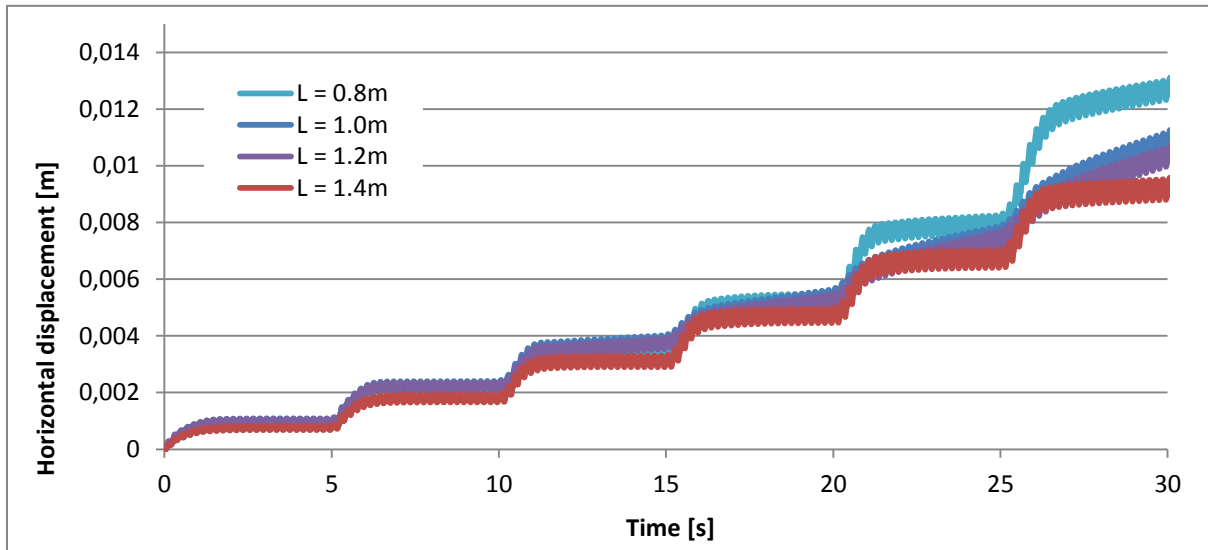


Figure 5.4 Top facing lateral displacements: Effect of reinforcement length

5.3 Effect on Reinforcement Connection Loads

The total connection load between the facing and the geo-synthetic reinforcements are shown in Figure 5.5 as a function of base input acceleration amplitudes for different levels of reinforcement axial stiffness. There are no significant changes in the total connection loads for varying stiffness' for base input amplitudes of 0.05 g and 0.15 g. However, the results at base input acceleration amplitude of 0.3 g indicate that stiffer reinforcements are subjected to increased axial loads. Individual connection loads are given in Appendix 1 as a function of the reinforcement's position above the toe. Here, no clear tendency as to how the connection loads strength affects this with varying base amplitudes is observed. Connection loads for different base amplitudes and reinforcement lengths were also investigated and are given in Appendix 1, no clear conclusions can be drawn from these results.

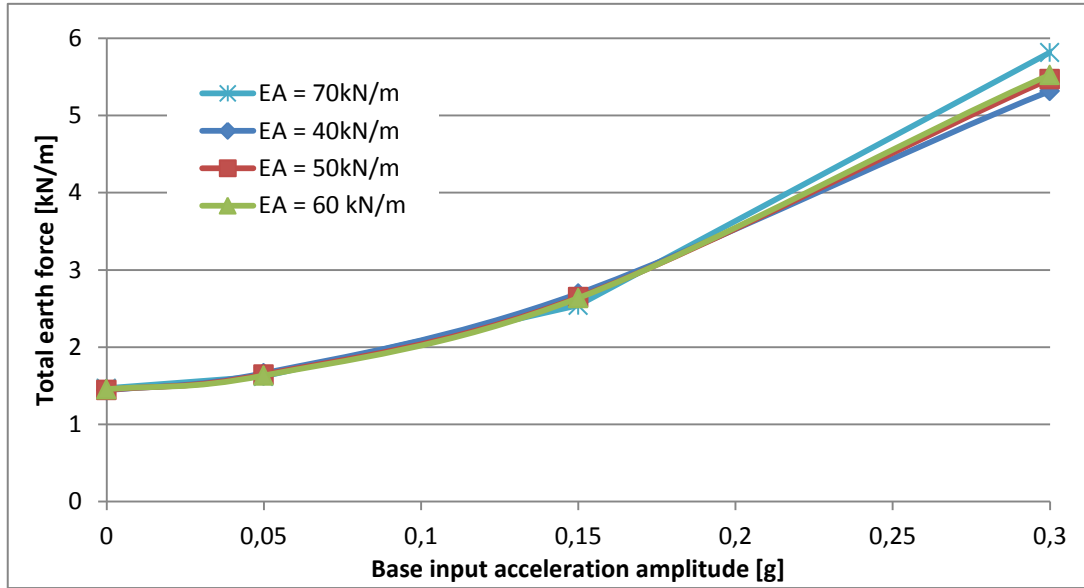


Figure 5.5 Total reinforcement connection loads

5.4 Comments and Discussions

For the lower base input amplitudes, the failure surface is shallow (see Figure 5.1a)) and most of the reinforcement layers (for the different lengths) are long enough to intersect the failure line and have sufficient pull-out resistance, i.e. they are all able to withstand the earth forces (both dynamic and static). For higher acceleration amplitudes the longer reinforcements are able to intersect the failure line with more of their reinforcement layers and are thus better capable to resist the earth forces (Zarnani, et al., 2011).

The failure surface becomes shallower with increasing axial reinforcement stiffness and reinforcement length, something which coincides with decrease in lateral wall displacements. The failure zone are only located behind the facing, i.e. it does not extend below the toe. Thus, the active earth force resultant from the dynamic excitation will act on the back of the facing. Understanding Newton's second law (force = mass · acceleration), it is reasonable to expect that the magnitude of soil mass in motion will affect the forces on the retaining wall. I.e. when the failure surface depth increases, the forces on the retaining wall increases and this results in larger facing displacements.

It is known (chapter 4) that the failure surface evolves from a single to a two-wedge mechanism. At what acceleration amplitude the mechanism changes (from single to two-wedges) is believed to be affected by the reinforcement properties. From Figure 5.1c) and Figure 5.2c) indications that a lowering of the axial stiffness and/or a shortening of the reinforcement length leads to a change in the failure surface shape; it is no longer a straight line for $EA=40$ kN/m and $L=0.8$ m at base input amplitudes of 0.30 g.

El- Emam & Bathurst (2007) found that "the magnitude of the total reinforcement connection loads decreased with increasing reinforcement length and decreasing stiffness", the same is not observed in the current study. The reason for this is not known, but; $R_{inter} = 0.8$, was used in the numerical model in the interface between the reinforcement's and the backfill, and this parameter is believed to affect the transfer of forces to the reinforcements. No detail study of the effect of R_{inter} was done, thus the effect of this parameter is unknown.

To get a better understanding of the stability of the numerical model (and also the effect of more reinforcement properties), a stability analysis should be carried out. This analysis should find how (and how much) the various model parameters (e.g. R_{inter} , stiffness and damping) affect the stability of the numerical model. Such an analysis has not been carried out in the current study due to limited time. This is a clear disadvantage and will decrease the reliability of the results presented.

Please note that the deviation tendency found in Figure 5.2 a) and c), opposed to Figure 5.2 b), are believed to be due to human error in extracting the results from PLAXIS, thus little attention should be made to the results in Figure 5.2 b).

5.5 Summary of Numerical Study on Effect of Reinforcement Parameters

This chapter describes the results from a numerical parameter study of the effect of reinforcement strength and length on the failure surface, wall displacements and reinforcement loads. The study was carried out using the PLAXIS model described in chapter 4 and thus the investigation covers acceleration amplitudes of up to 0.30 g. The major conclusions from the numerical results are:

- The failure surface becomes shallower with increasing axial reinforcement stiffness and reinforcement length.
- The magnitude of facing displacements is reduced with increasing axial stiffness and reinforcement length.
- A lowering of the axial stiffness and/or a shortening of the reinforcement length leads an earlier development of the two wedge failure mechanism.
- A sensitivity study should be carried out for the numerical model if it should be used for further studies of reinforcement parameters.

6 Literary Review: Analytical Methods for Seismic Design

There are a variety of different ways of calculating the seismic pressures on retaining walls. This chapter can be seen as a background for chapter 7. First, there is given a short overview of the various methods used for seismic design of reinforced soil walls. Then, more detailed descriptions of three pseudo-static methods are given.

In Table 6.1, the most well-known methods for calculation of the seismic pressures (and in some methods displacements) on a yielding retaining wall are presented. The cost of getting the necessary material parameters needed for an accurate finite element calculation is quite expensive (Kramer, 1996; Ausilio, et al., 2000). Therefore, most of the methods used to calculate such problems are simplified analytical methods, even though the finite element method is the most “all-inclusive” approach to solving such problems. In the literature and design codes reviewed in this study, the most commonly used type of simplified analytical methods is the pseudo-static.

Table 6.1 Dynamic pressures and displacements on retaining walls – Various calculation methods
(Kramer, 1996; Shukla, et al., 2002; Nouri, et al., 2005)

Type	Name	Additional information
Pseudo-static methods	Mononobe-Okabe method (M-O)	<ul style="list-style-type: none"> May be used for reinforced slopes, but primarily used for unreinforced slopes
	Two-part wedge method (TPW)	<ul style="list-style-type: none"> Based on the M-O method Often used for reinforced slopes Two wedge failure mechanism
	Logarithmic spiral method	<ul style="list-style-type: none"> Logarithmic spiral failure mechanism
	Circular slip method	<ul style="list-style-type: none"> Circular slip failure mechanism
	Vertical slice method (VSM)	<ul style="list-style-type: none"> Divides a logarithmic spiral failure mechanism in to vertical slices
	Horizontal slice method (HSM)	<ul style="list-style-type: none"> Combines a logarithmic spiral failure mechanism and the Mononobe-Okabe method.
Pseudo-dynamic methods	Steedman-Zeng method	<ul style="list-style-type: none"> Accounts for phase difference and amplification effects in the backfill
Displacement calculations	Newmark’s method	<ul style="list-style-type: none"> Used as a basis for other displacement methods
Whole falling mass equilibrium methods	Cullmann’s method	<ul style="list-style-type: none"> For analysis of homogeneous soils and specific failure surfaces
Numerical techniques	Finite element method	<ul style="list-style-type: none"> Can implement complex models for soil and reinforcement materials Used in the computer program PLAXIS
	Finite difference method	<ul style="list-style-type: none"> Used in the computer program FLAC

6.1 Introduction to Pseudo-Static Analysis

Pseudo-static analysis is one of the simplest approaches used in earthquake engineering to analyse the seismic response according to Melo & Sharma (2004). The pseudo-static analysis is basically a representation of the earthquake excitation by constant accelerations. Initial forces in the horizontal and vertical directions, F_h and F_v respectively, due to these accelerations are

$$F_h = k_h W \quad (6.1)$$

$$F_v = k_v W \quad (6.2)$$

Where W is the weight of the failure mass. The pseudo-static coefficients in the horizontal and vertical direction (k_h and k_v) is the ratio between the acceleration in the respective direction and the gravity constant (g) i.e. $k_h = \frac{\text{horizontal acceleration}}{g}$ and $k_v = \frac{\text{vertical acceleration}}{g}$. These forces act through the centre of the failure mass (Kramer, 1996).

A pseudo-static parameter is not able to represent all the effects of seismic loading, e.g. effect due to the duration of seismic loading, frequency content and soil acceleration amplification etc. Thus, finding a coefficient that fits perfectly is impossible, and according to Kramer (1996): "Selecting appropriate seismic coefficients is the most challenging part of the pseudo-static analysis".

Different codes and rules of practise have recommended coefficients for design; e.g. Eurocode (Europe), FHWA/AASHTO (the United States) and PIANC (international). Table 6.2 gives examples of recommended values of k_h , but generally the seismic coefficient should be based on the anticipated level of acceleration (Kramer, 1996). In the mentioned guidelines formulas for calculating k_h based on the acceleration amplitudes are given.

Table 6.2 Recommended horizontal seismic coefficients (Melo & Sharma, 2004)

Horizontal Seismic Coefficient, k_h	Description
0.05-0.15	Guidelines in the United States
0.12-0.25	Guidelines in Japan
0.1/0.2/0.5	"severe"/ "violent, destructive" /"catastrophic" earthquakes (Terzaghi, 1951)

6.2 Mononobe-Okabe Method (M-O)

This pseudo-static method was proposed in the 1920's by Okabe, Matsou and Mononobe to analyse seismic pressures. Later in the 1960's Seed and Whitman developed this method further and described how to estimate the dynamic earth pressure against a wall by using static forces to represent the inertial effects of earthquake loading .

6.2.1 Assumptions

There are three basic assumptions in the Mononobe-Okabe Method (Li & Aguilar, 2000):

- The retaining wall is assumed to move a sufficient distance at the base to mobilise the full shear strength of the backfill.
- One neglects the dynamic amplification and represents the earthquake loading through constant seismic coefficients.

According to Zarrabi-Kashani (1979), the critical failure surface for active earth pressure conditions is inclined at an angle

$$\alpha_{AE} = \phi - \psi + \tan^{-1} \left[\frac{-\tan(\phi - \psi - \beta) + C_{1E}}{C_{2E}} \right] \quad (6.6)$$

Where

$$C_{1E} = \sqrt{\tan(\phi - \psi - \beta)[\tan(\phi - \psi - \beta) + \cot(\phi - \psi - \theta)][1 + \tan(\delta + \psi + \theta) \cot(\phi - \psi - \theta)]}$$

$$C_{2E} = 1 + \{\tan(\delta + \psi + \theta)[\tan(\phi - \psi - \beta) + \cot(\phi - \psi - \theta)]\}$$

The solution by this method is based on the limit equilibrium of the soil wedge and one does not take in to account the wall (Caltabiano, et al., 2000). Also note that this method is subjected to the same limitations as the Coulomb theory. Even so, this method provides a simple way of estimating earthquake induced pressures on retaining walls (Kramer, 1996).

6.3 Two-Part Wedge Method (TPW)

Another limit-equilibrium (and pseudo-static method) is the two-part wedge method; as the name suggests the seismic pressures are calculated using two wedges. The assumptions from chapter 6.2.1 are still relevant.

The failure zone comprises of two masses (1 and 2) as described in Shukla et al. (2002), see Figure 6.2. Forces (P_1 and V_1) acting on the second wedge from the first is given by

$$P_1 = \frac{(1 \pm k_v)W_1 + \frac{\tan \phi_f \sin \theta_1 + \cos \theta_1}{\sin \theta_1 - \tan \phi_f \cos \theta_1} k_h W_1}{\lambda \tan \phi_f + \frac{\tan \phi_f \sin \theta_1 + \cos \theta_1}{\sin \theta_1 - \tan \phi_f \cos \theta_1}} \quad (6.7)$$

and

$$V_1 = \lambda P_1 \tan \phi_f \quad (6.8)$$

The quantity W is the weight of the soil wedge, θ is the angle of the failure surface and $\phi_f = \tan^{-1}(\tan \phi / FS)$, where ϕ is the friction angle and FS the factor of safety. Lambda (λ) is the inter-wedge shear mobilization ratio that varies between 0 and 1, and k_h and k_v are denoted as earlier.

In this study, a formulation proposed by Bathurst (1994) is used for determining the critical failure surface by trial. This technique assumes equilibrium in the horizontal direction. This renders the following equation for calculation of the horizontal active force acting on the retaining wall (P_{AE}):

$$P_{AE} = P_1 - \frac{\frac{\tan \phi_f \sin \theta_1 + \cos \theta_1}{\sin \theta_1 - \tan \phi_f \cos \theta_1} \sum T_{i1}}{\lambda \tan \phi_f + \frac{\tan \phi_f \sin \theta_1 + \cos \theta_1}{\sin \theta_1 - \tan \phi_f \cos \theta_1}} + k_h W_2 - \sum T_{i2} \quad (6.9)$$

$$- \frac{\tan \phi_f \cos \theta_2 - \sin \theta_2}{\cos \theta_2 + \tan \phi_f \sin \theta_2} [(1 \pm k_v)W_2 + V_1]$$

The critical geometry is found when $P_{AE}=0$. When calculating the failure surface, FS is set equal to 1. The tension mobilised in the respective reinforcement layer is given by (Reddy & Madhav, 2008):

$$T_i = 2\gamma h_i L_{ei} \tan \phi_r \quad (6.10)$$

Where h_i and L_{ei} is the depth and effective length of the reinforcement layer and ϕ_r is the angle of interface friction between the reinforcement and the soil.

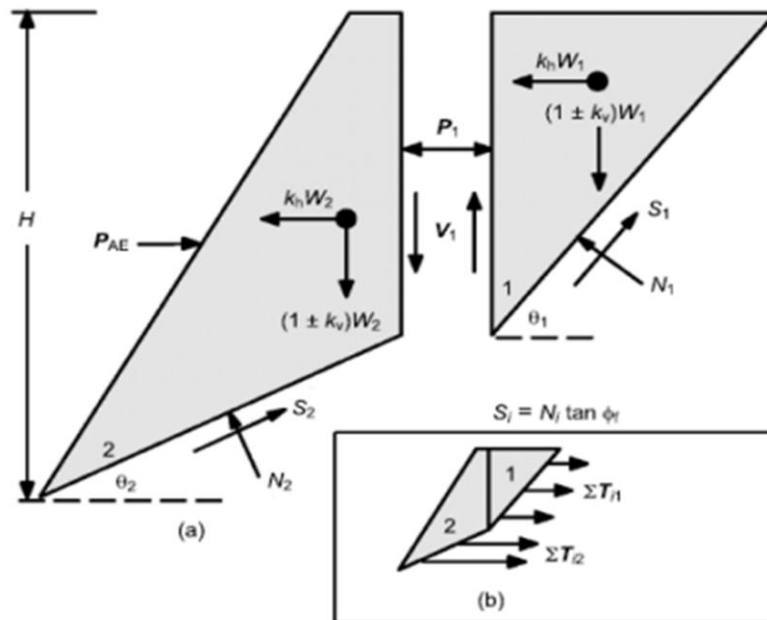


Figure 6.2 The two-part wedge method (Shukla, et al., 2002)

6.4 Horizontal Slice Method (HSM)

Earlier, the vertical slices method (VSM) was often used to analyse reinforced slopes. Here, the reinforcements cross slices and the forces mobilised appear as unknowns in the principal equations. The method of horizontal slices was proposed in 1992 by Lo and Xu to evade these unknowns.

6.4.1 Assumptions

This method divides the failure zone into a number of horizontal slices, and (as shown in Figure 6.3) the forces generated from the reinforcements do not intersect the horizontal slices. Inertia forces due to seismic waves are introduced as pseudo-static forces acting in the centre of gravity of each slice. Also, rigid-plastic behaviour is assumed in each slice. Coarse materials are usually used as backfill materials behind retaining walls; therefore pore-water pressures are neglected. Also, the soil is assumed to be cohesion less (Nouri, et al., 2005).

In addition, the following assumptions are given as described by Shahgholi et al. (2001):

- the vertical pressure on a horizontal slice under seismic loading is $(1 + k_v)\gamma h$, where γ is the unit weight of soil and h is the vertical distance between any point in soil mass and external borders of soil mass;
- the factor of safety is equal to $\frac{\text{available shear resistance}}{\text{required shear resistance}}$ and the same for all slices;
- the failure surface does not pass below the toe of the slope.

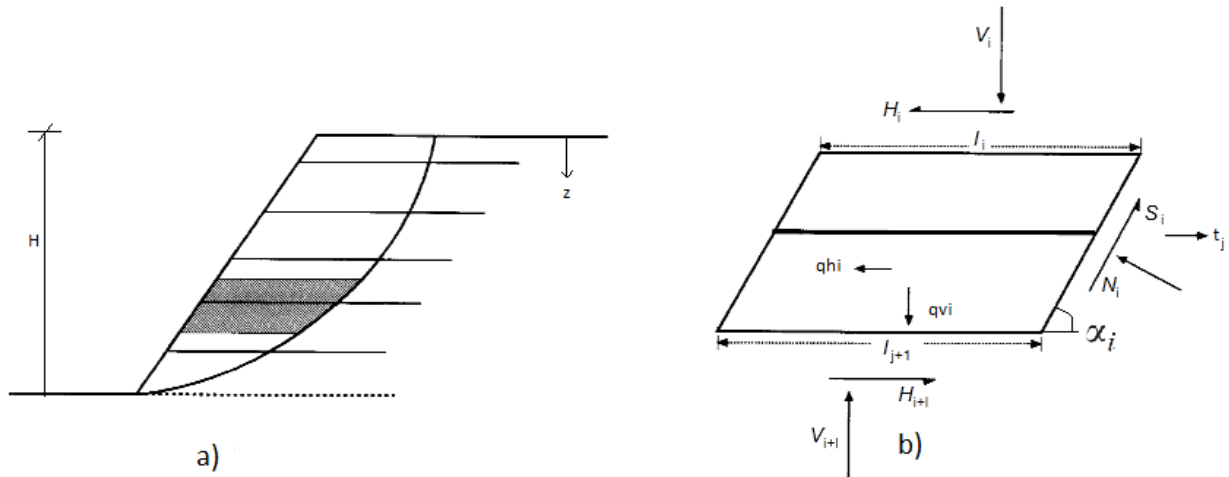


Figure 6.3 Horizontal slices method a) general b) one slice (Shahgholi, et al., 2001)

6.4.2 Formulation

By simplifying the method from 1992, Shahgholi, Fakher and Jones was able to make the method suitable for analysing the seismic forces on reinforced retaining walls (Nouri, et al., 2005). An additional development of this method was proposed by Choudhury et al (2006) for a retaining wall subjected to harmonic seismic acceleration.

The full formulation of the general HMS requires extensive mathematical derivation, thus only a simplified method is presented to illustrate the concept and the advantages of the method. A more complete formulation of the HMS is presented in Nouri et al. (2005) and in Shahgholi (2001). The following presentation is based on the work by Choudhury et al. (2006) and Ahmad & Choudhury (2008) and incorporates the horizontal seismic acceleration due to the shear wave velocity (V_s) in the soil.

The seismic inertia forces in the horizontal and vertical direction, q_{hi} and q_{vi} respectively can be expressed by

$$q_{hi} = m_i k_h g \sin\left(\frac{t}{T} - \frac{H-z}{V_s}\right) \quad (6.11)$$

$$q_{vi} = m_i k_v g \sin\left(\frac{t}{T} - \frac{H-z}{V_p}\right) \quad (6.12)$$

Where T is the period of seismic shaking, t is time and m_i is the mass of the i th slice. V_p is the primary wave velocity and z is the depth below the surface (Figure 6.3a). By considering Figure 6.3b the following equilibrium conditions can be obtained

$$\sum F_y = 0 \text{ (for the } i\text{th slice)} \Rightarrow V_{i+1} - V_i - W_i - q_{vi} + S_i \sin \alpha_i + N_i \cos \alpha_i = 0 \quad (6.13)$$

where

$$\tau_r = \frac{\tau_f}{FS} \Rightarrow S_i = \frac{1}{FS} (N_i \tan \phi) \quad (6.14)$$

FS is the factor of safety, τ_r the available shear resistance and τ_f the required shear resistance. ϕ is the soil friction angle.

By considering the equilibrium equation for the i th slice in the horizontal condition with FS=1, the tensile force (t_i) for a vertical slope can be expressed as

$$\sum F_x = 0 \text{ (for } i\text{th wedge)} \Rightarrow$$

$$t_i = q_{hi} + N_i \sin \alpha_i - S_i \cos \alpha_i \quad (6.15)$$

In this study, two failure surfaces (linear and polylinear) have been of interest, see Figure 6.4. The linear failure surface angle (α_{base}) is found by optimising the active earth pressure coefficient (K_{AE}) with respect to its maximum value by considering different angles (α_i) and values for t/T . The critical value for α_{base} is then chosen as the angle for all the slices and this gives the critical linear failure surface. The active earth pressure coefficient is given by

$$K_{AE} = \frac{1}{\tan \alpha_i} \frac{\sin(\alpha_i - \phi)}{\cos(\delta + \phi - \alpha_i)}$$

$$+ \frac{k_h}{2\pi^2 \tan(\alpha_i)} \left(\frac{TV_s}{H} \right) \frac{\cos(\alpha_i - \phi)}{\cos(\delta + \phi - \alpha_i)} m_1 \quad (6.16)$$

$$+ \frac{k_v}{2\pi^2 \tan(\alpha_i)} \left(\frac{TV_p}{H} \right) \frac{\cos(\alpha_i - \phi)}{\cos(\delta + \phi - \alpha_i)} m_2$$

where δ is the wall friction angle and

$$m_1 = 2\pi \cos \left(2\pi \left(\frac{t}{T} - \frac{H}{TV_s} \right) \right)$$

$$+ \left(\frac{TV_s}{H} \right) \left(\sin \left(2\pi \left(\frac{t}{T} - \frac{H}{TV_s} \right) \right) - \sin \left(2\pi \frac{t}{T} \right) \right) \quad (6.17)$$

$$m_2 = 2\pi \cos \left(2\pi \left(\frac{t}{T} - \frac{H}{TV_p} \right) \right)$$

$$+ \left(\frac{TV_p}{H} \right) \left(\sin \left(2\pi \left(\frac{t}{T} - \frac{H}{TV_p} \right) \right) - \sin \left(2\pi \frac{t}{T} \right) \right) \quad (6.18)$$

The critical polylinear failure surface is found by using the α_{base} angle as the angle for the first slice, i.e. the slice closest to the wall toe. Regarding the other slices, the angle that give the highest tensile force (using equation 6.15) are selected as the slice angle (α_i) for the respectable slice.

K_{AE} for the polylinear can be expressed as (Ling & Leshchinsky, 1998):

$$K_{AE} = \frac{\sum t_i}{0.5\gamma H^2} \quad (6.19)$$

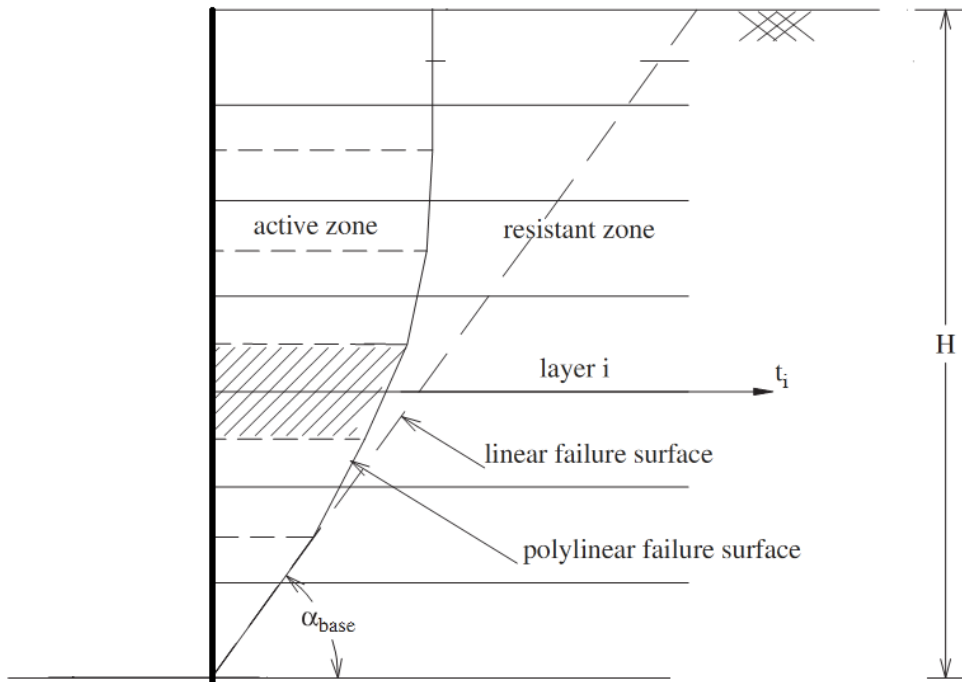


Figure 6.4 Polylinear and linear failure surfaces (Ahmad & Choudhury, 2008)

7 Shaking Table Experiments at RMC: Pseudo-Static Analysis

The technical computing language MATLAB (The Mathworks, Inc., 2011) was used to develop programs for calculating the pseudo-static failure surfaces and active earth pressures for the shaking table model. These programs are based on the pseudo-static methods described in chapter 6. MATLAB code is given in Appendix 2.

The purpose of this chapter is to verify the pseudo-static models and to find how suitable they are for calculating the failure surface and active earth forces acting on the retaining wall. This is done using results from the physical model presented in chapter 3. It should be noted that a numerical model (like the one presented in chapter 4) also can be used to verify analytical (pseudo-static) methods, but since this has not been the focus of this study it is not discussed further.

In the first part of this chapter the assumptions behind the pseudo-static calculations are presented. Later, the results from the pseudo-static calculations are presented and comparisons are made between these results and the results from the physical shaking table model.

7.1 Pseudo-Static Coefficient

The pseudo-static coefficient used in this chapter is based on direct measurements from the shaking table tests at RMC. El-Emam (2003) presents information about the soil amplification factor (AF) for the back fill surface specific for this models test (Figure 7.1). In simple terms, soil amplification is the ground's capacity to amplify seismic shaking. In this study, the soil amplification factor (AF) is defined as the ratio of the soil and rock response spectrum at the resonant peak. Values for the horizontal pseudo-static coefficient are calculated from the acceleration at the top of the backfill surface, using that:

$$k_h^{spes} = AF * \frac{a_b}{g} \quad (7.1)$$

Where a_b is the base input acceleration amplitude and k_h^{spes} is the pseudo-static coefficient based on data from the reduces-scale shaking table model test at RMC (chapter 3).

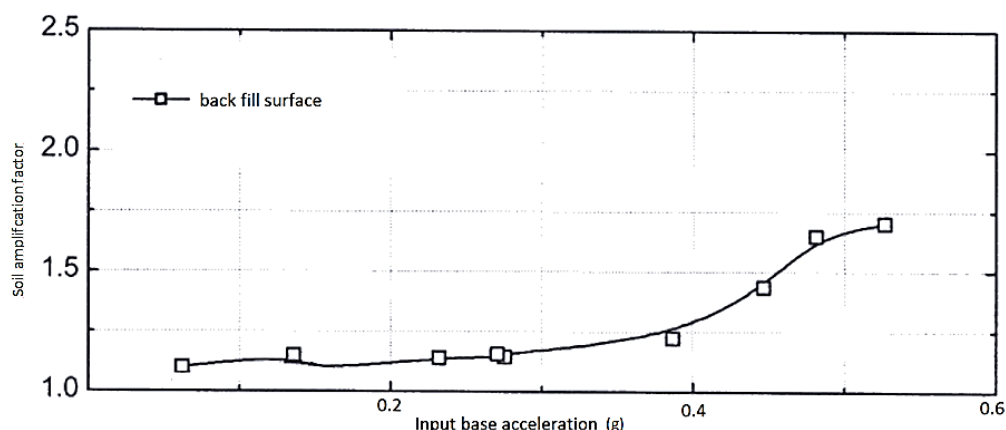


Figure 7.1 Outward soil amplification factor at backfill surface (El-Emam & Bathurst, 2004)

The vertical pseudo-static coefficient (k_v) was set to zero, while values for k_h^{spes} are presented together with the input base acceleration amplitude in Table 7.1.

Table 7.1 Horizontal pseudo-static coefficient

a_b	k_h^{spes}
0.05g	0.0549
0.15g	0.1663
0.30g	0.3498
0.40g	0.5163
0.50g	0.8288
0.60g	1.0154

7.2 Material Parameters

Table 7.2 shows the parameters used in the pseudo-static studies. The soil parameters are based on the information in El-Emam (2003) presented in chapter 3 and the wall-soil friction angle (δ) is set according to what was found in the numerical study by Zarnani et al. (2011).

Table 7.2 Material parameters in the pseudo-static studies

Property	Value
Friction angle, ϕ	51°
Unit weight of soil, γ	15.7 kN/m ³
Wall-soil friction angle, δ	44°
Shear wave velocity, V_s	68.8 m/s
Primary wave velocity, V_p	112.4 m/s

7.3 Failure Surface

The predicted failure surfaces from extensometer measurements (inferred failure zones) are shown in Figure 7.2 a)-f). Figure 7.2 f) also includes the observed failure surface (also referred to as the ultimate failure surface), indicated by the triangular-dashed line. The figures also shows the predicted failure surfaces using the Mononobe-Okabe method (M-O), the horizontal slices method (HSM) and the critical surfaces calculated using the two-part wedge method (TPW). Please note that the calculated failure surfaces, using the M-O method and the linear HSM, are so similar that the indicated failure lines overlap for most of the illustrations. The safety factors (see section 6.3) used in the two-part wedge calculations are presented in Table 7.3.

Table 7.3 Safety factors used for the two-part wedge calculations

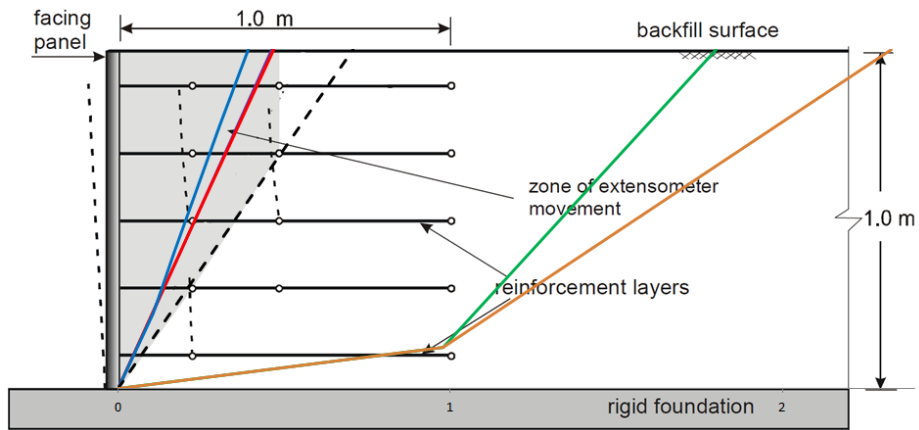
Pseudo-static coefficients (k_h^{spes})	TPW ($\lambda=0$)	TPW ($\lambda=1$)
0.0549	2.56	2.74
0.1663	2.03	2.15
0.3498	1.61	1.62
0.5163	1.33	1.34
0.8288	1.06	1.08
1.0154	1.0 (failure)	1.0 (failure)

The M-O method and the linear HSM overestimate the inclinations of the failure surface at the lower base acceleration amplitudes ($a_b \leq 0.40$ g, Figure 7.2 a)- d)), but these methods give the best prediction for the failure surface shape. At the higher amplitudes ($a_b > 0.40$ g) these methods under-predict the inclination of the failure surface.

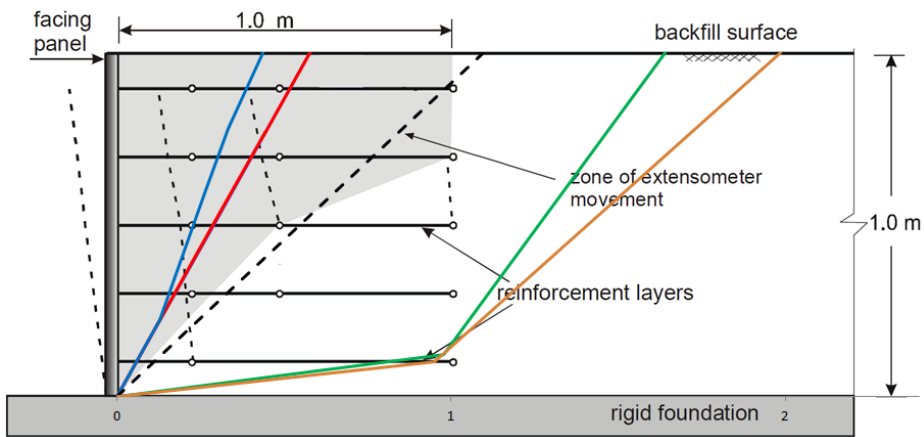
At a base input acceleration of about 0.60g, the shaking table model fails. The *ultimate failure surface* predicted using the TPW method (FS=1, see Table 7.3) with an inter-wedge shear mobilization of 0 fits reasonably well with the observed one. The same is not true for predictions using $\lambda=1$.

The TPW method generally predicts a failure surface that evolves (with increased higher base input acceleration amplitudes) by a reduction in the inclination of the first wedge; the point where the first and second wedge meets, only experiences small changes with increasing input amplitudes. At 0.50 g (Figure 7.2e)) and for $\lambda=0$, it is observed that there is an irregularity in the way the failure surface evolves. The TPW predicted failure surface “jumps” back and forth when the input base acceleration increases from 0.40 g to 0.50 g and back to 0.60 g, both with respect to the first wedge inclination and where the second wedge meets the first with respect to the lateral distance from the facing.

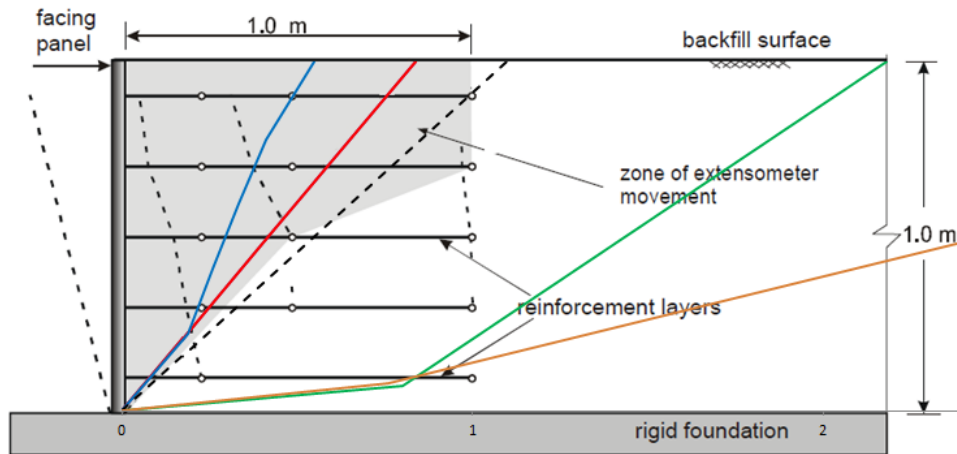
The failure surface predicted using the polylinear HSM does not resemble failure surface from El-Emam (2003) at any base input acceleration amplitudes.



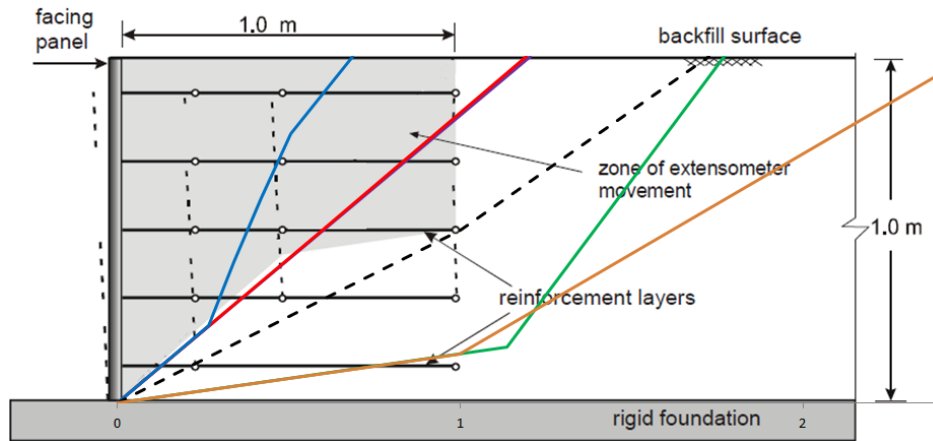
a) $a_b=0.05 \text{ g}$, $k_h^{\text{spes}}=0.0549$



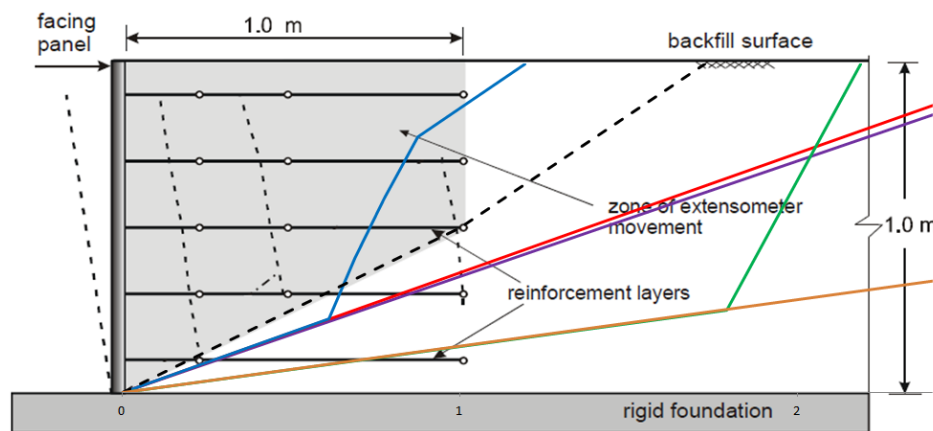
b) $a_b=0.15 \text{ g}$, $k_h^{\text{spes}}=0.1663$



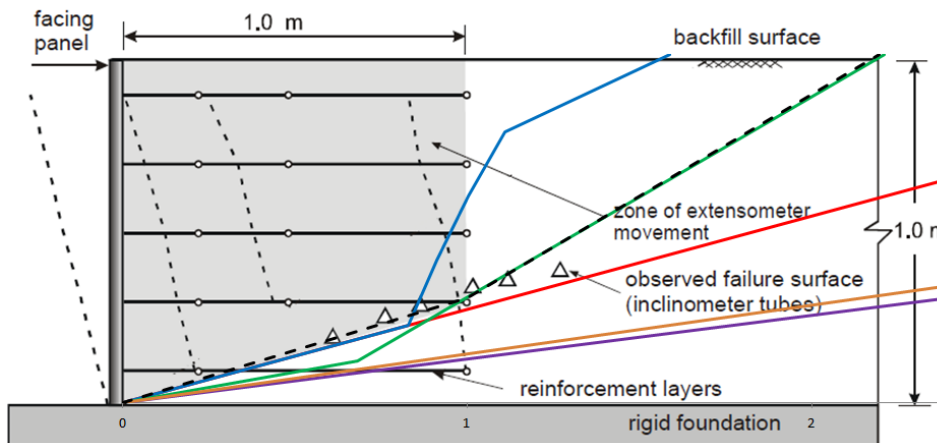
c) $a_b=0.30 \text{ g}$, $k_h^{\text{spes}}=0.3498$



d) $a_b=0.40\text{ g}$, $k_h^{spes}=0.5162$



e) $a_b=0.50\text{ g}$, $k_h^{spes}=0.8288$



f) $a_b=0.60\text{ g}$, $k_h^{spes}=1.0154$

- M-O
- Linear HSM
- Poly HSM
- Two-wedge ($\lambda=0$)
- Two-wedge ($\lambda=1$)
- - - Inferred failure zone

Figure 7.2 Observed and calculated failure surface geometry (El-Emam, 2003)
NOTE: The M-O and Linear HSM failure surface overlap in most of the illustrations above.

7.4 Earth Forces on the Retaining Wall

Figure 7.3 shows the earth forces on the retaining wall measured in the physical shaking-table model for different base input accelerations. The figure also shows the predicted horizontal active force acting on the retaining wall (P_{AE}) using the M-O, the HSM and the TPW method.

The M-O and the HSM predictions are in reasonable agreement with the measured values for input base accelerations up to 0.30g. For higher base amplitudes, these predictions overestimate the earth forces. P_{AE} predicted using polylinear HMS is in reasonable agreement with the measured values for all the studied base input acceleration amplitudes. The TPW method (both for $\lambda=0$ and $\lambda=1$) under-predicts the earth forces for all base input acceleration amplitudes.

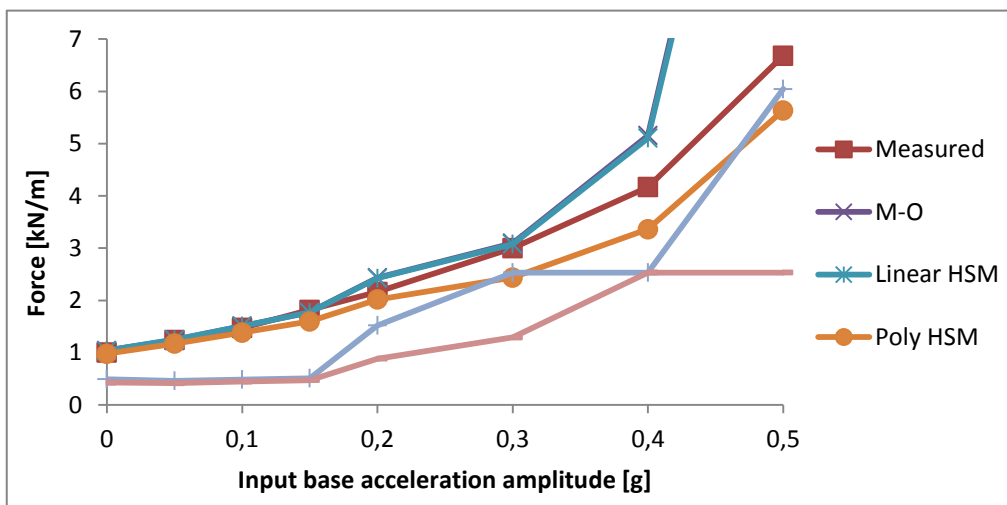


Figure 7.3 Total active earth force on the back of the facing.
NOTE: λ is denoted I in the figure

7.5 Comments and Discussions

An important assumption in pseudo-static theory is rigid soil behaviour. El-Emam & Bathurst (2004) showed that the entire wall system in the shaking table test does not move as a single body. Also, a single coefficient is used to represent the dynamic movement (k_h^{spes}). Thus, it is not reasonable to expect completely accurate predictions when using M-O, HSM and TPW. Even so, these methods are accurate in describing some aspects of the seismic loading on the retaining wall.

The numerical simulation conducted in this study and the numerical investigations by Zarnani et al. (2011) found that the failure mechanism evolves from a single to a two wedge mechanism as the base input acceleration increases. Since the TPW method is able to capture the two wedge mechanism, it is reasonable to expect this method to make a good prediction for the failure surface where this mechanism is fully developed (FS=1). A similar argument can be made to partly explain why the single wedge pseudo-static methods (M-O and linear HSM) gives the best prediction for the failure surface shape for the lower base input accelerations: The failure mechanism is a single wedge for the lower base input acceleration amplitudes.

Based on the results presented, these methods (M-O and linear HSM) seem useful for predictions up to acceleration amplitudes of 0.30g: The predicted and the physical failure surface shows the same tendency in how they develop (they have the same shape and becomes deeper with increasing amplitudes). The same is also observed in by Zarnani et al. (2011). Even so, it should be noted that the acceleration amplitude where the failure mechanism changes from a single wedge to a two wedge mechanism is not fixed and as shown previously (Chapter 5) it is influenced by the reinforcement properties. Thus, the “area” where these methods are applicable is not fixed, therefore an upper limit for use of these methods of 0.30 g cannot be assumed for all design situations.

As previously noted, the inter-wedge shear mobilization ratio (λ) lies between 0 and 1. In the results presented, there is a significant difference between results predicted using TPW with $\lambda=0$ and TPW with $\lambda=1$. But, the effects of λ has not been the focus in this study. Thus, investigations as to why $\lambda=0$ seems more suitable than $\lambda=1$ is not conducted. Additional information about the influence of λ can be found in Vieira (2008).

Both for $\lambda=0$ and $\lambda=1$, the TPW method accurately calculates at what base input amplitude failure occurs (FS=1, see Table 7.3). The TPW method ($\lambda=0$) prediction for the ultimate failure surface is accurate when compared to the one observed in the physical experiment (FS=1, $a_b=0.60g$). Also, the predicted P_{AE} using the TPW method ($\lambda=0$) is in reasonable compliance with the measured values. Even so, the TPW ($\lambda=0$) prediction is not accurate for lower base input acceleration amplitudes (FS>1, $a_b<0.60g$) and the predicted failure surface “jumps” back and forth; there is no clear tendency of how the mechanism develops. Thus, it is not possible to exclude the possibility that the compliance between the predicted ultimate failure surface using TPW ($\lambda=0$) and the observed failure surface is a coincidence.

The polylinear HSM method does not account for the moment equilibrium. Thus, the force in the horizontal direction might be reasonable and at the same time the inclination of the failure surface might be wrong. A better result for the predicted failure surface using the polylinear HSM is believed to be obtained if the moment equilibrium was satisfied in this approach. It should also be noted that

the polylinear HSM does not take the reinforcement length or stiffness in to consideration, thus making it unable to account for changes to these parameters.

7.6 Summary of the Pseudo-Static Analysis of the Shaking Table Experiments at RMC

This chapter describes the results of pseudo-static calculations using specific pseudo-static coefficients and the Mononobe-Okabe, the horizontal slices and the two-part wedge method. The calculations were carried out using MATLAB and the included results focuses on the failure surface geometry and total earth force on the back of the facing panel.

Furthermore, the major findings in this chapter were:

- This study has found notable differences in using the different pseudo-static methods. Neither the Mononobe-Okabe, nor the horizontal slice, or the two-part wedge method is able to predict both the failure surface and the earth forces for a wide range of acceleration amplitudes (0-0.60 g).
- The single wedge pseudo-static methods proved suited for calculating the failure surface and earth pressures for lower acceleration amplitudes (up to 0.30 g) in the physical model, but the failure depth is generally predicted as too shallow. But, it is noted that because these methods are unable to account for e.g. reinforcement stiffness, this is not necessarily true for all design situations.
- There are indications that the two-part wedge method is suited for predicting the ultimate failure surface, but further studies are needed to confirm this since no clear tendency in development of the predicted failure surface is observed.
- The polylinear HSM proves suited for predicting the total earth forces up to acceleration amplitudes of 0.60g, but are unable to account for reinforcement length or stiffness.

8 Pseudo-static Analysis: Different Guidelines

As noted in the introduction to the pseudo-static methods in chapter 6, “selecting appropriate seismic coefficients is the most challenging part of the pseudo-static analysis”. This chapter studies the horizontal pseudo-static coefficient effect on the Mononobe-Okabe method, but also the results from predictions using the polylinear horizontal method are presented. The first part of this chapter is a short presentation of relevant design codes (i.e. Eurocode 8, FHWA(2001)/AASHTO(2002) and PIANC(2001)) suggestions for the horizontal pseudo-static coefficient. This is followed by a study of the accuracy of these codes. This study is the basis for a proposal of a new way of determining the horizontal pseudo-static coefficient presented in the last part.

8.1 Guidelines for the Horizontal Pseudo-Static Coefficient

8.1.1 Eurocode 8

Eurocode 8: Part 5 (EC8) dictates that one shall use the following values for the horizontal seismic coefficient if specific values are not known

$$k_h^{EC} = \frac{S}{r} \alpha \quad (8.1)$$

Where α is the ratio of the design ground acceleration (a_g) on firm rock to the acceleration of gravity (g), i.e. $\alpha = a_g/g$. In this study, a_g is set equal to the amplitude of the input base acceleration (a_b).

The soil factor (S) is 1.6 for soft to medium firm cohesionless soils. Details' regarding the factor r are given in the following table and are valid for retaining walls up to 10 meter s high.

Table 8.1 Factor for calculation of the horizontal seismic coefficient according to the Eurocode

Type of retaining structure	r
Free gravity walls that can accept a displacement (d_r) up to $d_r=300\alpha S$ (mm)	2
Free gravity walls that can accept a displacement (d_r) up to $d_r=200\alpha S$ (mm)	1,5
Flexural reinforced concrete walls, anchored or braced walls, reinforced concrete walls founded on vertical piles, restrained basement walls and bridge abutments	1

8.1.2 FHWA(2001)/AASHTO(2002)

The Federal Highway Administration (FHWA, 2001) and the American Association of State Highway and Transportation Officials (AASHTO, 2002) proposes the same equation for calculating the horizontal seismic coefficient;

$$k_h^{FHWA} = \left(1.45 - \frac{a_{max}}{g}\right) \frac{a_{max}}{g} \quad (8.2)$$

Where a_{max} is taken as the Peak Ground Acceleration (PGA). In this study a_{max} is taken as the amplitude for the horizontal input base acceleration measured on the top of the retaining wall (i.e. $AF \cdot a_{base}$, see section 7.1).

8.1.3 PIANC (2001)

The Permanent International Association for Navigation Congresses (PIANC, 2001) suggest using the following formula for the horizontal seismic coefficient

$$k_h^{\text{PIANC}} = 0.5 \left(\frac{a_{\max}}{g} \right) \quad (8.3)$$

Where a_{\max} is as in FHWA(2001)/AASHTO(2002).

8.2 Predictions using EC8, PIANC (2001) and FHWA(2001)/AASHTO(2002)

8.2.1 Assumptions and Limitations

This chapter is only concerned with base input acceleration amplitudes up to 0.30 g. The values used for the horizontal seismic coefficient (k_h^{spes}), have so far been directly based on the peak acceleration measured on the shaking table backfill surface, and the maximum k_h^{spes} have been calculated as 1.0154. This is an unrealistic value to be used in real life earthquake engineering where k_h values over 0.30 are seldom used (Table 6.2), e.g. the FHWA (2001) and AASHTO (2002) do not use limit-equilibrium pseudo-static methods for sites with peak horizontal ground accelerations above $\sim 0.30g$.

M-O is used for evaluating the different codes with respect to the failure surface. Regarding the predicted active earth forces; results from M-O and polylinear HSM are discussed. Note that the same material parameters used in chapter 7 (see Table 7.2) are used in the following calculations. Also note that specific values for the horizontal pseudo-static coefficients are given in Appendix 3.

8.2.2 Failure Surface

The predicted failure surfaces using Mononobe-Okabe are presented in Figure 8.2 for different base input acceleration amplitudes. The different predictions are performed using codes described above (Eurocode 8, PIANC (2001) and FHWA (2001)/AASHTO(2002) respectively). Included in the figure are also predictions using k_h^{spes} and the failure surfaces measured by El-Emam (2003). All the studied approaches (different codes) predicts too shallow failure surfaces compared to what is measured in the physical model. Zarnani et al. (2011) found a same underestimation of the failure surface using FHWA (2001)/AASHTO (2002).

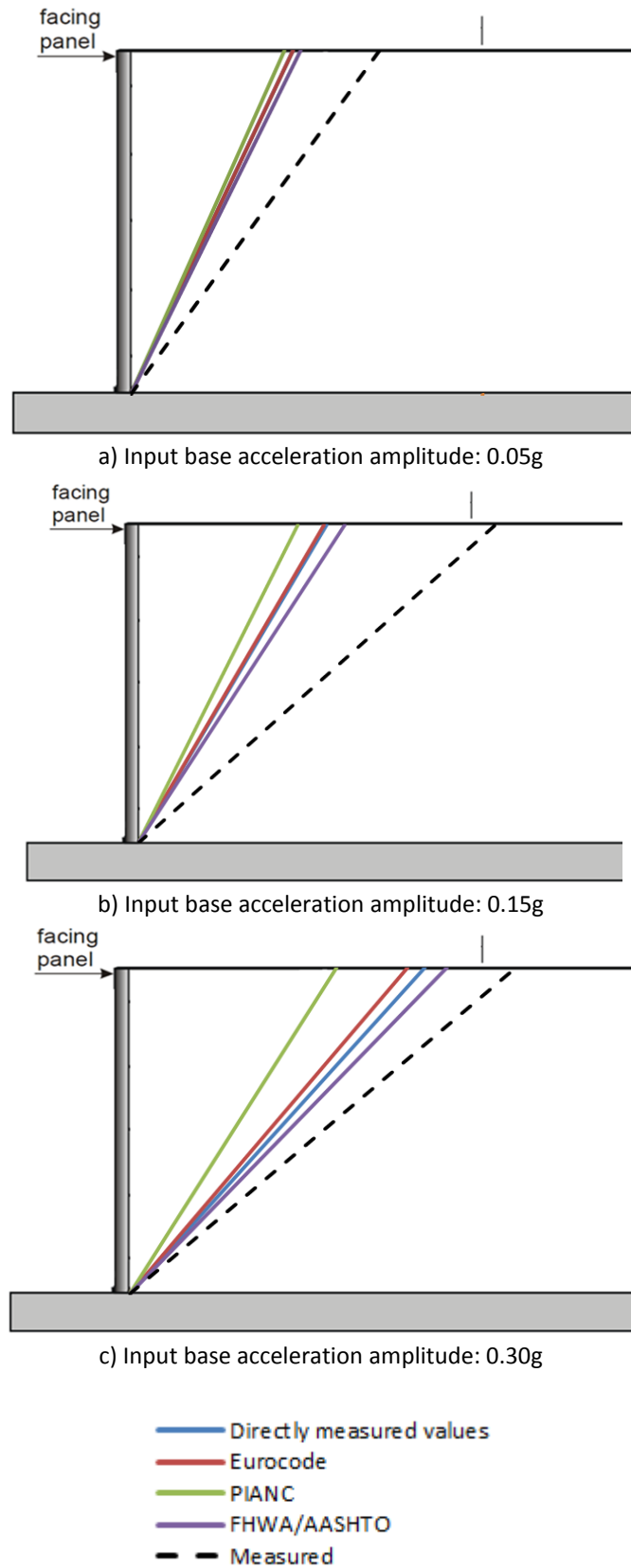


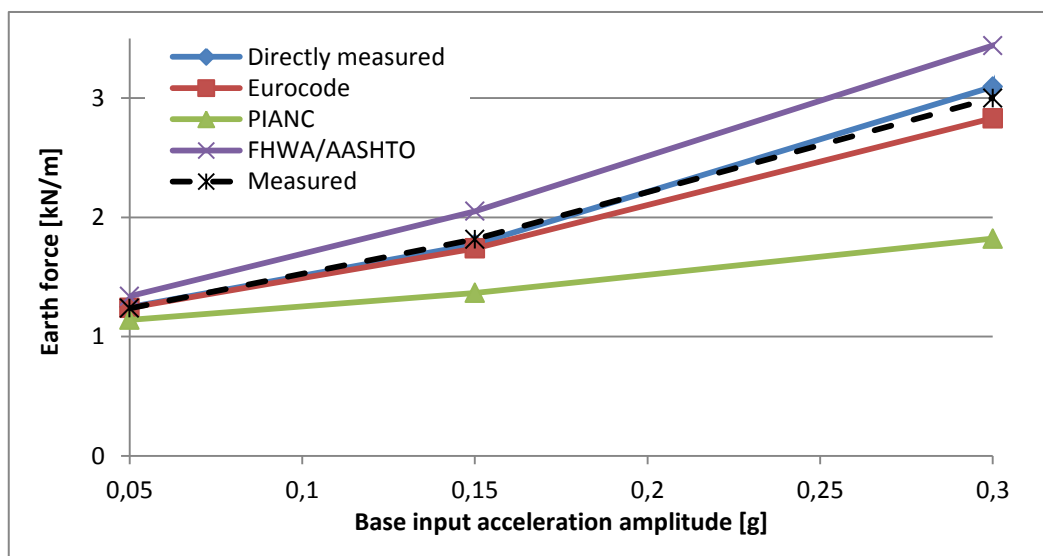
Figure 8.1 Predicted failure surfaces using M-O and Eurocode 8, PIANC (2001) and FHWA(2001)/AASHTO(2002) (El-Emam, 2003)

8.2.3 Earth Forces

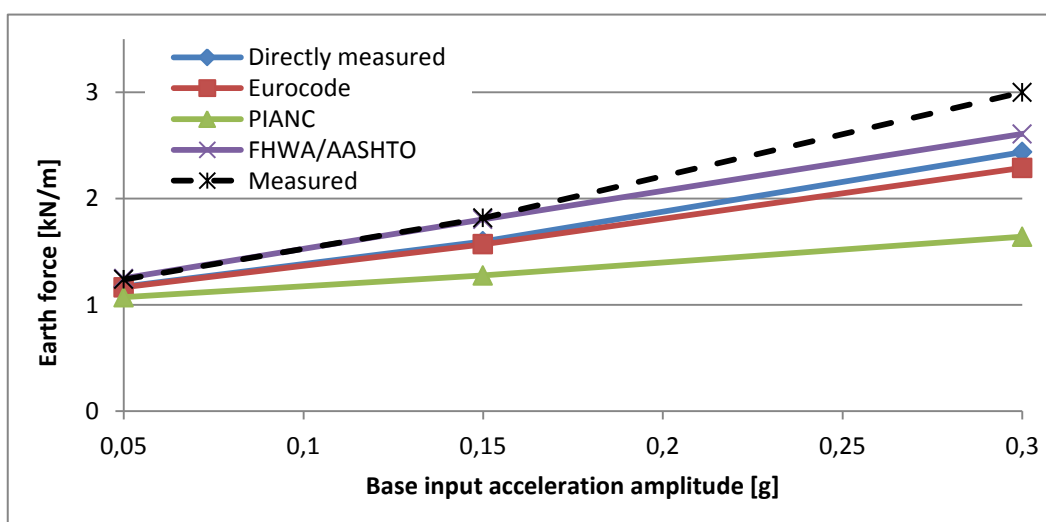
The predicted active earth forces calculated using the different design code guidelines for the horizontal pseudo-static coefficient are presented in Figure 8.2 for different base input acceleration amplitudes. Included are also measured values from the shaking table model (El-Emam, 2003).

Figure 8.2 a) presents data for predictions of the active earth forces using the M-O method. Results referred to as “Directly measured” and “Eurocode” (predicted using k_h^{spes} and k_h^{EC} respectively) are in reasonable good agreement with the measured values. FHWA (2001)/AASHTO (2002) estimations are conservative, e.g. at a base input amplitude of 0.30 g forces are overestimated by 44%. Predictions using PIANC (2001) under predict earth forces on the retaining wall.

When using the Polylinear HSM, all the suggested horizontal pseudo-static coefficients leads to a underestimation of the forces on the retaining wall (Figure 8.2b)). FHWA (2001)/AASHTO (2002) guidelines prove to be most accurate, but the forces are underestimated by 13 % for base input amplitude of 0.30g. Also here the predictions using PIANC (2001) guidelines are the least accurate.



a) Mononobe-Okabe



b) Polylinear HSM

Figure 8.2 Predicted active earth forces using Eurocode, PIANC and FHWA/AASHTO (El-Emam, 2003)

8.2.4 Observations

The horizontal pseudo-static coefficients suggested in the various codes are less suited for calculating the forces using the polylinear HSM than the M-O method. This suggests is that one pseudo-static coefficient is not necessarily well suited for use in different pseudo-static method, i.e. different methods require different guidelines for the pseudo-static coefficients.

FHWA (2001)/AASHTO (2002) prove best suited for predicting both the earth force and failure surface. The predicted active earth pressures are conservative and the predicted failure surface is closest to the ones measured in the physical model.

8.3 Predictions using ABC-coefficient

A new horizontal pseudo-static coefficient (k_h^{ABC-MO}) is suggested when calculating the failure surface and active earth force using the Mononobe-Okabe method (see equation 9.5). It is based on FHWA (2001)/AASHTO (2002) guidelines since these were found to be the most accurate:

$$k_h^{ABC} = (1.45A - \frac{a_{max}}{g}B) \frac{a_{max}}{g}C \quad (8.4)$$

where a_{max} is the Peak Ground Acceleration (PGA). A, B and C are constants.

FHWA (2001)/AASHTO (2002) guidelines under-predict the depth of the failure surface and slightly over-predict the earth force, i.e. k_h^{FHWA} is both too low and too high. Ideally k_h^{ABC-MO} should account for both these observations and thus predict a deeper failure surface and a lower earth force, but this is not possible with only one parameter. Thus, the following requirements were used to make it possible to find a suitable guideline for the pseudo-static coefficient:

- The predicted failure surface shall not under- or overestimate the failure surface with more than 20 % with regards to measured surfaces in El-Emam (2003).
- The predicted earth forces shall be conservative, i.e. higher than the measured values in El-Emam (2003).

The effects of A, B and C on the predicted inclination of the failure surface and active earth forces predicted using M-O were studied (Appendix 4). The observations made there, together with a trial procedure, lead to the following suggestion for calculating the horizontal pseudo-static coefficient:

$$k_h^{ABC-MO} = (1 - 1.3 \frac{a_{max}}{g}) (3.4 \frac{a_{max}}{g}) \quad (8.5)$$

8.3.1 Failure Surface

The predicted failure surface calculated using k_h^{ABC-MO} is presented in Figure 8.2 for different base input acceleration amplitudes. Included are also observed failure surfaces from the shaking table model (El-Emam, 2003) and predicted ones using FHWA (2001)/AASHTO (2002). Compared FHWA (2001)/AASHTO (2002), estimations using k_h^{ABC-MO} give a more accurate estimate for the failure surface for base acceleration amplitudes up to 0.30g.

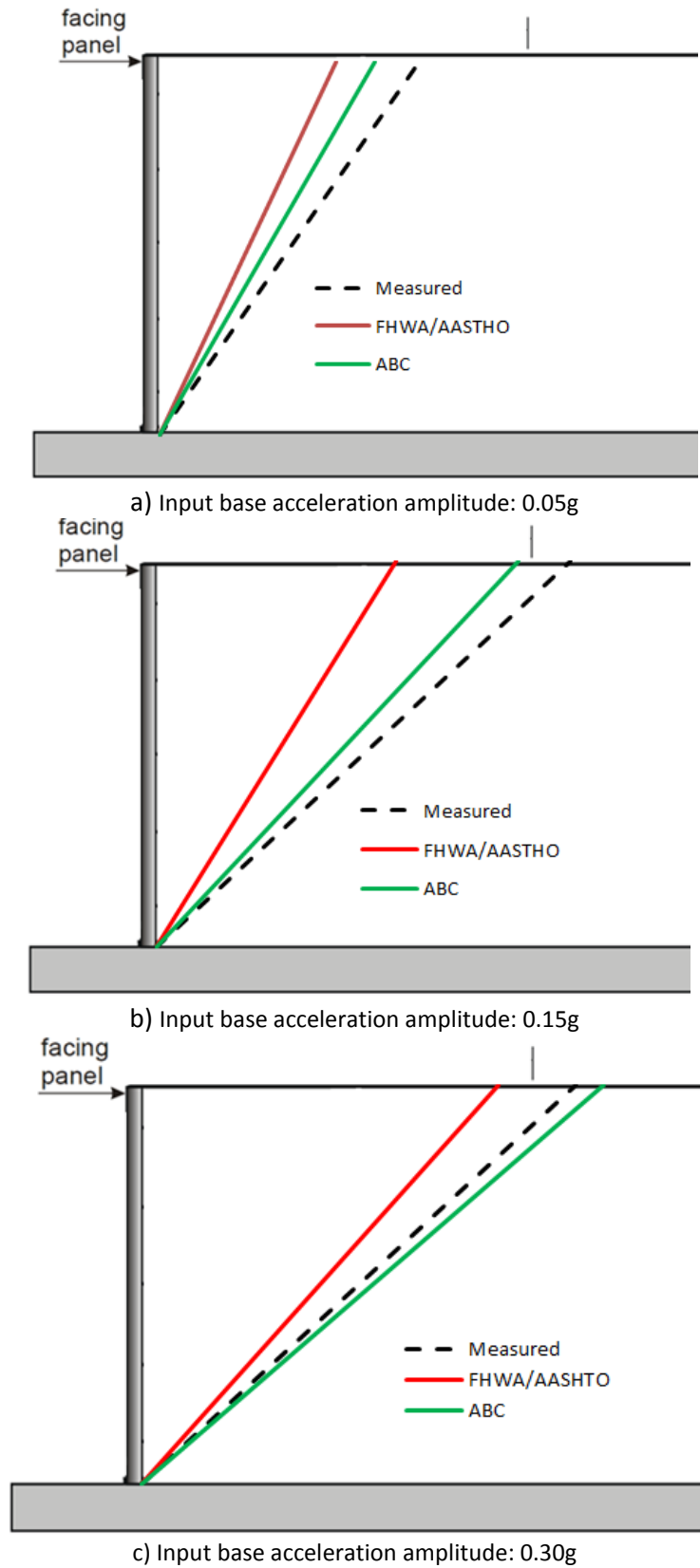


Figure 8.3 Failure surface predicted using k_h^{ABC-MO}

8.3.2 Earth Forces

In Figure 8.4 the predicted active earth forces using both FHWA (2001)/AASHTO (2002) guidelines and k_h^{ABC-MO} are presented for different base input accelerations. Included are also measured values from El-Emam (2003). The earth forces are generally over-predicted when using k_h^{ABC-MO} , up to two times the measured value at 0.15 g.

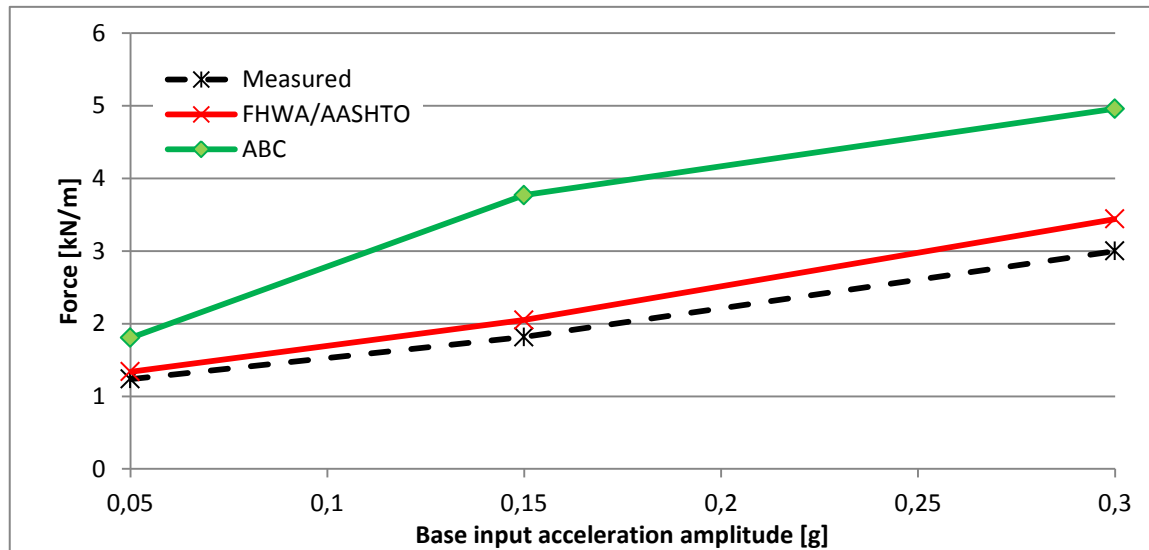


Figure 8.4 Active earth forces calculated using k_h^{ABC-MO}

8.4 Comments and Discussions

The main advantage of using k_h^{ABC-MO} when calculating the M-O failure surface is that the accuracy of the predicted failure surface is notably improved compared to other guidelines. Thus, the required reinforcement length estimation is improved. This contributes to a more secure seismic retaining wall design. Since the use of k_h^{ABC-MO} leads to an overestimation of the earth forces, it will lead to a more expensive earthquake design. The increased design forces will lead to the use of more resilient reinforcements and facing design.

The major issue with respect to the reliability of the proposed pseudo-static value is that the experimental data that it is based on is very limited; only a single shaking table model is studied. Furthermore, only two features of the shaking table model results are studied (predicted failure surface and active earth force). The need for further studies of reduced scale models is therefore necessary to prove the accuracy of this parameter. Thus, the proposed pseudo-static coefficient should be viewed as the start of a further development of the guidelines in FHWA (2001)/AASHTO (2002), i.e. a further optimisation of the three parameters (A, B and C respectively) is possible.

Equation 8.4 is basically a generalised expression for k_h^{ABC-MO} . By introducing a specific set of A, B and C's for the different pseudo-static methods (e.g. M-O, HSM and TPW method), k_h^{ABC} might be adapted for a variety of different pseudo-static methods. This might simplify the notations in design guidelines concerned with multiple methods and help making them more applicable.

8.5 Summary of the Pseudo-Static Analysis using Different Guidelines

This chapter presents the proposed horizontal pseudo-static coefficient from different guidelines (Eurocode 8, PIANC (2001) and FHWA(2001)/AASHTO(2002) respectively) and studies how suitable these guidelines are for predicting the failure surface and active earth forces for the shaking table test performed by El-Emam (2003) by using M-O method and HSM. Based on this study a new pseudo-static coefficient is suggested for use in the Mononobe-Okabe method (k_h^{ABC-MO}). The base input acceleration amplitudes (peak acceleration amplitudes) studied here range from 0.05 to 0.30g.

The major conclusions this chapter:

- FHWA (2001)/AASHTO (2002) is best suited for predicting the failure surface and active earth forces compared to the other design codes, but like the other codes it significantly underestimates the failures surface depth.
- The different pseudo-static methods require individually tailored guidelines for the pseudo-static coefficients, i.e. one k_h is not necessarily suited for use in multiple pseudo-static methods (e.g. M-O and HSM).
- Predictions using k_h^{ABC-MO} (and M-O) for the failure surface are more accurate than predictions using FHWA(2001)/AASHTO(2002), PIANC(2001) and Eurocode 8.
- Predictions using k_h^{ABC-MO} (and M-O) for the earth forces are very conservative; the earth forces are heavily overestimated.
- Further data is needed to verify k_h^{ABC-MO} .

9 Summary and Conclusions

The focus of this study is numerical and analytical design of geo-synthetic reinforced soil walls under dynamic loading. The major components are:

- Development and verification of a numerical PLAXIS model using physical model data to simulate the behaviour of a reduced-scale shaking test.
- A numerical parameter study of the effects of reinforcement length and strength on the failure surface, facing displacements and reinforcement loads.
- A comparison of the physical model results with the Mononobe-Okabe, horizontal slices and two-part wedge method.
- A comparison of different codes for seismic design using the Mononobe-Okabe method
- A suggestion for selecting the horizontal pseudo-static coefficient to improve design using the Mononobe-Okabe methods.

In this chapter, the final conclusions of this thesis are presented. Also, the major limitations and suggestions to future studies are presented.

9.1 Limitations

General limitations:

- The major limitation in this study is that *only* a single reduced-scale shaking table model is used as background for the numerical and pseudo-static investigations (and simulations).
- Only horizontal excitation is considered.
- Cohesion and effects of wet soil are neglected; the backfill soil is dry and cohesionless.

Limitations in the numerical simulations and in the numerical results:

- The hardening soil model is not able to account for softening due to soil dilatancy and effects due to cyclic loading.
- Data from triaxial and oedometer testing on the backfill material is not available.
- The effects of numerical instability on the numerical results are unknown since a sensitivity study is not conducted.
- Specific details concerning the initial excitation of the physical model experiment is unknown.

Limitations concerning the pseudo-static predictions:

- Investigations of the accuracy of different pseudo-static methods are limited to the Mononobe-Okabe, horizontal slices and two-part wedge method.
- Concerning the Horizontal Slices Method; the simple formulation by Choudhury et al. (2006) and Ahmad & Choudhury (2008) is used, i.e. moment equilibrium is not considered.
- The investigation of current design codes is limited to FHWA (2001)/AASHTO (2002), PIANC (2001) and Eurocode 8.
- Only active earth forces have been considered.

9.2 Conclusions

The final conclusions are:

- A numerical model has been developed using PLAXIS 2D Dynamics and verified using a reduced-scale shaking table model. PLAXIS 2D Dynamics proved capable of creating a numerical model based on results of physical experiments, but there are significant limitations to this model. Therefore, the developed model is only suitable for simulating soil and retaining wall behaviour up to a base input acceleration amplitude of 0.30g.
- A lowering of the axial stiffness and/or a shortening of the reinforcement length, leads to an earlier development of the two-wedge failure mechanism. Also, the failure surface becomes shallower and the magnitude of the facing displacements is reduced with increasing axial stiffness and reinforcement length.
- No conclusive results were found concerning the effect of reinforcement stiffness and length on the reinforcement loads.
- The numerical parameter study suggests that pseudo-static methods that do not account for key reinforcement properties (e.g. the Mononobe-Okabe and the horizontal slices method) are not suited for use in seismic design where an accurate prediction of the failure surface is vital.
- The accuracy of pseudo-static models has been studied using programmes developed in MATLAB. This study has shown large variations between, and in, the accuracy of the Mononobe-Okabe, horizontal slices and two-part wedge method for predicting active earth forces and the failure surface for different acceleration amplitudes.
- Neither the Mononobe-Okabe, nor the horizontal slice, or the two-part wedge method is able to predict both the failure surface and the earth forces for a wide range of acceleration amplitudes (0-0.60 g). The different methods are best suited for predictions either before or after the development of the two-wedge failure mechanism.
- The single-wedge pseudo-static methods (Mononobe-Okabe and linear horizontal slices method) are suitable for predicting the failure surface *shape* up to the critical acceleration (in this study, approximately 0.30 g), but when using guidelines in FHWA (2001)/AASHTO (2002), Eurocode 8 and PIANC (2001) the failure surface depth is under-predicted.
- Single-wedge pseudo-static methods are reasonably accurate in predicting the active earth forces for the physical model for acceleration amplitudes up to acceleration amplitudes of 0.30 g.
- The two-part wedge method is able to predict the ultimate failure using $\lambda=0$, but is not possible to exclude the possibility that this is coincidence. Thus, the two-part wedge method might be accurate in calculating the ultimate failure surface, but further studies are needed to confirm this.

- The polylinear HSM are reasonably accurate for predicting the total earth forces for a wide range of acceleration amplitudes, but is not suited for predicting the failure surface. Special consideration should be taken when using this pseudo-static model since it is unable to account key reinforcement parameters (e.g. reinforcement length and strength).
- A review of current guidelines or seismic design has shown that: FHWA (2001)/AASHTO (2002) guidelines for the horizontal pseudo-static coefficient give more accurate predictions (for both the failure surface and earth forces) than PIANC (2001) and Eurocode 8, when using the Mononobe-Okabe method.
- On the basis of this review, a simple pseudo-static coefficient has been proposed. This coefficient has been shown to give better estimations for the failure surface than FHWA (2001)/AASHTO(2002), but use of this leads to an overestimated active earth force.

9.3 Possible Future Work

The following work is suggested as a continuation of the work in this thesis:

- The numerical model should be subjected to a more detailed sensitivity study to test the robustness of the numerical results.
- The numerical model could be developed further, either using PLAXIS 2D Dynamics or an alternative finite element program (e.g. ABAQUS FEA), by incorporating soil softening in the material model.
- Verification of the Mononobe-Okabe, horizontal slices and two-part wedge method using the developed numerical model, this should also include vertical acceleration.
- Verification of the Mononobe-Okabe, horizontal slices and two-part wedge method using other physical models.

10 References

- AASHTO, A. A. o. S. H. a. T., 2002. *AASHTO*, Washington, DC: Standard Specifications for Highway Bridges.
- Ahmad, S. M. & Choudhury, D., 2008. Pseudo-dynamic approach of seismic design for waterfront reinforced soil-wall. *Geotextiles and Geomembranes* 26, 8 February , pp. 291-301.
- Auleda, M., 2011. *Upcommons UPC*. [Online]
Available at: <http://upcommons.upc.edu/pfc/bitstream/2099.1/3423/13/40055-13.pdf>
[Accessed 03 06 2012].
- Ausilio, E., Conte, E. & Dente, G., 2000. Seismic stability analysis of reinforced slopes. *Soil Dynamics and Earthquake Engineering*, 27 January, pp. 159-172.
- Bathurst, R. & Hatami, K., 1998. Seismic response analysis of a geosynthetic reinforced retaining wall. *Geosynthetics International*, 5, - -, pp. 127-166.
- bv, P., Version 1. *PLAXIS-GiD Materail Models Manual*, Delft, The Netherlands: Plaxis bv.
- Cai, Z. & Bathurst, R., 1996. Seismic-induced permanent displacement of geosynthetic-reinforced semental retaining walls. *Canadian Geotechnical Journal*, - -, pp. 937-955.
- Caltabiano, S., Cascone, E. & Maugeri, M., 2000. Seismic stability of retaining walls with surcharge. *Soil Dynamics and Earthquake Engineering*, - December, pp. 469-476.
- Choudhury, D., Nimbalkar, S. S. & Mandal, J., 2006. Comparison of Pseudo-Static and Pseudo-Dynamic Methods for Seismic Earth Pressure on Retaining Wall. *Jorunal - Indiam Geophysical Union Vol.10, No.4*, - October, pp. 263-271.
- Dowrick, D., 1977. *Earthquake resistant design*. 1. red. Berkeley, California: John Whiely & Sons, Ltd..
- El-Emam, M. M., 2003. *PhD Thesis: Behaviour of Reinforced Soil Walls under Earthquake Loading*. - red. Kingston, Ontario, Canada: Queen's University.
- El-Emam, M. M. & Bathurst, R. J., 2004. Experimental design, instrumentation and interpretation of reinforced soil wall response using a shaking table. *International Journal of Physical Modelling in Geotechnics*, - -, pp. 13-32.
- El-Emam, M. M. & Bathurst, R. J., 2005. Facing contribution to seismic response of reducedscale reinforced soil walls. *Geosynthetics International*, 10 July, pp. 215-238.
- El-Emam, M. M. & Bathurst, R. J., 2007. Influence of reinforcement parameters on the seismic response of reduced-scale reinforced retaining walls. *Geotextiles and Geomembranes* 25, - -, pp. 33-49.
- European committee for standardization , 2004. *Eurocode 8: Design of structures for ertquake resistande Part 5: Foundations, retaining structures and geotechnical aspects*, Brussels: In Norway; Standard Norge .

- Fakher, A., Nouri, H. & Shahgholi, M., 2002. Limit equilibrium in reinforced soil walls subjected to seismic loads. *Proceedings of the Third Iranian International Conference on Geotechnical Engineering and Soil Mechanics*, pp. 281-286.
- FHWA, 2001. *Mechanically stabilized earth walls and reinforced soil slopes: design and construction guidelines*, Washington, DC, USA: Federal Highway Administration and National Highway Institute.
- Hatami, K. a. B. R., 2000. Effect of structural design on fundamental frequency of reinforced-soil retaining walls. *Soil Dynamics and Earthquake Engineering* 19, 5 March, p. 137–157.
- Hatami, K. & Bathurst, R., 2000. Effect of structural design on fundamental frequency of reinforced-soil retaining walls. *Soil Dynamics and Earthquake Engineering*, 19, - -, pp. 137-157.
- Haugen, E., 2011. *Master's thesis: Earthquake response of retaining walls*, Trondheim: NTNU.
- Holst, M., 2011. *Prosjektoppgave i TBA4510 Geoteknikk FDP: Samvirke mellom jord og konstruksjon*, Trondheim: NTNU.
- Iai, S., 1989. Similitude for Shaking Table Tests on Soil-Structure-Fluid Model in 1g Gravitational Field. *Soils and Foundations Vol. 29*, - -, pp. 105-118.
- Itasca Consultion Group, 2001. *FLAC - Fast Lagrangian Analysis of Continua*. Minneapolis U.S.A.: Itasca Consultion Group.
- Kanade, P. & Gakki, D., 1997. *Dynamic analysis and earthquake resistant design: Strong motion and dynamic properties, Volume 1*. Tokyo: Gihodo Shuppan Co Ltd..
- Kramer, S. L., 1996. *Geotechnical Earthquake Engineering*. Upper Saddle River, New Jersey 07458: Prentice-Hall, Inc..
- Ling, H. & Leshchinsky, D., 1998. Effects of vertical acceleration on seismic design og geosynthetic-reinforced soil structures. *Géotechnique* 48 No. 3, pp. 347-373.
- Liu, M. & Gorman, D., 1995. Formulation of Rayleigh Damping and Its Extensions. *Computers & Structures Vol. 57*, - February , pp. 277-285.
- Li, X. & Aguilar, O., 2000. Elastic Earth Pressure on Rigid Walls Under Earthquake Loading. *Journal of Earthquake Engineering*, 4 5, pp. 415-435.
- Madabhushi, S., 1990. *Numerical simulation of initial celocity/displacement conditions i a dymamic centrifuge test*. Cambridge U.K.: Cambridge University.
- McCarthy, D. F., 1998. *Essentials of Soil Mechanics and Foundations*. 5. red. Columbus, Ohio: Prentice hall.
- Melo, C. & Sharma, S., 2004. *SEISMIC COEFFICIENTS FOR PSEUDOSTATIC SLOPE ANALYSIS*. Vancouver, B.C., Canada, 13th World Conference on Earthquake Engineering.
- Nordal, S., 2011. *Geotechnical Engineering, Advanced Course - Lecture notes and background material*, Trondheim: NTNU - Geotechnical Division.

- NORSAR Engineering, 2011. *EC8 Regulations for Structural Design*. [Online]
Available at: <http://www.norsar-engineering.com/sd.php>
[Accessed 3 June 2012].
- Nouri, H., Fakher, A. & Jones, C. J. F. P., 2005. Development of Horizontal Slice Method for seismic stability analysis of reinforced slopes and walls. *Geotextiles and Geomembranes*, 29 November, pp. 175-187.
- PIANC, 2001. *Seismic Design Guidelines for Port Structures*, Balkema, Rotterdam: Permanent International Association for Navigation Congresses.
- Plaxis bv, 2010. *Dynamics manual Version 9.0*. [Online]
Available at: <http://ebookbrowse.com/plaxis-2d-v9-0-7-dynamics-manual-pdf-d321363898>
[Accessed 1 June 2012].
- Plaxis bv, 2011. *PLAXIS 2D*. Delft, The Netherlands: Plaxis bv.
- Plaxis bv, 2011. *Plaxis 2D Reference Manual*. Delft, The Netherlands: Plaxis bv.
- Plaxis, 2011. *Plaxis Materials model manual*, Delft, the Netherlands: Plaxis bv.
- Reddy, G. N. & Madhav, M. R. E. S., 2008. Pseudo-static seismic analysis of reinforced soil wall - Effect of oblique displacement. *Geotextiles and Geomembranes* 26, 13 February, pp. 393-403.
- Schanz, T., Vermeer, P. A. & Bonnier, P. G., 1999. *The hardening soil model: Formulation and verification*. Rotterdam: Beyond 2000 in Computational Geotechnics.
- Shahgholi, M., Fakher, A. & Jones, C. J. F. P., 2001. Horizontal slice method of analysis. *Géotechnique*, 8 August, pp. 881-885.
- Shukla, S. K., Bathurst, R. J., Hatami, K. & Alfaro, M. C., 2002. *Geosynthetics and their application Ch. 14. Geosynthetic-reinforced soil walls and slopes - seismic aspects*. 1 red. London: Thomas Telford Publishing .
- Strømmen, E. N., 2010. Auto spectral density. I: E. N. Strømmen, red. *Theory of Bridge Aerodynamics*. 2 red. Trondheim: Springer-Verlag, pp. 32-35.
- Strømmen, E. N., 2010. *Theory of Bridge Aerodynamics 2ed*. Trondheim: Springer-Verlag.
- Terzaghi, K., 1951. Mechanism of landslides. *Geological Society of America*, - -, pp. 83-123.
- The Mathworks, Inc., 2011. *MATLAB R2011a*, Kista, Sweden: The Mathworks, Inc..
- Vieira, C., 2008. *Geosynthetic reinforced soil retaining walls and slopes. Seismic behaviour and design methodologies*. Ph.D Thesis, Porto: University of Porto, Portugal.
- Waterman, D., 2006. *Structural elements in Plaxis: Structural elements and excavations*. Chile: Plaxis BV.
- Zarnani, S. & Bathurst, R. J., 2009. Influence of constitutive model on numerical simulation EPS seismic buffer shaking table tests. *Geotextiles and Geomembranes*, 27(4), - 4, pp. 308-312.

Zarnani, S., El-Emam, M. M. & Bathurst, R. J., 2011. Comparison of numerical and analytical solutions for reinforced soil wall shaking table tests. *Geomechanics and Engineering*, Vol. 3, No. 4, 16 November, pp. 291-321.

Zarrabi-Kashani, K., 1979. *MSc paper: Sliding of Gravity Retaining Wall During Earthquakes Considering Vertical Acceleration and Changing Inclination of Failure Surface*. Massachusetts: Massachusetts Institute of Technology.

Appendixes

Appendix 1 – Reinforcement connection loads

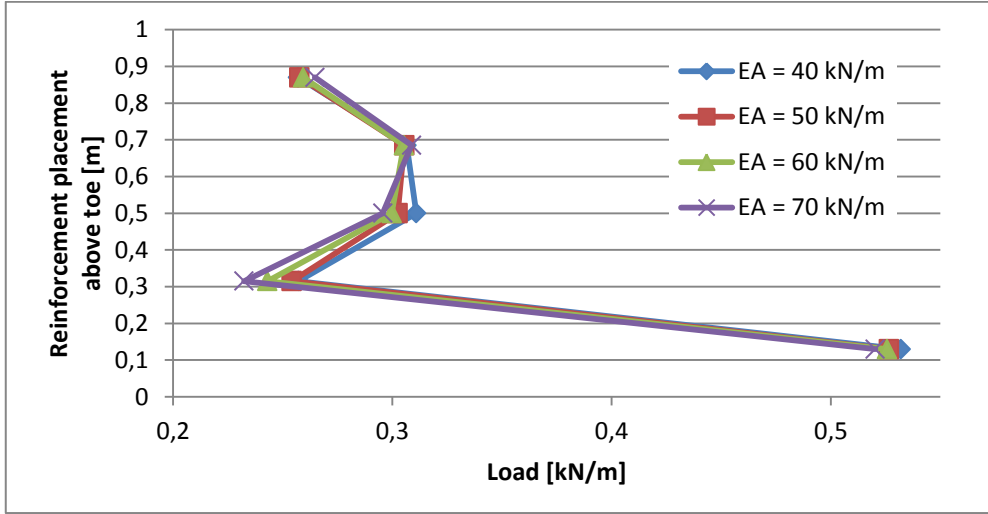
Appendix 2 – Pseudo-static methods – MATLAB code

Appendix 3 – Horizontal Pseudo-static Coefficients from Current Seismic Design Codes

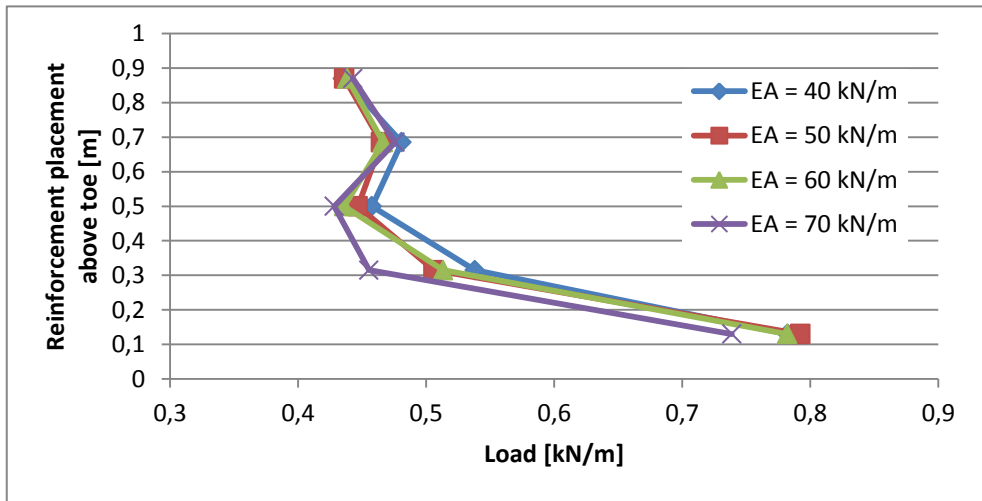
Appendix 4 – Effect of Changing A, B and C

Appendix 1 – Reinforcement connection loads

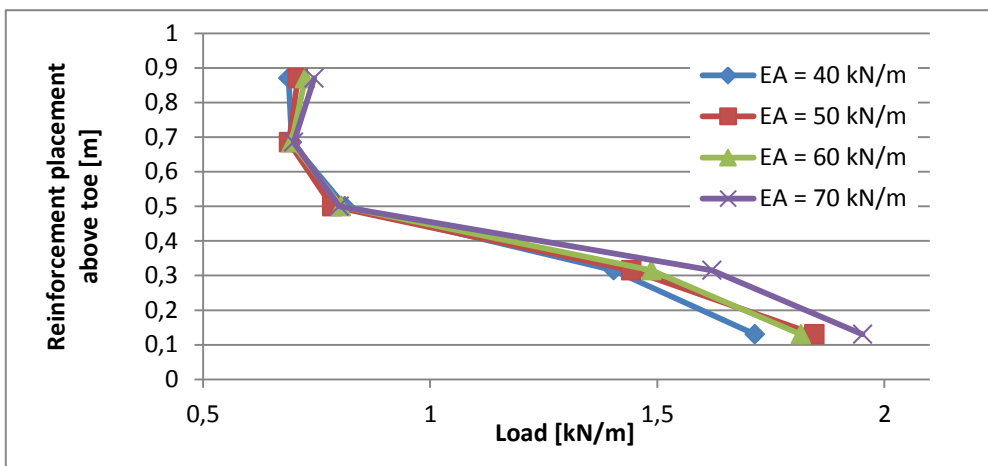
Effect of reinforcement stiffness



a) Input base amplitude: 0.05g

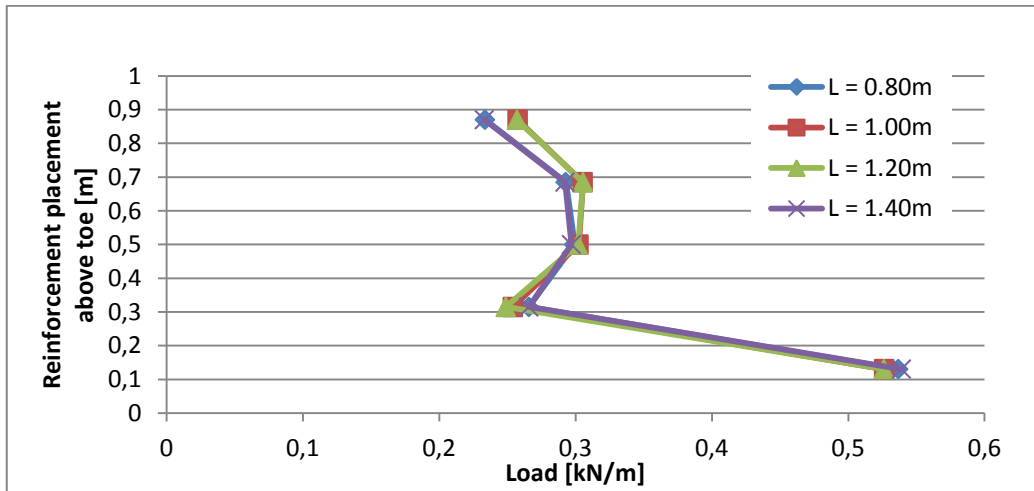


b) Input base amplitude: 0.15g

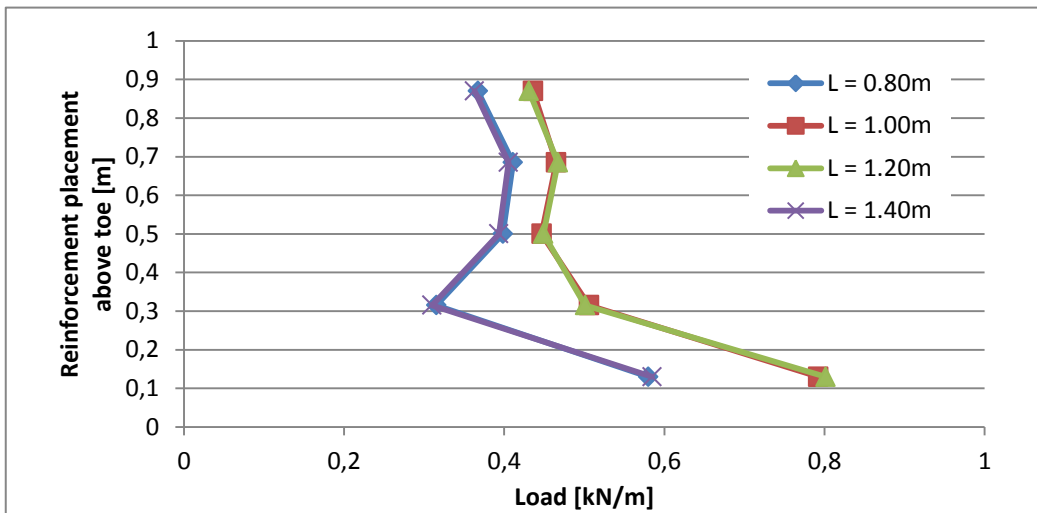


c) Input base amplitude: 0.30g

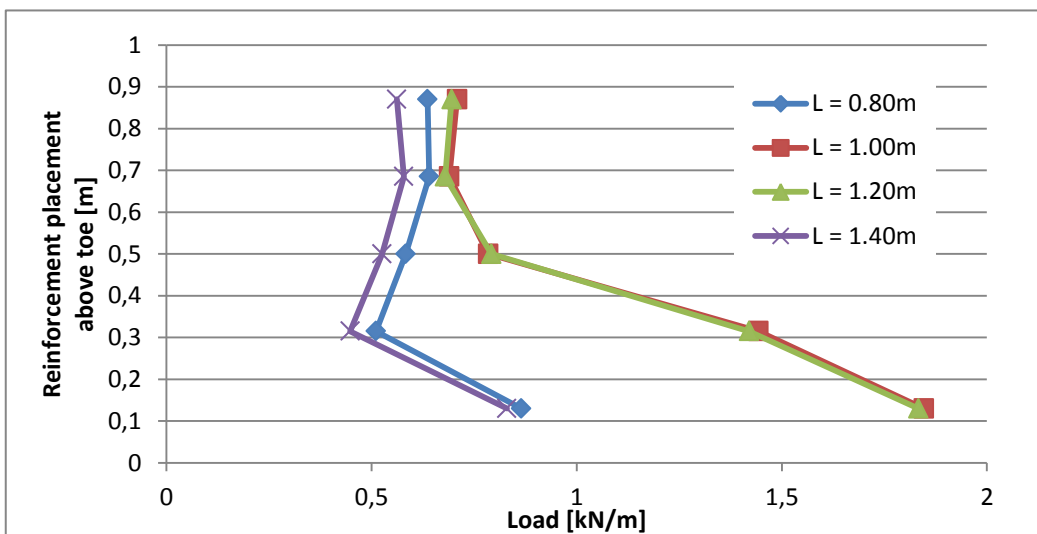
Effect of reinforcement length



Input base amplitude: 0.05g



Input base amplitude: 0.15g



Input base amplitude: 0.30g

Appendix 2 – Pseudo-static methods – MATLAB code

It is assumed that the basics of MATLAB are known to the reader and that the theory in section 6.2-6.4 is read. Thus, please note that the comments in these MATLAB codes are restricted to describing the general steps of these programs and cannot be analysed without additional information (chapter 6).

Mononobe-Okabe method

```
clear all
close all

%% Input
phi=[insert value];    %Soil friction angle [deg]

delta=[insert value]; %Wall friction angle [deg]
beta=[insert value];  %Backfill surface inclination [deg]
omega=[insert value]; %Facing inclination, zero=vertical [deg]

gamma=[insert value]; %Unit soil weight [kN/m3]
H=[insert value];    %Wall height [m]

kh=[insert value];   %Horizontal pseudo-static coefficient
kv=[insert value];   %Vertical pseudo-static coefficient

n=[insert value];    %Number of reinforcements
Sv=[insert value];   %The reinforcement vertical spacing [m]
L=[insert value];    %Reinforcements length [m]

%% Transferring degrees to radians
psi_rad=atan(kh/(1-kv));

phi_rad=(phi*2*pi)/360;
delta_rad=(delta*2*pi)/360;
beta_rad=(beta*2*pi)/360;
omega_rad=(omega*2*pi)/360;

%% Failure surface inclination
C1E=sqrt(tan(phi_rad-psi_rad-beta_rad)*(tan(phi_rad-psi_rad-
beta_rad)+cot(phi_rad-psi_rad-
omega_rad))*(1+tan(delta_rad+psi_rad+omega_rad)*cot(phi_rad-psi_rad-
omega_rad)));

C2E=1+(tan(delta_rad+psi_rad+omega_rad)*(tan(phi_rad-psi_rad-
beta_rad)+cot(phi_rad-psi_rad-omega_rad)));

alfa_AE_rad=phi_rad-psi_rad+atan((-tan(phi_rad-psi_rad-beta_rad)+C1E)/C2E);
alfa_AE=alfa_AE_rad*360/(2*pi);

%% Calculating reinforcements placement above toe
if mod(n,2) == 0
    for i=1:1:n
        h(i)=(H/2)-(Sv/2)-(((n/2)-1)*Sv)+(i-1)*Sv;
    end
else
    for i=1:1:n
        h(i)=(H/2)-(((n-1)/2)*Sv)+(Sv*(i-1));
    end
end
```

Appendix 2 – Pseudo-static methods – MATLAB code

```
%% Calculating KAE and PAE
KAE=((cos(phi_rad-omega_rad-
psi_rad))^2)/((cos(psi_rad)*((cos(omega_rad))^2)*cos(delta_rad+omega_rad+ps
i_rad))*((1+sqrt((sin(delta_rad+phi_rad)*sin(phi_rad-beta_rad-
psi_rad))/(cos(delta_rad+omega_rad+psi_rad)*cos(beta_rad-omega_rad))))^2))
PAE=0.5*KAE*gamma*(H^2)*(1-kv)

%% Calculating reinforcement loads
for j=1:1:n
    Lt(j)=L-(h(j)/tan(alfa_AE_rad));
    if Lt(j)>0
        T(j)=2*(Lt(j)*gamma*(H-h(j)))*tan(phi_rad);
    else
        T(j)=0;
    end
end

end

%Display failure surface inclination
disp('failure line incl, alfa_AE')
disp(alfa_AE)

%Plot reinforcements and failure surface
x0=[0 L 0 0 L 0 0 L 0 0 L];
y0=[h(1) h(1) h(1) h(2) h(2) h(2) h(3) h(3) h(3) h(4) h(4)];

plot(x0,y0);
hold on

top=1/tan(alfa_AE_rad);

x1=[0 top];
y1=[0 1];

plot(x1,y1);
hold on
```

Two-part wedge method

```

clear all
close all

%% Input
phi=[insert value];           %Soil friction angle [deg]
gamma=[insert value];        %Unit soil weight [kN/m3]
H=[insert value];            %Wall height [m]
lamda=[insert value];        %inter-wedge shear mobilization ratio
                                %0<=Lambda<=1

kh=[insert value];           %horizontal pseudo-static coefficient
n=[insert value];            %Number of reinforcements
Sv=[insert value];           %The reinforcements vertical spacing [m]
L=[insert value];            %Reinforcements length [m]

%% Zeroing of parameters
H1=0;                         %Height of 1st wedge
H2=0;                         % = H-H1
H1_div_H=0;                   % = H1/H
teta2=0;                      %angle between the horizontal plane and
                                %the inclination of the "2nd" wedge's
                                %surface
tetal=0;                      %angle between the horizontal plane and
                                %the inclination of the "2nd" wedge's
                                %surface
dif=0.01;                     %Selected interval of studied values of
H1/H

L1=0;                         %Width of 1st Wedge
L2=0;                         %Width of 2st wedge

Lt=zeros(n,1);
T1=0;
T2=0;
k=1;
Test=0;
resulttrac=1;
FS=1;

phi_rad=(phi*2*pi)/360;
phi_rad_f=phi_rad;

Results=zeros(10000000,16);
Results(:,10)=10;
h=zeros(n,1);                 %%Reinforcements position above toe [m]

%% Calculating reinforcements placements above toe
if mod(n,2) == 0
    for i=1:1:n
        h(i)=(H/2)-(Sv/2)-((n/2)-1)*Sv+(i-1)*Sv;
    end
else
    for i=1:1:n
        h(i)=(H/2)-(((n-1)/2)*Sv)+(Sv*(i-1));
    end
end

```

Appendix 2 – Pseudo-static methods – MATLAB code

%%Calculations of the critical failure surface, i.e. the one with the lowest safety factor (FS)

```

for FS=1:0.01:20
    if Test<=4
        phi_rad_f=phi_rad/FS;

    for teta2=5:1:90
        teta2_rad=teta2*2*pi/360;

    for teta1=teta2:1:90
        teta1_rad=teta1*2*pi/360;

        for H1_div_H=0:dif:H
            H1=H*H1_div_H;
            H2=H-H1;

            A1=1/(sin(teta1_rad)-(tan(phi_rad_f)*cos(phi_rad_f)));
            B1=(tan(phi_rad_f)*sin(teta1_rad))+cos(teta1_rad);

            L2=H2/tan(teta2_rad);
            L1=H1/tan(teta1_rad);

            W1=gamma*L1*H1*0.5;
            W2=gamma*((H+H1)/2)*L2;

            P1=(W1+(B1*A1*kh*W1))/((lamda*tan(phi_rad_f))+(B1*A1));
            V1=lamda*P1*tan(phi_rad_f);

            A2=1/((tan(phi_rad_f)*sin(teta2_rad))+cos(teta2_rad));
            B2=(tan(phi_rad_f)*cos(teta2_rad))-sin(teta2_rad);

            T1=0;
            T2=0;

            for j=1:1:n
                if h(j)<=H2
                    Lt(j)=L-(h(j)/tan(teta2_rad));

                    if Lt(j)>0
                        T(j)=2*(Lt(j)*gamma*(H-h(j)))*tan(phi_rad_f);
                    else
                        T(j)=0;
                    end
                    T2=T2+T(j);
                else
                    Lt(j)=L-L2-((h(j)-H2)/tan(teta1_rad));
                    if Lt(j)>0
                        T(j)=2*(Lt(j)*gamma*(H-h(j)))*tan(phi_rad_f);
                    else
                        T(j)=0;
                    end
                    T1=T1+T(j);
                end
            end
        end
    end
end

```

Appendix 2 – Pseudo-static methods – MATLAB code

```

        PAE=P1-((B1*A1*T1)/((lamda*tan(phi_rad_f))+ (B1*A1)))+(kh*W2)-
T2-((B2*A2)*(W2+V1));

        T_total=T(1)+T(2)+T(3)+T(4);

        KAE=(2*T_total)/(gamma*(H^2));

        Results(k,:)=[teta2 teta1 H1_div_H H1 H2 L1 L2 PAE KAE FS T(1)
T(2) T(3) T(4) 0 T_total];

        if abs(PAE)<=0.01
        if KAE>0
        Test=1+Test;
        x= [0 L2 L1+L2];
        y= [0 H2 H];

        x0=[0 L 0 0 L 0 0 L 0 0 L];
        y0=[h(1) h(1) h(1) h(2) h(2) h(2) h(3) h(3) h(3) h(4) h(4)];

        plot(x0,y0);
        hold on

        plot(x,y,'-.or')
        ylim([0 H])
        hold on
        PAE2=P1+(kh*W2)-(A2*A2)*(W2+V1);
        KAE2=(2*PAE2)/(gamma*(H^2));
        Results_relevat(resultttrac,:)=[teta2 teta1 H1_div_H H1 H2 L1 L2
PAE KAE FS T(1) T(2) T(3) T(4) 0 T_total];
        resultttrac=1+resultttrac;
        end
        end
        k=k+1;
        end
    end
end
end

```

Appendix 2 – Pseudo-static methods – MATLAB code

Horizontal slices method - Linear and polylinear

%All relevant notations are as described in chapter 6.4.

close all

clear all

%Input

phi=[insert value]; %Soil friction angle[deg]

delta=[insert value]; %Wall friction angle[deg]

kh=[insert value]; %Horizontal pseudo-static coefficient

kv=[insert value]; %Vertical pseudo-static coefficient

gamma=[insert value]; %Unit soil weight [kN/m3]

H=[insert value]; %Wall height [m]

Vs=[insert value]; %Shear wave velocity [m/s]

Vp=[insert value]; %Primary wave velocity

n=[insert value]; %Number of reinforcements => number of slices

Sv=[insert value]; %The reinforcement vertical spacing [m]

L=[insert value]; %Reinforcements length [m]

T=[insert value]; %Period of seismic shaking

t=[insert value]; %Time

%%Calculation: linear HSM

alfa=0;

% Transferring degrees to radians

phi_rad=(phi*2*pi)/360;

delta_rad=(delta*2*pi)/360;

%%Calculating alfa_base by trying different values of t and inclination angle (here "alfa" is inclination angle).

Kae_matrix=zeros(100000,3);

j=1;

for t=0:0.01:10

for alfa=15:1:90

 alfa_rad=(alfa*2*pi)/360; %Converts alfa to radians

 m1=2*pi*cos(2*pi*((t/T)-(H/(T*Vs))))+((T*Vs)/H)*(sin(2*pi*((t/T)-(H/(T*Vs))))-sin(2*pi*(t/T))));

 m2=2*pi*cos(2*pi*((t/T)-(H/(T*Vp))))+((T*Vp)/H)*(sin(2*pi*((t/T)-(H/(T*Vp))))-sin(2*pi*(t/T))));

 %Calculating different values for linear KAE and stores relevant

 %information in a matrix ("Kae_matrix")

 Kae0= (1/(tan(alfa_rad)))*((sin(alfa_rad-phi_rad))/(cos(delta_rad+phi_rad-alfa_rad)));

 Kae1=((kh*T*Vs*m1)/(2*(pi^2)*H))*(cos(alfa_rad-phi_rad)/((tan(alfa_rad)*cos(delta_rad+phi_rad-alfa_rad))));

 Kae2=((kv*T*Vp*m2)/(2*(pi^2)*H))*(sin(alfa_rad-phi_rad)/((tan(alfa_rad)*cos(delta_rad+phi_rad-alfa_rad))));

 Kae=Kae0+Kae1+Kae2;

Appendix 2 – Pseudo-static methods – MATLAB code

```

Kae_matrix(j,1)=alfa;
Kae_matrix(j,2)=t;
Kae_matrix(j,3)=Kae;

j=j+1;
end
end

%Calculates the correct value of the linear KAE and displays it:
Maximum_Kae=max(Kae_matrix(:,3));
disp('KAE_linear')
disp(Maximum_Kae)

%Finds relevant value for the time:
for j=1:1:100000
    if Kae_matrix(j,3)==Maximum_Kae
        alfa_base=Kae_matrix(j,1);
        t_used=Kae_matrix(j,2);
    end
end

alfa_base_rad=(alfa_base*2*pi)/360; %Makes the alfa base angle in to
radians

%%Calculation: polylinear HSM

%Accounts for n being similar or odd
h=zeros(n,1); %Reinforcements position above toe [m]
if mod(n,2) == 0
    for i=1:1:n
        h(i)=(H/2)-(Sv/2)-(((n/2)-1)*Sv)+(i-1)*Sv;
    end
else
    for i=1:1:n
        h(i)=(H/2)-(((n-1)/2)*Sv)+(Sv*(i-1));
    end
end

%Calculates the height from the toe to the top of the slices
dz_top=zeros(n,1); %height from the surface to the top of the slice
for j=1:1:n-1
    dz_top(j)=(h(j)+h(j+1))/2;
end
dz_top(n)=H;

%Calculates slice thickness
dz=zeros(n,1); %slice thickness
dz(1)=dz_top(1);
for k=2:1:n
    dz(k)=dz_top(k)-dz_top(k-1);
end

%creating different matrixes for use later
l=zeros(90,n+1); %Top width of slice
l_0=zeros(n+1,1); %Bottom width of slice
V=zeros(90,n+1); %Top inter wedge force
V_0=zeros(n+1,1); %Bottom inter wedge force
W=zeros(90,n); %Weight of slice
m=zeros(90,n); %Mass of slice [1000*kg/m]
qv=zeros(n,1); %As described in theory

```

Appendix 2 – Pseudo-static methods – MATLAB code

```

qh=zeros(n,1);           %As described in theory
av=zeros(n,1);           %As described in theory
ah=zeros(n,1);           %As described in theory
tensile=zeros(90,n);     %Tensile force
N=zeros(90,n);           %As described in theory
S=zeros(90,n);           %As described in theory

%Implementing initial conditions from linear HSM (geometry and forces from
bottom slice)
alfa_slice_1=zeros(n,1);
alfa_s=zeros(90,n);

l_0(2)=dz(1)/tan(alfa_base_rad);
alfa_slice_1(1,1)=alfa_base;
alfa_slice_0=alfa_base;
z=zeros(n+1,1);
z(1)=0;
z(n+1)=H;

t_summert=0; %Zeros the parameter that describes the total tensile forces

%%Finds geometry of all wedges (except the bottom one which was found above
%by using linear HSM) and calculates corresponding forces.

for i=2:1:n
    av(i)=kv*9.81*sin(pi*2*((t_used/T)-((H-dz_top(i))/Vp)));
    ah(i)=kh*9.81*sin(pi*2*((t_used/T)-((H-dz_top(i))/Vs)));

    %Tries different angles from alfa_base to vertical (0-90) and
    %calculates the corresponding forces
    for alfa_slice=alfa_base:1:90
        alfa_slice_rad=(alfa_slice*2*pi)/360;

        alfa_s(alfa_slice,i)=alfa_slice;

        V_0(i)=l_0(i)*(1+kv)*gamma*(H-dz_top(i-1));

        l(alfa_slice,i+1)=l_0(i)+abs((dz(i)/tan(alfa_slice_rad)));

        V(alfa_slice,i+1)=l(alfa_slice,i+1)*(1+kv)*gamma*(H-dz_top(i));

        W(alfa_slice,i)=((l_0(i)+l(alfa_slice,i+1))/2)*dz(i)*gamma;
        m(alfa_slice,i)=W(alfa_slice,i)/9.81;

        N(alfa_slice,i)=((V(alfa_slice,i+1)-
        V_0(i))+W(alfa_slice,i))/((tan(phi_rad)*sin(alfa_slice_rad))+cos(alfa_slice
        _rad));
        S(alfa_slice,i)=N(alfa_slice,i)*tan(phi_rad);

        tensile(alfa_slice,i)=-
        (S(alfa_slice,i)*cos(alfa_slice_rad))+((N(alfa_slice,i))*sin(alfa_slice_rad
        ))+(m(alfa_slice,i)*ah(i));

        z(i)=z(i-1)+dz(i-1);
    end

    %Finds maximum tensile force,
    Maximum_tensile(i)=max(tensile(:,i));

```

Appendix 2 – Pseudo-static methods – MATLAB code

```

%Finds the corresponding geometry to the maximum tensile force, i.e.
%the critical surface for the ith slice, and stores the inter-wedge
%forces and the correct geometry
for p=1:1:90
    if tensile(p,i)==Maximum_tensile(i)
        t_summert=tensile(p,i)+t_summert; %Ads max tensile
                                           %force to the total
                                           %tensile force

        alfa_slice_1(i)=alfa_s(p,i);
        alfa_slice_0=alfa_s(p,i);
        l_0(i+1)=l(p,i+1);
        V_0(i+1)=V(p,i+1);

    end
end
end

%Calculates forces from the first (bottom) slice
av(1)=kv*9.81*sin(pi*2*((t_used/T)-((H-dz_top(i))/Vp)));
ah(1)=abs(kh*9.81*sin(pi*2*((t_used/T)-((H-dz_top(1))/Vs))));

W(:,1)=l_0(2)*dz(1)*0.5*gamma;
m(:,1)=W(alfa_slice,i)/9.81;
V(:,2)=l_0(2)*(1+kv)*gamma*(H-dz_top(1));
N(:,1)=((V(alfa_base,2))+W(alfa_base,1)+(m(alfa_base,1)*av(1)))/((tan(phi_r
ad)*sin(alfa_base_rad))+cos(alfa_base_rad));
S(:,1)=N(alfa_base,1)*tan(phi_rad);
tensile(:,1)=-
(S(alfa_base,1)*cos(alfa_base_rad))+((N(alfa_base,1))*sin(alfa_base_rad))+
(m(alfa_base,1)*ah(1));

%Sums all the tensile forces and calculates the poly linear
%earth prefficient
t_summert=tensile(1,1)+t_summert;
KAE_polylinear=t_summert/(0.5*gamma*(H^2));

%Plot and displays results
disp('KAE_polylinear')
disp(KAE_polylinear)
figure
    plot(l_0(:),z(:),'-or')
    ylim([0 H])
    hold on

x0=[0 L 0 0 L 0 0 L 0 0 L];
y0=[h(1) h(1) h(1) h(2) h(2) h(2) h(3) h(3) h(3) h(4) h(4)];
    plot(x0,y0);
    hold on

x1=[0 H/tan(alfa_base_rad)];
y1=[0 H];
x2=[l_0(:);z(:)];
    plot(x1,y1);
    hold on

%Calculates and displays PAE (both linear and polylinear)
PAE_linear=0.5*Maximum_Kae*gamma*(H^2)
PAE_polylinear=0.5*KAE_polylinear*gamma*(H^2)

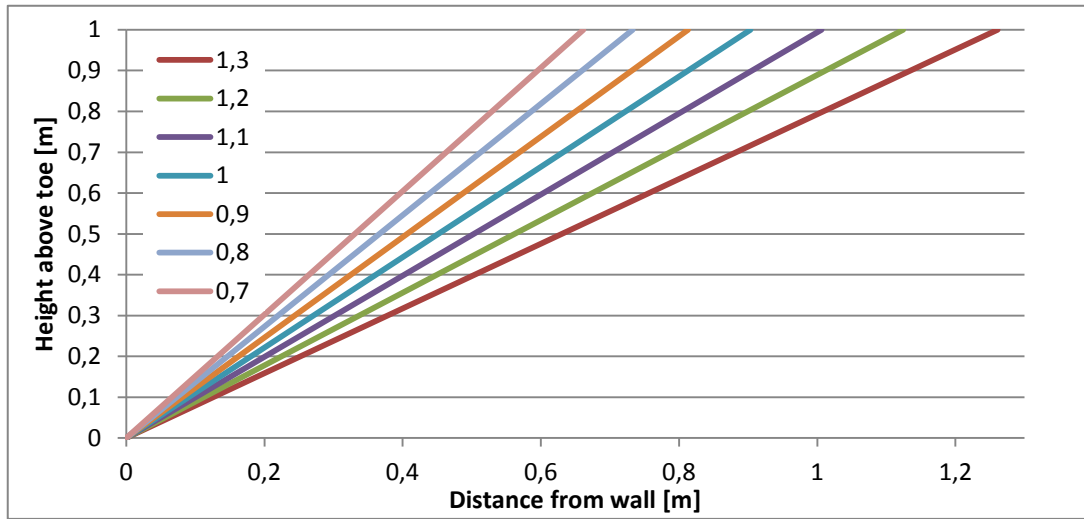
```

Appendix 3 – Horizontal Pseudo-static Coefficients from Current Seismic Design Codes

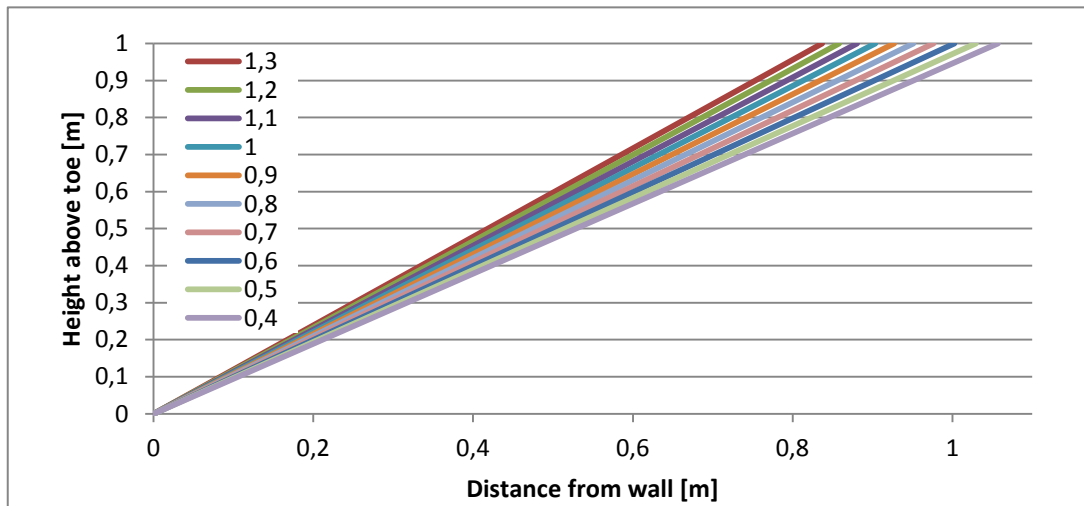
Input acceleration amplitude	k_h^{spes}	k_h^{EC}	k_h^{PIANC}	k_h^{FHWA}
0.00g	0	0	0	0
0.05g	0.0549	0.0533	0.0275	0.0766
0.15g	0.1663	0.1600	0.0832	0.2135
0.30g	0.3498	0.3200	0.1749	0.3848
0.40g	0.5163	0.4267	0.2582	0.4821
0.50g	0.8288	0.5333	0.4144	0.5149

Appendix 3 – Horizontal Pseudo-static Coefficients from Current Seismic Design Codes

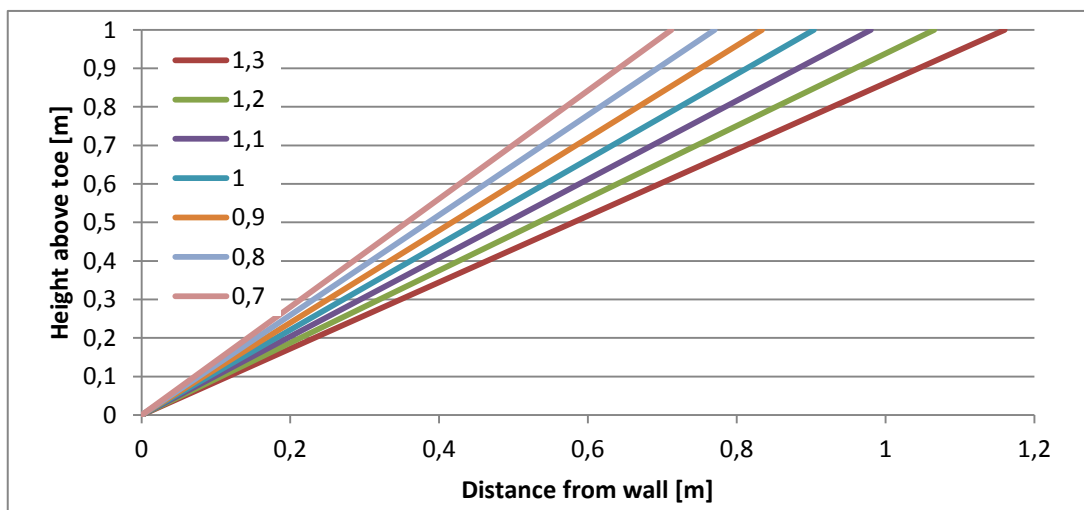
Appendix 4 - Effect of changing A, B and C Failure surface



Failure surface for different values of A ($a_{max}=0.30g$)

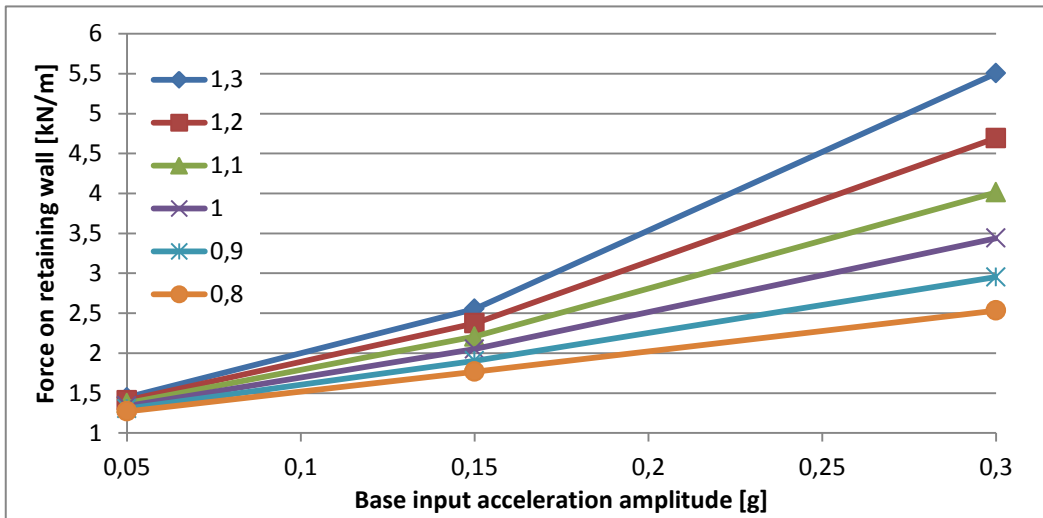


Failure surface for different values of B ($a_{max}=0.30g$)

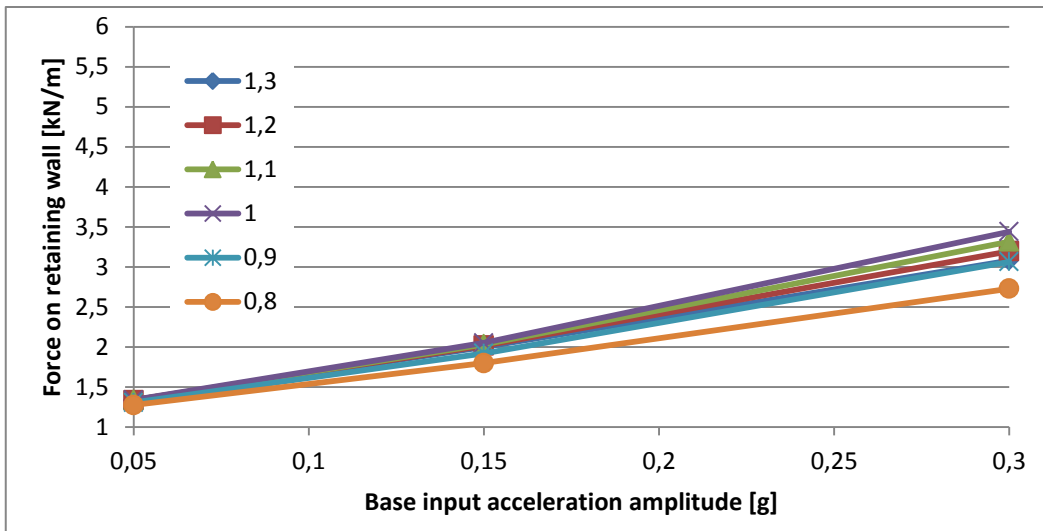


Failure surface for different values of C ($a_{max}=0.30g$)

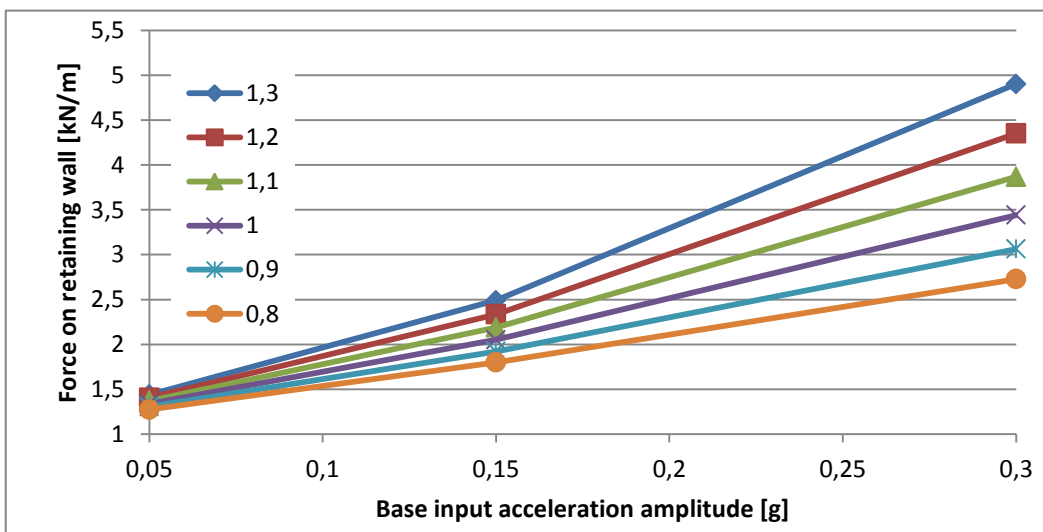
Active earth forces



Earth forces for different values of A



Earth forces for different values of B



Earth forces for different values of C